This thesis deals with the fabrication and characterization of novel all-fiber components for access networks. All fiber components offer distinctive advantages due to low forward and backward losses, epoxy free optical path and high power handling. A novel fabrication method for monolithic 1x4 couplers, which are vital components in distributed passive optical networks, is realized. The fabrication method differs from conventional structures with a symmetric coupling profile and hence offers ultra wideband performance and easy process control. New structure for 1x4 couplers, by fusing five fibers is proposed to achieve high uniformity, which gives equivalent uniformity performance to 1x4 planar lightwave splitters. Isolation in fused fiber WDM is improved with integration of long period gratings. Packaging techniques of fused couplers are analyzed for long term stability.
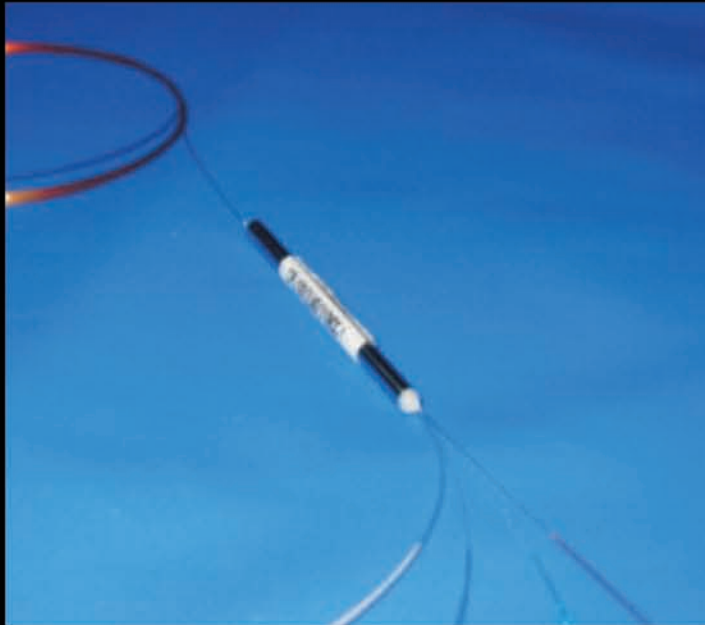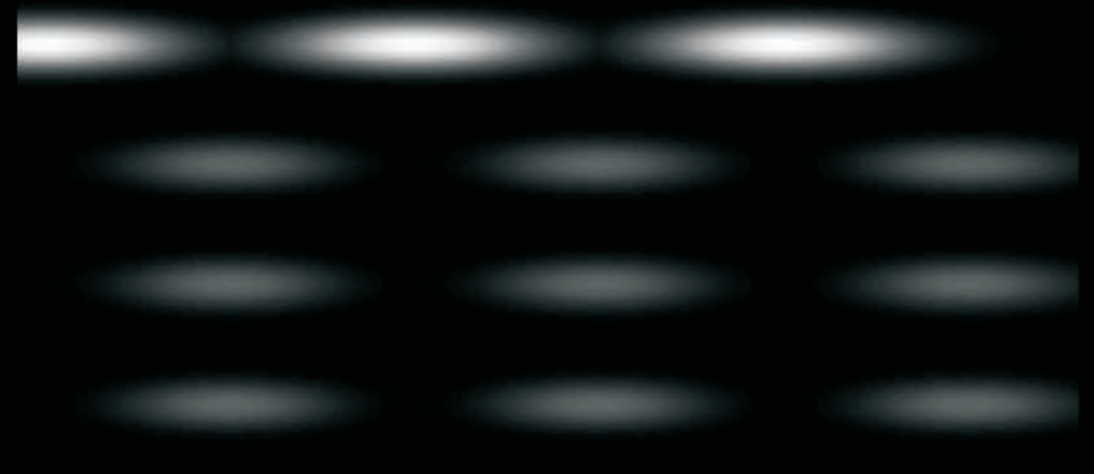
Ph. D Thesis

Samuel Varghese

December 2008

Ph. D Thesis

Fabrication and Characterization of All-Fiber Components for Optical Access Networks

Samuel Varghese

International School of Photonics
Cochin University of Science and Technology

Fabrication and Characterization of All-Fiber Components for Optical Access Networks

Samuel Varghese K

Ph. D Thesis submitted in fulfillment of the requirements of the degree of Doctor of Philosophy to the

International School of Photonics
Cochin University of Science and Technology
Cochin, 682 022, Kerala, India

December 2008

**Fabrication and Characterization of
All-Fiber Components for Optical Access Networks**
Ph. D Thesis in the field of Photonics

Author:
Samuel Varghese
Research Fellow,
International School of Photonics,
Cochin University of Science and Technology,
Cochin – 682022, India.
Email: zamvargheze@gmail.com

Research Advisors:
Dr. V. P. N Nampoori
Professor & Director,
International School of Photonics,
Cochin University of Science and Technology,
Cochin – 682022, India.
Email: nampoori@gmail.com

Dr. C. P. Girijavallabhan
Professor,
International School of Photonics,
Cochin University of Science and Technology,
Cochin – 682022, India.
Email: gvallabhan@gmail.com

International School of Photonics
Cochin University of Science and Technology
Cochin – 682022, India
URL: www.photonics.cusat.edu

December 2008

Front Cover: Density plot of optical power along the propagation direction of a
monolithic 1x4 coupler
Back Cover: Photograph of monolithic 1x4 coupler

Dedicated to

My Loving Family

CERTIFICATE

Certified that the work presented in the thesis entitled *"Fabrication and Characterization of All-Fiber Components for Optical Access Networks"* is based on the original work carried out by Mr. Samuel Varghese K, under my guidance and supervision at the International School of Photonics, Cochin University of Science and Technology, Cochin, India and has not been included in any other thesis submitted previously for award of any degree.

Cochin – 682022
29th December 2008.

Prof. V. P. N. Nampoori
(Supervising Guide)

DECLARATION

Certified that the work presented in the thesis entitled ***"Fabrication and Characterization of All-Fiber Components for Optical Access Networks"*** is based on the original work done by me, under the guidance and supervision of Prof. V. P. N. Nampoori, Professor and Director, International School of Photonics, Cochin University of Science and Technology, Cochin, India and the co-guidance of Prof. C. P. G. Vallablan at the International School of Photonics, Cochin University of Science and Technology, Cochin, India and it has not been included in any other thesis submitted previously for award of any degree.

Cochin – 682022   Samuel Varghese
29th December 2008.

Preface

Passive Optical Network (PON) is one of the leading broadband access technologies today. All-fiber technology offers a versatile platform, for realizing a variety of components for passive optical networks, owing to its capability of keeping the integrity of signal transmission with low loss and high power handling. All-fiber components find applications as branching and multiplexing elements in PONs and in fiber amplifiers.

In passive optical networks, many end users share the same central office equipment and fiber infrastructure through 1xN optical splitters. The design and fabrication technologies of 1xN fused biconical tapered couplers are very well established, provided N=2. But the accepted PON system calls for 1x4 splitter followed by 1x8 splitters. Fused coupler fabrication is relatively simple as compared to the competitive technologies like Planar Lightwave Circuits (PLC), which requires semiconductor fabrication process. Thus in a PON system, for 1xN splitter requirements, when N=4, fused coupler is more economical and whereas when N≥4, PLC may be the option due to its merits. It has to be noted that cascading of 1x2 couplers to realize 1x4 or 1x8 splitters is not preferred due to the higher insertion loss and reduction in reliability factor. Methods to achieve wideband performance of monolithic fused couplers are not established well. Monolithic 1xN couplers are difficult to fabricate, due to the complex coupling signatures of the device. Moreover, in monolithic couplers, it is difficult to achieve broadband performance from 1250 to 1650nm, for the faithful transmission at multiple wavelengths for bundled transmission of video, data and voice. In the work reported here, the focus has been to arrive at a novel design to realize wavelength independent monolithic 1x4 splitters, fabricate them, and characterize them for the performance and reliability. Part of the studies has been devoted to realize all-fiber high isolation wavelength division multiplexers and mode conditioning elements, which are also vital components in optical access networks.

Chapter 1 reviews the architecture of PON network as well as various optical technologies used in PON. Copper based access solutions are not capable of supporting the evolving high bandwidth services and hence optical access networks are considered as the promising solution for next generation services. The point-to-multipoint (P2MP) Passive Optical Network architecture is the most attractive solution since it shares the cost of the fiber plant among different customers and also offers lower operating cost owing to its passive nature. The basic architecture of a passive optical network is explained along with its advantages, power budget and

multiple access options. Passive Optical Network contains only passive components like splitters and WDMs. The major technologies for realizing the splitters, viz., fused fiber technology and planar waveguide technology are reviewed. The components based on fused fiber technology are attractive since it offers an all-fiber solution.

Chapter 2 describes the underlying theory and the operating principles of fused couplers. Fused couplers, are important passive components in fiber communication systems that perform signal splitting, wavelength multiplexing, filtering etc. Fused couplers are formed by joining two or more independent optical fibers; the claddings of the fibers are fused in a small region. This chapter describes the basic theory and fabrication of fused fiber couplers. Chapter 2 also describes the salient features of the automated fabrication set-up designed in-house for realizing fused coupler based branching components. The important control parameters for fusion and tapering include pulling speed, the flame temperature and flame brush width. All these parameters are precisely controlled in the automated fabrication process. This chapter describes the detailed process flow and the effect of different control parameters on fabrication. The importance performance parameters of the couplers include splitting ratio, excess loss, insertion loss and directivity. This chapter also describes the measurement setup and procedure for measuring those parameters.

Following the above, different fabrication methods for realizing wavelength independent 1x4 couplers are reviewed. In *Chapter 3*, the power coupling profile in four fiber structures is analyzed and a new method for the fabrication of 1x4 monolithic coupler is proposed. This method alleviates the need for preprocessing of individual fibers that are fused and allows easy fabrication of wavelength insensitive device. Important features of the process developed here are the symmetric power transfer to all coupled fibers and the ultra wide band performance. To establish the process and device reliability, many devices are built and the repeatability of parameters like insertion loss, polarization dependent loss and uniformity are analyzed. The response of the coupler is studied for bidirectional applications. From the studies a model is suggested to predict the back reflection of the device. This method can be extended for realizing wavelength independent couplers.

Uneven port-to-port uniformity causes different optimum reach conditions for data transmission at different wavelengths. The port-to-port uniformity of the fused coupler is generally spectrally dependent, owing to the different spectral dependence of the throughput and coupled ports of the coupler. Hence, if all the power can be

transferred to the coupled fibers, it is possible to achieve the same spectral dependence for all the splitted signals. This helps to reduce the wavelength dependence of uniformity. As described in *Chapter 4*, this is done by fusing five fibers together and completely transferring the throughput fiber to the coupled fibers. By adjusting the process parameters it is possible to keep nominal power in the throughput port, which can be used for the in-situ monitoring of the signal flowing through the splitter.

Fused coupler technology can be used to build wavelength division multiplexers (WDMs). However, the isolation reported in fused WDM is 17-20 dB, whereas the requirement is 30-35 dB. *Chapter 5* deals with a method to improve the isolation in fused WDMs by integrating long period gratings (LPGs). LPGs act as a spectrally sensitive loss element by rejecting a narrow band signal and hence help in improving the isolation of fused WDMs. A low cost fabrication method based on electric arc using a splicing machine is utilized to realize this. Methods are devised to reduce the polarization sensitivity of such devices by rotating the fiber during the fabrication.

Multimode fiber based access networks are affected by differential mode delay, arising from the interaction between laser spot and index profile defects. Thus single mode sources shall be conditioned for gigabit transmission over multimode fiber; conventionally done with offset launching. In *Chapter 6*, a method to achieve mode conditioning with all-fiber approach is proposed. LPGs are fabricated at the single mode-multimode fiber interface and the device is packaged. The sensitivity of the fabrication process is studied for parameters such as position of the grating at the single mode-multi mode interface etc.

Reliability is one of the critical issues faced by today's passive optical component manufacturers and suppliers, which forms the subject matter of *Chapter 7*. Fused coupler packaging approach is analyzed to improve the impact resistance and thermal stability. The present work suggests achieving thermal matching of the adhesive using quartz filling and improvement in adhesion by changing the surface roughness of the substrate. A method to improve the ruggedness of the device is suggested by redefining the fixing points of the fused region inside the quartz substrate. Chapter 8 includes general conclusions based on the research with possible work for further research in this direction.

List of Publications

International Journals

1. **Samuel Varghese**, Suresh Nair, V.P.N.Nampoori and C.P.Girijavallabhan, "Grating Assisted Control of Isolation in All-fiber WDMs", *Microwave and Optical Technology Letters*. (*Communicated*)

2. **Samuel Varghese**, Suresh Nair, V.P.N.Nampoori and C.P.Girijavallabhan, "Monolithic fused 1x4 couplers with high uniformity", *J. Optics Communications*. (*Accepted for publication*)

3. **Samuel Varghese**, Muhammed Iqbal, Suresh Nair, V.P.N.Nampoori and C.P.G.Vallabhan, "Fabrication and characterization of monolithically fused wavelength independent 1x4 couplers" *Fiber and Integrated Optics,* 26, pp.245-254, 2007.

Patents

1. Suresh Nair, **Samuel Varghese**, Muhammed Iqbal, Yoshitaka Koshiba, "Method of building truly fused 1x4 couplers with ultra broadband spectral performance; low polarization sensitivity and high impact resistance and couplers build therefore", *Journal of the Patent Office*, India 25, 19867, 2007

International Conferences

1. **Samuel Varghese**, Biji Mathew, Muhammed Iqbal, Abraham Thomas, Suresh Nair, "Highly reliable planar splitters designed for FTTH application", *PHOTONICS 2006, Eighth International Conference on Optoelectronics, Fiber Optics and Photonics, Hyderabad, December 2006.*

2. **Samuel Varghese**, Anees P, Suresh Nair, "An edge filter interrogation scheme for distributed FBG sensing", *PHOTONICS 2006, Eighth International Conference on Optoelectronics, Fiber Optics and Photonics, Hyderabad, December 2006.*

3. **Samuel Varghese**, Muhammed Iqbal, Baiju C. B, Hari. K, Abraham Thomas, Suresh Nair, "Design Improvements of fused couplers for PON Applications", *PHOTONICS 2004, Seventh International Conference on Optoelectronics, Fiber Optics and Photonics, Cochin, December 2004.*

4. **Samuel Varghese**, Priyamvada, Majo Mary Mathew, Swarish. S, Suresh Nair, "A novel real time Remote Fiber Monitoring System", *Seventh International Conference on Optoelectronics, Fiber Optics and Photonics, Cochin, December 2004*.

5. Ajith Kumar P.T, Prasannan. G, S. Ambadiyil and **Samuel Varghese**, "Performance analysis and material dependence of micro-holographic optical elements as couplers for fiber optic communications", *Proceedings of SPIE Vol.5005, IS&T/SPIE's 15th Annual Symposium on Electronic Imaging – Science and Technology, January 2003, Santa Clara, California, USA.*

6. **Samuel Varghese**, Suresh Nair, "Studies on improvement of isolation in fused fiber wavelength division multiplexers", *PHOTONICS 2002, Sixth International Conference on Optoelectronics, Fiber Optics and Photonics, Mumbai, December 2002*.

7. **Samuel Varghese**, Muhammed Iqbal, Suresh Nair, "Development of IEEE 802.3z compliant mode conditioning patchcord for Gigabit Ethernet LANs and its reliability studies", *PHOTONICS 2002, Sixth International Conference on Optoelectronics, Fiber Optics and Photonics, Mumbai, December 2002*.

8. **Samuel Varghese**, Suresh Nair, "Design and fabrication of flat response interleaver for high channel count DWDM Applications", OPTONICS-2001, *Second International Conference and XXVII Annual convention of Optical Society of India, Thiruvananthapuram, 2001*

National Conferences

1. Anees. P, **Samuel Varghese K**, Suresh Nair, "Interrogation System for FBG based Smart Sensors", *National Conference on Recent Trends in Opto-electronics and Laser Technology, NCOL, April, Thiruvananthapuram 2007*.

2. **Samuel Varghese**, Suresh Nair, V.P.N. Nampoori, "Fabrication and performance analysis of Long Period Fiber Bragg Gratings based on Electric Arc technique", *DAE-BRNS National Laser Symposium, Thiruvananthapuram, November 2002*.

Acknowledgements

This thesis is a culmination of many years of effort where I have been accompanied and supported by many. I am extremely grateful to my supervisors, Prof. V. P. N. Nampoori and Prof. C. P. Girijavallabhan. I would like to thank them for taking responsibility of my Ph.D. studies and for their generous support. I am indebted to Prof. Nampoori for his continuous guidance, encouragement and for his suggestions for improving my thesis. His enthusiasm, simplicity and commitment to science deeply impressed me. I express my gratitude to Prof. C. P. Girijavallabhan, who inspired me with his clarity of thoughts and comments. His suggestions always added another dimension of perfection to my work.

My special and sincere thanks to Dr. Suresh Nair, CTO, NeST group for his support, advice and of being a source of optimism. He was the main inspiration for initiating this research. I feel motivated and energized every time, after my discussion with him. I am grateful to him for his insightful and constructive review comments. It would not have been possible to do this work without his guidance and support.

I would like to express my gratitude to the visionary leaders of NeST, Dr. Javad Hassan, Mr. N. Jehangir and Mr. U. M. Shafi, for allowing me to do scientific research in a highly motivated industrial environment. My personal regards to Dr. P. T. Ajithkumar, C-DIT, Trivandrum, who nourished my interest in optics and inspired me to continue research. My special thanks to Prof. P. Radhakrishanan, Prof. V. M. Nandakumaran and Mr. Kailasnath for their kind support.

I was privileged to have the generous support from my colleagues at NeST family, especially Biji Mathew and Muhammed Iqbal. I am also indebted to all my colleagues at NeST R&D Centre. It has been a pleasure and interesting experience to work with them and without their contribution this work would have been much more difficult. I acknowledge the cooperation of my co-researchers at International School of Photonics, whom I have had the pleasure to work with.

Warmest thanks to my wife Neeba for always being by my side, supporting and encouraging me to be on track. I thank my beloved parents for their blessings and love. My family deserves special mention for their inseparable support and prayers. I would like to thank everyone who was important to the successful realization of thesis. Finally, I praise God almighty for strengthening me throughout my life and especially to do this work.

Samuel Varghese

List of Abbreviations

AWG	Arrayed Waveguide Grating
BER	Bit Error Rate
BPON	Broadband Passive Optical Network
BR	Back Reflection
BW	Bandwidth
CATV	Community Antenna TV
CO	Central Office
CPR	Coupled Power Ratio
CR	Coupling Ratio
CTE	Coefficient of Thermal Expansion
CWDM	Coarse Wavelength Division Multiplexing
DAC	Data Acquisition Card
DEMUX	Demutliplexer
DMD	Differential Mode Delay
DSL	Digital Subscriber Line
DUT	Device Under Test
DWDM	Dense Wavelength Division Multiplexing
E/O	Electrical-to-OpticaI
EDFA	Erbium Doped Fiber Amplifier
EL	Excess Loss
EPON	Ethernet Passive Optical Network
FBG	Fiber Bragg Grating
FBT	Fused Biconical Taper
FSAN	Full Service Access Network
FTTB	Fiber-To-The-Building
FTTC	Fiber-To-The-Curb
FTTH	Fiber-To-The-Home
FTTx	Fiber-To-The-x
FWHM	Full Width at Half Maximum
GbE	Gigabit Ethernet
GPON	Gigabit Passive Optical Network
GRIN	Graded Index
HA	Humidity Aging
HOM	Higher Order Modes
IEEE	Institute of Electronics and Electrical Engineers
IL	Insertion Loss
IOM	Intermediate Order Modes
ITU	International Telecommunication Union
LAN	Local Area Network

LED	Light Emitting Diode
LOM	Lower Order Modes
LPG	Long Period Gratings
MCC	Motor Control Card
MCP	Mode Conditioning Patchcable
MMF	Multi Mode Fiber
MPD	Modal Power Distribution
MUX	Multiplexer
NRZ	Non-Return to Zero
O/E	Optical-to-Electrical
ODN	Optical Distribution Network
OLT	Optical Line Terminal
ONT	Optical Network Terminal
ONU	Optical Network Unit
OSA	Optical Spectrum Analyzer
P2MP	Point-to-Multi-Point
P2P	Point-to-Point
PC	Personal Computer
PDL	Polarization Dependent Loss
PLC	Planar Lightwave Circuit
PON	Passive Optical Network
PRBS	Pseudo Random Binary Sequence
RH	Relative Humidity
Rx	Receiver
SASA	Splitter Array Sub Assembly
SEM	Scanning Electron Microscope
SMF	Single Mode Fiber
TC	Temperature Cycling
TDL	Temperature Dependent Loss
TDM	Time Division Multiplexing
TDMA	Time Division Multiple Access.
TFF	Thin Film Filter
Tx	Transmitter
UV	Ultraviolet
VCSEL	Vertical Cavity Surface Emitting Laser
WDDM	Wavelength Division De-Multiplexer
WDM	Wavelength Division Multiplexer

Contents

Chapter 1
Optical Access Networks

Passive Optical Networks (PONs) are emerging as the ultimate solution for high speed access networks. All-fiber components are ideal for passive optical networks because of many inherent advantages such as low forward and return losses and high power handling capability. This chapter reviews the architecture and optical component technologies used in PON. This chapter also presents the relevance of the research work.

Since its conception [1-3] in late 1980's, Passive Optical Network (PON) is emerging as a promising solution for "last mile" access, because of the potential of optical transmission and the advantages of PON's architecture. PON based broadband access systems have now adopted for wide-scale deployments in Asia, Europe and North America [4], owing to the growing need for broadband access and maturing of the relevant technologies. However, PON technologies are still in the process of evolution to cater to the growing need of economic broadband access.

After a quick overview of access network principles in section 1.1, this chapter continues with a description of optical access network topologies (section 1.2). Section 1.3 introduces the basic architecture of PON, its advantages, optical power budget and the evolution of PON standards. Section 1.4 describes the various optical technologies for power splitting and wavelength division multiplexing.

1.1 Broadband Access Networks: An Overview

Access network is the network between Central Office (CO) and end users and is traditionally called last-mile networks. They are also called first-mile networks in recent years as they are the first segment of the broader network seen by users of telecom services [4]. The "last mile" is the most expensive part of the network because there are far more end users than backbone nodes [5]. Example of access networks are i) twisted copper pairs connecting to each individual household ii) residential coaxial cable drops from community antenna TV (CATV) service providers. Wi-Max is another type of access technology which uses radio waves for last-mile connectivity. Traditionally, optical fibers have been widely used in backbone networks because of their huge available bandwidth and very low loss. However, until the beginning of this century, fiber has not been used as the technology of last-mile connection.

The most widely deployed "broadband" solutions today are Digital Subscriber Line (DSL) and Cable Modem networks. There were 367.7 million broadband subscribers globally at the end of the first quarter of 2008 and 65% of them are using the DSL technology [6]. Although broadband copper-based access networks provide much higher data rate than 56 Kbps dial-up lines, they are unable to provide enough bandwidth for the tremendous growth of Internet traffic, emerging services such as Video-On-Demand, High Definition Television and interactive gaming, or two-way video conferencing. The maximum physical reach of DSL is about 6km @ 2Mbps and

0.3km @ 53Mbps [7]. The physical reach and channel capacity of DSL almost have reached the limitations of the available copper cabling.

In the last decades, optical networks have experienced substantial growth with the deployment of optical fiber in metro and core network segments. DWDM (Dense Wavelength Division Multiplexing) based high capacity systems provide ever increasing bandwidth to meet the growing needs of both voice and data communication [8]. However, optical fiber access networks are far behind and just beginning to penetrate a market largely dominated by copper-based solutions. Local Area Networks (LANs) using emerging fiber technology can provide a high-capacity, high-speed access network system that is inexpensive, simple, scalable, and capable of delivering bundled voice, data and video services to an end-user over a single fiber plant.

1.2 Optical Fiber Access Networks

Local loops using optical fiber for access connections are called fiber-in-the loop systems [9-12]. Fiber access systems are also referred to as fiber-to-the-x (FTTx) system, where ''x'' can be ''home,'' "building", ''curb,'' ''premises,'' etc., depending on how deep in the field fiber is deployed or how close it is to the user. In a fiber-to-the-home (FTTH) system, fiber is connected all the way from the service provider to household users. In an FTTC system, fiber is connected to the curb of a community where the optical signal is converted into the electrical domain and distributed to end users through twisted pairs. Therefore, an FTTC system can also be regarded as a hybrid fiber twisted pair system.

FTTx which brings high-capacity optical fiber networks closer to the end users, appears to be the best candidate for the next-generation access network. FTTx is considered an ideal solution for access networks because of the inherent advantages of optical fiber in terms of low cost, huge capacity, small size and weight, and its immunity to electromagnetic interference and crosstalk. Today, the maximum demonstrated information capacity of an optical fiber exceeds 100 Tb/s for a typical DWDM system with coherent detection [8]. Because of the costs involved, such systems probably will be limited to core and backbone networks. Since optical fibers are widely used in backbone networks, Wide Area Networks, and Metropolitan Area Networks, the implementation of the FTTx in access networks will complete the all-optical-network revolution.

Fiber access systems can be point-to-point (P2P) or point-to-multi-point (P2MP). Moreover, they can use an active remote distribution node such as an Ethernet switch or a simple passive splitter as the remote distribution node used in power splitting PONs. Figure 1.1 depicts different architectures of fiber access networks, assuming a number of N end nodes:

a. In the first architecture, there is a direct Point-to-Point (P2P) link between the CO and each end user, so N fibers and 2xN transceivers are needed to support N customers. The speed of the terminal equipment equals to the data rate for end users.

b. In the second architecture, there is a P2P link between the CO and the curb switch while the links between the curb switch and the end users are also P2P. So the link between the CO and the curb switch is now shared between the N end users. This approach needs 2x(N+l) transceivers (1 at the CO, N+1 at the curb switch and N at the end user side). The speed requirement of the terminal equipment also is the data rate for end users;

c. In the third architecture, the CO and end users are connected by a Point-to-Multi-Point (P2MP) link. Compared with the second architecture, the curb switch is now replaced by a wavelength multiplexer/demultiplexer. As each user has its own corresponding transceiver at the CO side, this architecture needs 2xN transceivers. The required speed of the terminal equipment is the same as a and b;

d. The last architecture shares the same topology as the previous one with a passive optical splitter/coupler instead of the WDM and it reduces the cost further by sharing a single transceiver at the CO side among all the end users. Then only N+1 transceivers are needed in total. The speed of the terminal equipment equals to the sum of data rate for all end users.

The network topology of the last two architectures is normally referred as a PON, where only passive optical devices are used, namely fibers and splitters or combiners. Various solutions based on a shared PON network architecture are adopting different transfer technologies, to support integrated services and multiple protocols. The PON architecture was proposed as a way to share the large fiber bandwidth among many users through a passive splitter, and hence improve the per user cost of FTTH. In fact, NTT adopted P2P architectures in some early FTTH trials [13]. Another type of PON called WDM-PON uses a wavelength multiplexer as the remote distribution node [12]. PON architectures will be described in detail in the following sections. Although FTTH was in trial for a long time since its proposal, the high cost of fiber-optic

components and lack of killer applications for the high bandwidth offered by optical fibers have been barriers to its real applications.
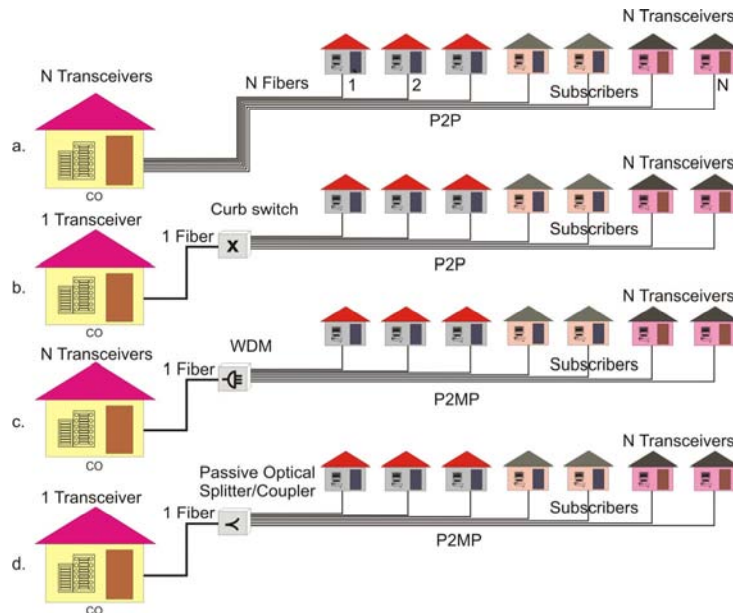
Figure 1.1: Different architectures of access network

1.3 Basic Architecture of a PON

Figure 1.2 depicts a common PON architecture supporting different FTTx scenarios. The optical elements used in such networks are only passive components, such as fibers, splitters/couplers and connectors. The optical path that consists of these components is called the Optical Distribution Network (ODN). The Optical Line Terminal (OLT) resides in the CO, connecting the optical access network to an IP, ATM, or SONET backbone. An Optical Network Unit (ONU) is located at the curb (FTTC solution), or an Optical Network Terminal (ONT) is located at the end user location (FTTH, FTTB solutions), to provide broadband voice, data, and video services with guaranteed Quality of Service. While FTTB and FTTH solutions have fiber reaching all the way to the customer premises, FTTC may be the most economical deployment today [14]**,** leaving room for alternative technologies such as DSL or even wireless to implement the last drop.
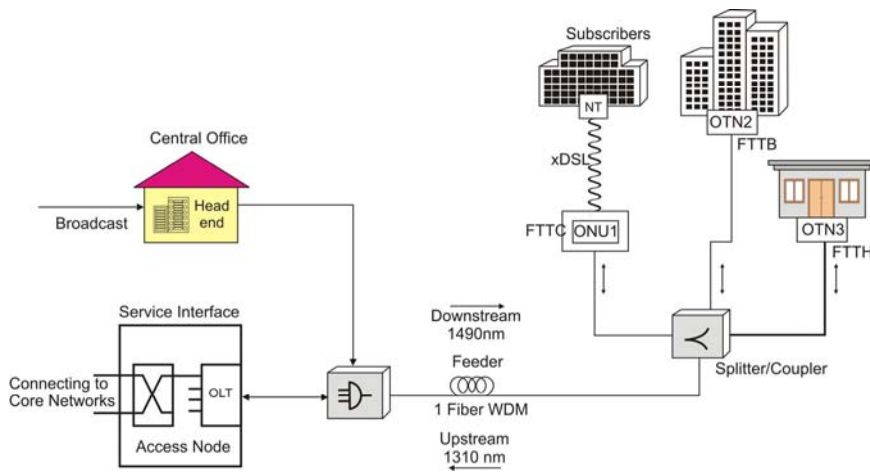
Figure 1.2: PON Architecture (FTTx Scenario)

All transmission over the ODN of the PON occurs from or towards the OLT, as ONUs or ONTs do not communicate directly with each other. The P2MP transmission from the OLT to ONUs/ONTs is called Downstream, and the P2MP transmission from ONUs/ONTs to the OLT is called Upstream. In most PON implementations, the downstream and upstream optical signals in the drop section, close to an ONT, are shared over a single fiber for cost reasons. Closer to the OLT, in the feeder section, it is more common to use separate fibers for up- and downlink. The wavelengths of uplink and downlink signals can be the same, but usually separate wavelength bands are used, as this makes the network more robust against optical reflections, and reduces the losses associated with up- and downlink combination and splitting. Upstream and downstream signals are multiplexed (combined) or demultiplexed (split) from the fiber using coarse WDM filters at the CO and the subscriber premises.

1.3.1   Advantages of PON Architecture

PON technology is getting more and more interest from the telecom industry as a future-proof "last mile" solution. The benefits of using broadband PON local access networks are numerous, and list a few:

> ➢ A PON allows for longer physical reach. While the DSL maximum physical reach is about 6 km, a PON local loop can operate at distances of over 20 km

without amplification, as today's optical fiber has much less attenuation than any copper wire.

➢ Since numerous end nodes share the feeder section fiber(s) between the CO and the passive optical splitter/combiner, a PON minimizes fiber deployment in both the local exchange and the local loop.

➢ In a PON, E/O components and electrical devices at the CO are shared amongst a large number of subscribers, saving expensive high-speed electrical and optical equipment.

➢ Due to the high data capacity of fiber, a PON can provide much higher line rates than alternative access technologies. The standardized maximum downstream and upstream line rate of an FSAN PON today is standardized at 2488 Mbps

➢ Since the bandwidth of a PON is shared by all subscribers, it provides the possibility to use the bandwidth more efficiently by Dynamic Bandwidth Allocation [15, 16]. Hence, the line rate exceeds the available average bandwidth of each PON subscriber by nearly the PON splitting factor. This is especially valuable for accommodating burst traffic, as a single subscriber can communicate at the full line rate during limited time intervals. In contrast, DSL assigns *a* complete P2P link to a single subscriber, so a subscriber cannot exceed the peak subscriber rate and free CO transmission capacity, due to inactive subscribers, cannot be reused.

➢ As a P2MP network, a PON allows for downstream video broadcasting.

➢ A PON can reduce the cost of maintenance dramatically, because it eliminates the necessity of installing multiplexers and demultiplexers in the splitting locations, thus relieving network operators from the gruesome task of maintaining and providing power to electrical devices in the field. Instead of active devices in these locations, a PON has optical passive components that can even be buried into the ground at the time of deployment:

➢ A PON easily upgrades to higher bit rates or additional wavelengths. If a new subscriber wants to join the PON, there is no need to add extra hardware at the CO side, while DSL requires the installation of a new transceiver in the local exchange. When new technologies that support higher bit rates become available, only the end equipment like OLTs and ONTs needs to be extended or replaced.

1.3.2   PON Multiple Access Technology

In the downstream direction, the OLT laser is modulated with a mix of broadcast (all ONTs), narrowcast (some ONTs) and P2P information using a suitable multiplexing mechanism. In fact, PON downstream technology borrows a lot from other continuous, single talker fiber networks. Sharing the feeder section of a PON for upstream communication however is a much more uncommon and difficult task, as a multiple access technology is required that avoids collision between signals transmitted by the different ONTs. Collisions cannot be permitted as the high network delay and data rates would cause excessive network time-outs. The available solutions for multiple access are Wavelength Division Multiple Access, Time Division Multiple Access (TDMA), Sub Carrier Multiple Access and Code Division Multiple Access [17-20].
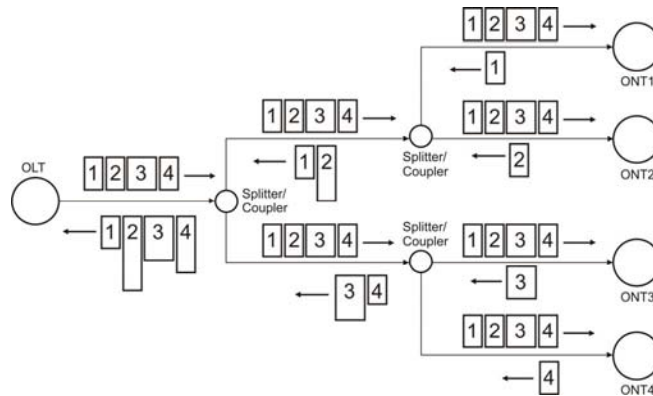
Figure 1.3: Signal transmission in a TDM/TDMA PON

TDMA is the most efficient and most adopted PON multiple access technology today, and allocates the upstream communication of each ONT into time slots that are separated in time upon arrival at the OLT. An ONT can only transmit data within the time slots allocated to it. TDMA gives each ONT a pre-allocated but variable fraction of the single wavelength upstream capacity. Only one transceiver is needed in the OLT (Figure 1.1 d), no matter how many ONTs are connected to it, as long as the downstream optical power budget is not exhausted. Hence TDMA PONs provide an economical solution for the "last mile problem". The signal transmission over a TDM/TDMA PON is illustrated in Figure 1.3. In downstream the data is broadcast across the P2MP ODN from the OLT at the CO side to the ONTs receiving a single wavelength. As each ONT receives all the data, the OLT must label each packet with the ID of the intended recipient. The signal received by each ONT is in

Continuous-Wave mode as in a P2P link, since the OLT is always the only talker. There is no rapid change of the signal amplitude and phase. From this CW downstream, a system clock is extracted from the downstream receiver that is used to synchronize the ONT upstream transmission. During normal operation of a TDMA-PON, each ONT only turns on its laser and transmits a burst of data in its granted time slot, and then quickly shuts its laser off to avoid interfering with other ONTs. This is referred to as burst mode operation. Because the ONTs are at different locations, the drop sections show different fiber lengths with different optical loss, and the amplitude and phase of the upstream signals vary rapidly, from burst to burst, upon arrival at the OLT. In a TDMA-PON each upstream burst is preceded by a burst preamble, allowing the OLT receiver circuits to perform on-the-fly amplitude, clock phase and data recovery. The intervals between bursts also contain guard times to account for the finite switch on/off times of the ONT laser sources.

1.3.3 Optical Power Budget of a PON

The upstream optical power budget of a PON is the difference in dB between the (worst case) upstream optical power launched into the fiber by an ONT and the receiver sensitivity of the OLT. In practice, the minimum and maximum loss an optical signal may experience on its way from OLT to ONT, or when traveling in the opposite direction, is clearly specified. For class A, B and C optical distribution network, the minimum/maximum path loss are 5~20, 10~25 and 15~30 respectively. These losses are mainly due to fiber attenuation, which increases with fiber length, and the 1xN power reduction in each broadband 1xN splitter or combiner. When the PON splitting factor is made high, to support a large number of ONTs from a single OLT the optical losses due to the power splitting and combining will consume most of the optical power budget. So typically a PON may have a high split, but then the maximum range is limited or vice versa. In Equation 1.1, α is the fiber attenuation factor and L is the length of fiber.

$$P_{transmitted} - P_{sensitivity} \geq P_{penalty} + \alpha L + P_{splitter} \qquad (1.1)$$

1.3.4 Wavelength Plan in PON

FSAN (Full Service Access Network) study group standardized PONs specifying the 1490 nm wavelength band for downstream signal transmission, the 1310 nm wavelength band for upstream transmission, and 1550 nm as an enhancement band for broadcast services such as CATV (Community Antenna Television) via this

broadband overlay. The schematic of the wavelength allocation plan is shown in Figure 1.4. The network installers normally use an out of band test wavelength at 1625nm, for trouble shooting the network.
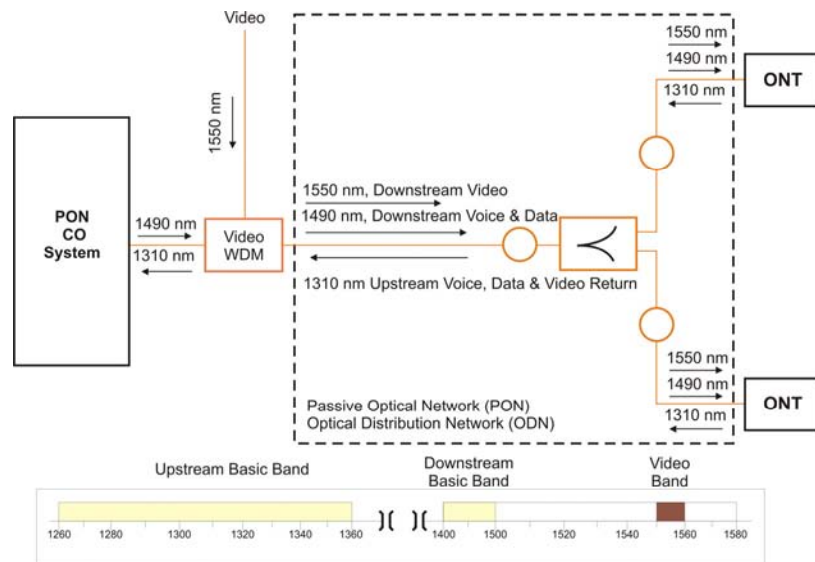
Figure 1.4: ITU-T G.983.3 PON Wavelength Allocation Scheme

1.3.5 Signal Splitting in TDM-PON

The purpose of power splitting include: (1) sharing the cost and bandwidth of OLT among ONUs and (2) reducing the fiber mileage in the field. Apart from the simple one-stage splitting strategy (Figure 1.5 (a)), splitters may also be cascaded in the field as shown in Figure 1.5 (b). In the most extreme case, the feeder fiber forms an optical bus and ONUs are connected to it at various locations along its path through 1:2 optical tap splitters as shown in Figure 1.5 (c). The actual splitting architecture depends on the demography of users and the cost to manage multiple splitters. In a bus or tree architecture like Figure 1.5 (c), if all the splitters have the same power splitting ratio, the furthest ONU will suffer the most transmission and splitting loss and become the system bottleneck. Splitters with uneven splitting ratios may be used to improve the overall power margin. However, such optimization requires stocking non-uniform splitters and is hence difficult to manage. From a management point of view, it is usually simpler to have a single splitter for distribution in the field, which makes splicing easier and minimizes connector and splicing losses. However, distributed splitting architecture is more advantageous when serving clusters of customers, randomly distributed. An example of a distributed splitter solution would

be the 1x8 split at the local convergence points with a 1x4 split at each of the network access points.
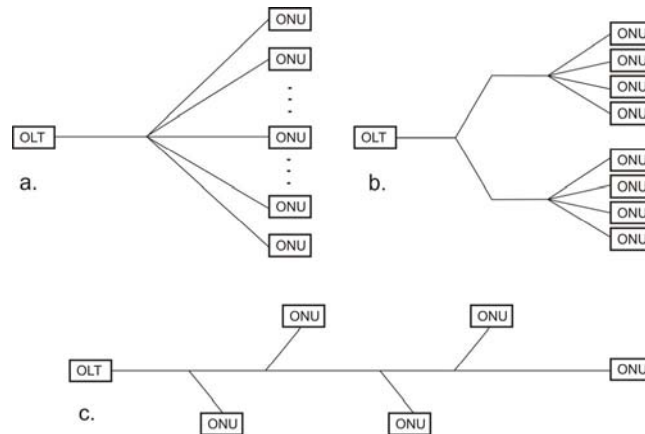
Figure 1.5: Splitting strategies in a TDM-PON: (a) one-stage splitting
b) multi-stage splitting and (c) optical bus

Most of the commercial PON systems have a splitting ratio of 1:16 or 1:32. A higher splitting ratio means that the cost of the PON OLT is better shared among ONUs. However, the splitting ratio directly affects the system power budget and transmission loss. The ideal splitting loss for a 1:N splitter is 10*log(N) dB. To support large splitting ratio, high power transmitters, high sensitivity receivers, and low-loss optical components are required. Higher splitting ratio also means less power left for transmission fiber loss and smaller margin reserved for other system degradations and variations. Therefore, up to a certain point, higher splitting ratio will create diminishing returns. Studies showed that economically the most optimal splitting ratio is somewhere around 1:40 [12].

A high splitting ratio also means the OLT bandwidth is shared among more ONUs and will lead to less bandwidth per user. To achieve a certain bit error rate (BER) performance, a minimum energy per bit is required to overcome the system noise. Therefore, increasing the bit rate at the OLT will also increase the power (which is the product of bit rate and bit energy) required for transmission. The transmission power is constrained by available laser technology (communication lasers normally have about 0–10 dBm output power) and safety requirements issued by regulatory authorities [13].

1.3.6 Evolution of PON Standards

Today's PON standards represent the different views and attitudes of two distinct standardization groups looking at problems and finding solutions towards the future of the telecommunication market. Broadband PON (BPON) and Gigabit PON (GPON) are mainly motivated by groups of network providers, who want a high performance platform that can provide full services to end users. Ethernet PON (EPON), which optimizes simplicity rather than performance, presents the consideration of some equipment vendors. The strengths and weakness of the respective standards result from the different considerations.

In 1998 ITU-T released G.983.1, the first in a series of G.983.x recommendations commonly referred to as ATM-PON or Broadband PON (BPON), and drafted by the FSAN study group [21]. It was a first attempt at a PON standard. Various physical layer parameters have been specified in G.983.1 [21], such as the line coding (NRZ with scrambling), minimum receiver sensitivity, minimum and maximum transmit power values both in upstream and downstream. The next-generation ITU-T PON standard is GPON and was designated ITU-T G.984.x. GPON retains the strengths of BPON, corrects its weaknesses, and increases the bit rate to the gigabit range. Concurrent in time, the IEEE has developed an Ethernet-based protocol referred to as EPON [22]. EPON is part of the IEEE Ethernet in the Last Mile initiative and was designated 802.3ah. Although the transport mechanism for EPON is based on Ethernet, there are substantial differences imposed by the very nature of an access network.

1.4 Optical Technologies and Components of PON

The optical technologies for access network have been advancing at a rapid rate, with goals of achieving performance and high reliability in addition to manageability, ease of installation, and upgradeability. Each of these goals bears a direct contribution to the overall capital and operational expenditures of the network. For widespread uptake and deployment, it is imperative that the network be cost competitive to current access technologies. In this section, optical technologies that have been developed to achieve these goals are compared.

Optical power splitter is the central component in a power-splitting passive optical network where its primary function is to split the optical power at the common port equally among all its output ports. The major technologies used to make power splitters include fused fiber technology and planar lightwave circuit (PLC)

12

technology. High reliability, low cost per port, low insertion loss, and high splitting ratio uniformity are essential for splitters for use in passive optical networks. Many leading service providers and component manufacturers consider wavelength division multiplexing (WDM) network as the preferred upgrade solution in order to satisfy high and increasing bandwidth demands. In a WDM-PON, each user is assigned with their own downstream/upstream wavelength channels, enabling dedicated and potentially symmetric downstream/ upstream bandwidths. An arrayed waveguide grating (AWG) serves as the passive WDM mux/demux or a passive WDM routing component at the remote node, replacing the optical power splitter in a power-splitting PON.

1.4.1 Power Splitting Technologies

In a power-splitting PON, an optical power splitter in the outside plant is physically connected to the CO, with a feeder fiber. It also connects to a number of ONUs via a series of distribution fibers. There are different technical technologies used for signal splitting in FTTH system [23]:

> - Fused or fused biconical taper (FBT) couplers
> - Planar splitter or planar lightwave circuits (PLCs)
> - Fused coupler arrays
> - Monolithic fused couplers

In a PON-FTTH network, in order to split the incoming signal from the central office to subscribers, regardless of the fabrication technology used and/or the protocol adopted (B-PON, E-PON or G-PON), the passive optical splitter has to guarantee at least four key parameters: broad operating wavelength range, low insertion loss and uniformity in any operating conditions, small footprint and long-term reliability. Aside from uniform loss, the insertion loss of splitters is an important parameter in network implementation that influence system performance and the overall cost per drop. Lower insertion loss splitters will extend the reach and number of customers that can be accommodated within the same PON, yielding higher revenue per PON for service providers.

1.4.1.1 Fused Fiber Technology

A fused coupler is a structure formed by joining two independent optical fibers [24], as shown schematically in Figure 1.6. The claddings of the fibers are fused in a small

region. FBT devices work as a result of an energy transfer by coupling between optical fiber cores [25]. Consider two parallel single-mode optical fibers in close proximity. If the evanescent tails of each waveguide have considerable overlap, it can be shown that there are two possible solutions for mode propagation in the two waveguide structure. These are the so-called supermodes or Eigenmodes. The two solutions have symmetric and non-symmetric energy distributions and differing propagation constant values. As the relative phases of the modes change, the energy is shared between the two fibers. At matching and mismatched phases, the energy is alternately maximized in each fiber core, i.e. the energy pulses back and forth between the waveguides. In other words, the energy can be split evenly or unevenly down the fibers. The energy transfer is dependent on the core separation (2r) and the interaction length (z).
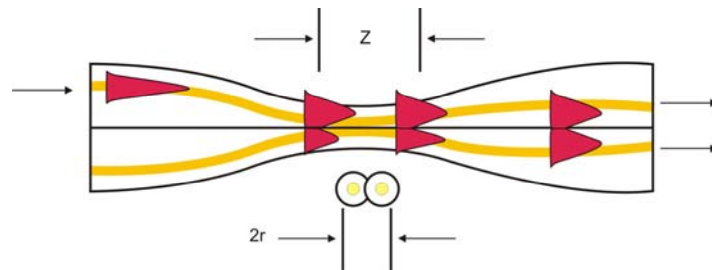
Figure 1.6: Fused coupler technology

A 2x2 coupler is formed, since two separate fibers are fused. To obtain a 1x2 coupler (or splitter) one of the input fibers is cut and terminated suitably to avoid back-reflections from that end. The 1x2 coupler is then mounted on a glass or quartz plate (see Figure 1.7) and put into a metal tube [24], typically of 3 mm diameter. The advantage of this optical coupler type is that the optical signal is always traveling through the same material and therefore offers a reduced loss.

Figure 1.7: Photograph of a 1x2 Fused Coupler

1.4.1.2 Planar Lightwave Circuit Technology

The second type of splitter is made up of integrated optical circuit assembled with an input and an output fiber array as shown in Figure 1.8 [26]. Central to the splitter is a

PLC chip comprising of optical waveguides fabricated on a planar substrate, typically made of silicon or quartz, to form a cascade of Y-branches. For a 1xN splitter, one side of the PLC chip is aligned to a fiber whereas the opposite side is aligned to an array of N fibers, as shown in Figure 1.8. The number of power-splitting fan outs in a PON is typically 16 and 32, but with an increasing demand of up to 64, makes the alignment of the fiber array to the PLC chip more challenging [27].
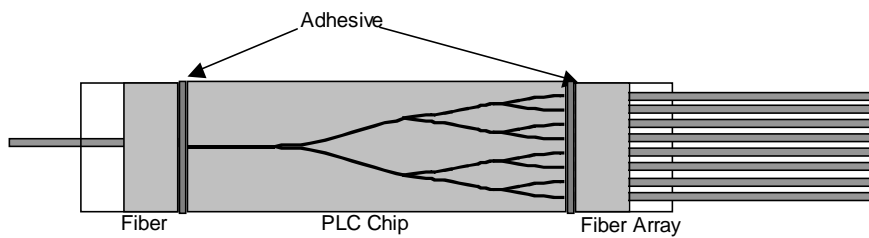
Figure 1.8: Internal structure of a 1x8 PLC splitter

There are three principal fabrication processes for Planar Lightwave Circuits (PLC) [28-33], Ion exchange with glass substrate, Plasma-enhanced chemical vapor deposition and Flame hydrolysis deposition. The differences between the three processes lie in the "generation" or building-up of the waveguide in which the light will propagate. The principle outcome of all these technologies is ultimately the same: to generate a structure in which light can propagate without loss and still behave like an optical fiber. All processes mentioned have a structure at the end (doped glass), which has a different refractive index than the surrounding material (also Glass). The difference in the refractive index allows the waveguide to mimic the performance of an optical pure fiber which is also constructed with glass having a different refractive index.

Compared to fused biconical-taper-based splitters, PLC technology allows for chip-size devices with the potential of integrating multiple functions, e.g. WDM coupler, onto a single chip. It also enables a uniform loss over a wide operating range of wavelengths from 1250 nm to 1625 nm [27, 34-37]. A PLC-based splitter suffers excess insertion loss from fiber array alignment to the PLC chip, fiber array uniformity caused by pitch and depth inaccuracies in the v-grooves of fiber array block that holds the fiber array, splitting ratio uniformity caused by imperfections in the PLC chip due to manufacturing, inherent chip material loss, and connector loss.

1.4.1.3 Fused Fiber Arrays

To create a more complex structure than 1x2 or 2x2 configurations, 1x2 fused coupler components are concatenated by splicing the output arms of the first coupler to the input arm of the second one and so forth [38]. This is done repeatedly to achieve the desired output power ratio and number of ports required. The series of cascaded fused couplers and the respective splices are usually housed and protected in robust plastic packaging.

1.4.1.4 Monolithic Fused Couplers

Another configuration to achieve multiple output ports is accomplished by fusing more than two fibers together [39]. This method helps to minimize the number of components. In practice, only 1x3 and 1x4 fused components have found extensive use.

1.4.2 WDM Technologies

Wavelength division multiplexer (WDM) is a passive component which is designed to split/combine signals, at two different wavelengths [40, 41]. A very common wide channel spacing WDM is 980/1550nm WDM, used extensively in Erbium Doped Fiber Amplifier (EDFA), where the pump and signal at these two wavelengths are multiplexed in the amplifying (Erbium-doped) fiber [42]. An alternative pump or signal combining WDM for EDFAs is 1480/1550 nm WDM, which is a narrow channel WDM [43]. Another variety of WDM, which is extensively used for telecommunication applications is a 1310/1550 nm WDM, which is also referred to as "Classical WDM" in order to distinguish it from dense WDMs (DWDMs) [44].

In FTTH, typically, voice and data operate at 1490 nm and 1310 nm, in downstream and upstream directions. Video usually operates at 1550 nm wavelength band. The signals are then combined onto a single fiber using wavelength division multiplexing (WDM) techniques and distributed to end users via passive optical splitters. Also, the WDM technology has been considered as one of the most graceful upgrade paths beyond power-splitting PONs to support more users at higher bandwidths. For an upgrade in the outside plant, the power splitter in the remote node of a power-splitting PON is replaced with an arrayed waveguide grating (AWG). In a 1xN configuration, an AWG serves as a wavelength router or a demultiplexer because a composite WDM signal launched into the input port is separated into individual channels by the device [45–47].

16

1.4.2.1 Fused Fiber WDM

A fused WDM is a symmetric 2x2 FBT coupler which can take two inputs at two different wavelengths, from the two input ports, and combines them at one output port. On the other hand, if these two signals are injected into the same input port, they will separate out at the two output ports. Such a design owes its origin to the fact that for a given coupler, the coupling coefficients and the effective lengths of interaction at two different wavelengths say 1310 and 1550nm are different. Therefore the splitting ratios at these wavelengths are usually different. For a coupler to function as a WDM at these two operating wavelengths, the fabrication process has to be tailored such that the splitting ratio of the device is maximum at one wavelength and minimum at the other wavelength [48, 49]. This implies that all of the input power at one wavelength will emerge at one output port, all input power at the second wavelength will emerge at the second output port.

1.4.2.2 Filter WDM

Filter based WDMs are assembled as shown schematically in Figure 1.9. Light from fiber is collimated using a suitable collimator and is allowed to fall on a suitable filter. The filter selectively reflects a wavelength and is focused back to the fiber on the same side by the collimator. The transmitted light is focused to another fiber by a collimator. WDMs can also be realized by reflective optics as shown in Figure 1.10, as suggested by Kapany et al [50]. This configuration comprises a transparent imaging element having a curved reflective surface at one end and pre-aligned fiber insertion holes at the other end. The transparent element is characterized by an index of refraction equal to that of the fiber core, and the fibers are glued in their respective holes with index matching cement.
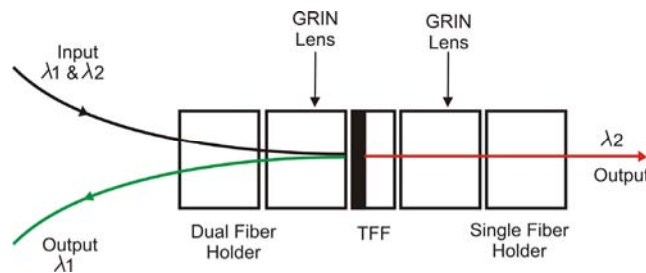

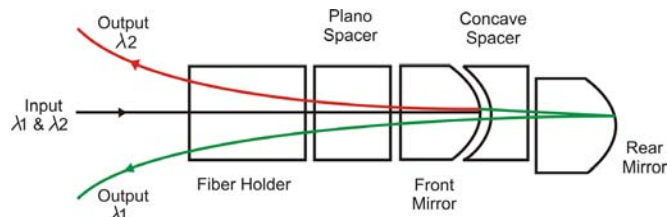Figure 1.9: Thin Film Filter based WDM

Figure 1.10: Reflective Optics based WDM

1.4.3 Mode Conditioning in Multimode Networks

Local Area Networks (LANs) often employ multimode fibers tuned for use with Light Emitting Diodes (LEDs) that is having limited modulation capability. In order to support high speeds as per Gigabit Ethernet requirements, the systems need laser sources such as Fabry-Perot (FP) lasers or Vertical Cavity Surface Emitting Lasers (VCSEL). The larger core diameter of the multimode fiber results in the laser signal disintegrating into an uneven distribution among all the modes and this degraded optical power profile, often translates into bit errors. The smaller spot sizes concentrate energy near the centers of the multimode fibers and hence are particularly sensitive to any central irregularity in the refractive index profile. Thus the launch dependent modal power distribution of multimode fiber combined with Differential Mode Delay (DMD) can cause serious problems in Gigabit Ethernet LANs. To address these needs, and hence to achieve useful link distances at Gigabit speeds, the signal from the single mode must be adapted to the multimode fiber. This adaption is conventionally done using an optical mode conditioning patch cable (MCP), which is an optical mode conditioner for efficiently conditioning a single mode optical signal propagating in a single mode optical fiber for propagation within a multimode optical fiber [51]. A lateral launching technique is well known for obtaining a better bandwidth– distance product by launching a small light spot with a radial offset from the multimode fiber core center [52]. Long period gratings, which acts as a spectrally sensitive loss element, by coupling light from lower order modes to higher order modes [53] can be effectively used to achieve modal power distribution in multimode Gigabit Ethernet networks.

1.4.4   Possible Evolution Scenarios of PON System

Besides the high capacity, a cost effective PON system requires a high split factor (large number of subscribers) and *a* long reach, to achieve an increased sharing of the fiber plant and the centralized equipment, a flexible and cost-effective deployment,

18

and a high bandwidth usage. High split factor and long physical reach are two conflicting requirements when the optical power budget is limited. Eventually, higher line rates normally result in lower receiver sensitivity, which will decrease the optical power budget. A possible evolution scenario for the PON system to increase the physical reach and the split factor is to deploy optical amplification in the PON system. Experimental systems, such as Super PON have shown that it is possible to increase the split factor to 1:2048 or extend the physical reach to 135 km by the use of optical amplifiers [54]. This kind of system however requires a new standard and may only be economical on a longer term. Although a pure WDM-PON is not a cost-effective option, the combination of WDM and TDM-PON can be very attractive to increase the data capacity over a shared PON fiber plant.

1.4.5 All-Fiber Technology

All-fiber components are formed by transforming the properties of optical fiber itself, either by heating, tapering or by changing the refractive index. All-fiber approach is preferred for realizing a variety of components for passive optical networks, owing to its capability of keeping the integrity of signal transmission with low forward and return losses and high power handling [24]. Fused fiber technology and Long Period Gratings are two prominent technologies that contribute to all-fiber platform. In these methods, the signal never leaves the fiber and hence the integrity of the signal is preserved. In fused fiber method, the basic fabrication process involves stretching a pair of single mode fibers together, which are held in intimate contact across a short unjacketed length, in a high temperature flame. This process of heating and stretching results in narrowing of the two fibers into a single biconical tapered junction. Such components are also some times called fused biconical tapered (FBT) couplers.

In planar lightwave circuit splitters, epoxy comes in the optical path and hence may not be ideal for power splitting applications such as high power analog video transmission. Also, planar lightwave circuit splitters are not cost competitive for low port counts, less than eight. On the other hand wideband fused couplers are limited in port count by two. Cascading of 1x2 couplers affects the uniformity of the 1xN splitters as well as its reliability. 1x4 splitters are vital components in passive optical networks, where distributed splitting is preferred [55]. Monolithic 1x4 couplers are attractive solution that can offer the advantages of PLC splitter (high port count) and fused couplers (epoxy free optical path). However, methods to achieve wideband

performance of monolithic couplers are not established well, which is one of the main focuses of this research.

Long period gratings (LPG) are formed by making periodic index perturbations along the length of the fiber. LPGs help to couple power from core modes to the cladding modes of the fiber. The most prominent reason for the successful incorporation of LPGs in communication systems is the fact that they provide a mechanism for producing wavelength dependent attenuation in the transmission. Fused coupler technology can also be used to realize wavelength division multiplexers, but the isolation is limited. Combining the LPG with fused WDMs can offer all-fiber WDMs with isolation greater than 30 dB.

1.5 Conclusions

Among the different optical access architectures, Passive Optical Network provides unique advantages because of its passive nature and reduced operational costs. The advantages of PON architecture as well as main optical technologies and components for passive optical networks are discussed in detail. All-fiber technology based on fused coupler and long period grating offers a versatile platform for realizing a variety of components for passive optical network applications. The present work focuses on developing fused monolithic 1x4 coupler and high isolation fused WDMs. Details of the work are given in subsequent chapters of the thesis.

References

1. J. R. Stern, J. W. Ballance, D. W. Faulkner, S. Hornung and D. B. Payne, "Passive Optical Local Networks for Telephony Applications and Beyond", Electronics Letters, Vol. 23, pp. 1255-1257, 1987.
2. Donald. E.A. Clarke and Tetsuya Kanada, "Broadband: The Last Mile", IEEE Communications Magazine, Vol.31, pp. 94-100, 1993.
3. Yih-Kang Maurice Lin, Dan R. Spears, and Mih Yin, 'Fiber-Based Local Access Network Architectures", IEEE Communications Magazine, Vol. 27, pp. 64-73, 1989.
4. Cedric F. Lam, Passive Optical Networks Principles and Practice, Ch. 1, pp. 1-17, 2007

5.   James F. Mollenauer, "Functional Requirements for Broadband Wireless Access Network"', IEEE 802 Broadband Wireless, Access Study Group, March 5, 1999.

6.   Fiona Vanier, World Broadband Statistics Report – Q1 2008, www.point-topic.com, 2008

7.   Timo Smura, "Techno-economical analysis of IEEE 802.16a-based fixed wireless access networks", PhD thesis, Helsinki University of Technology, 2004.

8.   G. P. Agrawal, "Fiber-Optic Communications Systems", 3rd edition, Wiley 2002.

9.   N. J. Frigo, ''A survey of fiber optics in local access architectures,'' in Optical Fiber Telecommunications, III A, edited by I. Kaminow and T.L. Koch, pp. 461–522, Academic Press, 1997.

10. E. Harstead and P. H. van Heyningen, ''Optical Access Networks,'' in Optical Fiber Teclecommunications, IV B, edited by I. Kaminow and T. Li, pp. 438–513, Academic Press, 2002.

11. S. S. Wagner, H. Kobrinski, T.J. Robe, H.L. Lemberg, and L.S. Smmot, ''Experimental demonstration of a passive optical subscriber loop architecture,'' Elect. Lett., Vol.24, pp. 344–346, 1988.

12. S. S. Wagner and H. L. Lemberg, ''Technology and system issues for a WDM-based fiber loop architecture,'' IEEE J. Lightwave Tech., Vol.7, pp.1759–1768, 1989.

13. H. Shinohara, ''Broadband access in Japan: rapidly growing FTTH market,'' IEEE Commun. Mag., pp.72–78, Sept. 2005.

14. X. Z. Qiu. J. Vandewege. F. Fredricx, P. Vetter, "Burst mode transmission in PON access systems", The 7th European Conference on Networks and Optical Communications, NOC'2002, Darmstadt, Germany, pp. 127-132, 2002.

15. ITU-T Recommendation G983.4, "A broadband optical access system with increased service capability using dynamic bandwidth assignment", Nov. 2001.

16. Ryosuke Nishino, Yoshihiro Ashi, "Development of Dynamic Bandwidth Assignment Technique for Broadband Passive Optical Networks", FTTH Conference 2004.

17. Ton Koonen, "Fiber-optic techniques for broadband access networks", Telektronikk, Vol. 101, pp. 49-65, 2005.

18. John E. George, "Optical System Design Considerations for FTTP Networks". FTTH Conference 2004.

19. Eyal Shraga. "GPON and EPON (GE-PON) Economical Comparison", FlexLight, White Papers, 2005.

20. ITU-T Recommendation G983.1, "Broadband Optical Access System Based on Passive Optical Networks", Nov. 2001.

21. ITU-T Recommendation G983.3, "A broadband optical access system with increased service capability by wavelength allocation", 2001

22. FlexLight Networks and BroadLight, "Comparing Gigabit PON Technologies: ITU-T G.984 GPON vs. IEEE 802.3ah EPON". White Paper, May 2004.

23. "Passive Splitters for FTTH-PON Applications", White paper available at www.ftthcouncil.org, June 2004.

24. F. Gonthier, "Fused couplers increase system design options", Laser Focus World Magazine, pp. 83-88, June, 1998

25. D. Salazar, M. A. Felix, J. A. Valenzuela, H. Marquez, "A simple technique to obtain fused fiber optic couplers", Instrumentation and Development, Vol.5, pp. 170-174, 2001

26. S. Varghese, Biji Thomas, M. Iqbal, Abraham Thomas, Suresh Nair, "Highly reliable planar splitters designed for FTTH application" Proceedings of Eighth International Conference on Optoelectronics, Fiber Optics and Photonics (Photonics-2006), Hyderabad, pp.32, 2006

27. I. B. Sohn, M. S. Lee, J. Y. Chung, ''Fabrication of optical splitter and passive alignment technique with a femtosecond laser,'' IEEE Photonics Technology Letters, Vol.17, pp. 2349–2351, 2005.

28. R.A. Betts, "Fabrication techniques for integrated optics devices", Physics in Technology, Vol. 14, pp. 194-198, 1983

29. Katsunari Okamoto, "Recent progress of integrated optics planar lightwave circuits", Optical and Quantum Electronics, Vol. 31, pp.107-129,1999

30. M. Kawachi, "Silica waveguides on silicon and their application to integrated components," Opt. Quantum Electron., Vol. 22, pp. 391- 416, 1990.

31. S. Suzuki, M. Yanagisawa, Y. Hibino, and K. Oda, "High-density integrated planar lightwave circuits using SiO_2–GeO_2 waveguides with a high refractive index difference," J. Lightwave Technol., Vol. 12, pp. 790–796, 1994.

32. Navarro, Anthony G., "Silica Waveguide Design and Fabrication using Integrated Optics: A Link to Optical VLSI Photonics Integration for Semiconductor Technology", 22nd Annual Microelectronic Engineering Conference, pp.68, May 2004

33. A. Himeno, K. Kato, and T. Miya, "Silica-based planar lightwave circuits," J. Select. Top. Quantum Electron., Vol. 4, pp. 913–924, 1998.

34. K. Okamoto, ''Planar Lightwave Circuits for FTTH and GMPLS,'' in Proc. of APOC 2006, paper 6351–28, Kwangju, Korea. Sept. 3–7, 2006.

35. E. Edmon, K.G. McCammon, R. Estes, J. Lorentzen, ''Chapter 2: Today's broadband fiber access technologies and deployment considerations at SBC,''

Broadband optical access and FTTH, ed. Chin-Lon Lin, Chap. 3, p17, John Wiley & Sons, 2006.

36. R. Gritters, H. Taguchi, and A. Geraci, ''Low Insertion Loss PLC Splitters for Improved PON Performance,'' White paper from Seikoh Gaiken USA, Fiber optic product news http://www.fpnmag.com

37. K.A. McGreer, H. Zu, C. Ho, N. Kheraj, Q. Zhu, M. Stiller, and J. Lam, ''Planar lightwave circuits for PON applications'' Proc. of OFC, paper NWD4, Mar., 2006.

38. Shigehito Yodo, Akio Hasemi and Masanobu Shimizu, "Single mode 1x8 Fused Couplers", Proceedings of 5th Conference on Optical/Hybrid Access Networks, Canada, pp. 4.05/01 - 4.05/06, September, 1993

39. J. W. Akrwright and D. B. Mortimore, "Monolithic MxN single-mode fused fiber couplers using capillary tube technology", E-FOC 91 Proceedings, pp. 246-251, June 1991

40. H. A. Roberts, "Single-mode fused wavelength division multiplexer", SPIE Proceedings – fiber optic couplers, connectors and splice technology II, 574, pp. 100-104, 1985.

41. J. M. Senior and S. D. Cusworth, "Devices for wavelength Multiplexing and Demulitiplexing ", IEE Proceedings, Pt.J, 136, pp. 183-185, 1989.

42. F. Gonthier, D. Ricard, S. Lacroix, and J. Bures, "2x2 multiplexing couplers for all-fiber 1.55μm amplifiers and lasers", Electronic Letters, Vol.27, pp.42-44, 1991.

43. J. D. Minelly and M. Suyama, "Wavelength combining fused-taper couplers with low sensitivity to polarisation for use with 1480 nm-pumped erbium doped fiber amplifiers", Electronic Letters, Vol. 26, pp. 523-524, 1990.

44. S. S. Orlov, A. Yariv and S. V. Essen, "Coupled mode analysis of fiber optic add-drop filters for dense wavelength-division multiplexing", Optics Letters, Vol. 22, pp. 688-690, 1997.

45. M.K. Smit, ''Progress in AWG design and technology'' Proc. of 2005 IEEE IEEE/LEOS Workshop on Fibers and Optical Passive Components, pp.26–31, 2005.

46. M.K. Smit, ''New focusing and dispersive planr component based on an optical phased array,'' Elect. Letters, Vol.24, pp385–386, 1988.

47. H. Takahashi, S. Suzuki, K. Kato, and I. Nishi,''Arrayed-waveguide grating for wavelength division multi/demultiplexer with nanometer resolution,'' Elect. Letters, Vol.26, pp87–88, 1990.

48. C. M. Lawson, P. M. Kopera, T. Y. Hsu, and V. J. Tekippe, "In-line single-mode wavelength division multiplexer/demultiplexer", Electronic Letters, Vol. 20, pp. 963 -966, 1984.

49. P. Roy Chaudhuri, B. P. Pal, and M. R. Shenoy, "Modeling fused 2x2 all-fiber coupler components", Proceedings of National Symposium on Advances in Microwaves and Lightwave, New Delhi, pp. 57-62, 2000.

50. Narinder S. Kapany, Fred C. Unterleitner, "Fiber Optics Communications Module", US Patent 4329017, 1982

51. IEEE 802.3z, "Information Technology - Telecommunication & Information Exchange Between Systems - LAN/MAN - Specific Requirements - Part 3: Carrier Sense Multiple Access with Collision Detection (CSMA/CD) Access Method and Physical Layer Specifications", 2002.

52. L. Raddatz, I.H. White, D.G. Cunningham, and M.C. Nowell, "An experimental and theoretical study of the offset launch technique for the enhancement of the bandwidth of multimode fiber links", J Lightwave Technology, Vol. 16, pp. 324–331, 1998

53. W. T. Chen and L. A. Wang, "Optical coupling between singlemode fibers by utilizing long period fiber gratings", Electronics Letters, Vol.35, pp. 421 – 423, 1999

54. R. P. Davey, P. Healey, I. Hope, P. Watkinson, D. B. Payne, Oren Marmur, Jorg Ruhmann, Yvonne Zuiderveld, "DWDM reach extension of a GPON to 135km", Journal of Lightwave Technology, Vol. 24, pp. 29-31, 2006.

55. Samuel Varghese, Suresh Nair, "FTTH compliant truly fused 1x4 couplers for passive optical network applications", White paper available from SFO Technologies, www.nestgroup.net , 2008

Chapter 2
Fused Fiber Couplers:
Basic Theory and Automated Fabrication

Fused couplers are made by joining two independent optical fibers, which work on the basic principle of coupling between parallel optical waveguides. The fabrication process and the performance parameters of these devices are reviewed. The different process parameters that control the performance as well as the recipe for realizing wavelength insensitive coupler are discussed in this chapter.

Fused couplers, are important passive components in fiber optic communication systems, that perform functions such as light branching and splitting in passive networks [1], wavelength multiplexing / de-multiplexing [2], filtering [3], polarization selective splitting [4] and wavelength independent splitting [5]. Fused couplers are formed by joining two independent optical fibers; where the claddings of the fibers are fused over a small region. The devices work as a result of energy transfer between the optical fiber cores.

This chapter describes the theoretical background of coupling mechanism in optical directional couplers. The light propagation in tapered fiber and fused couplers are also reviewed. Section 2.5 describes salient features of the automated fabrication setup designed in-house for fused couplers. The fabrication system involves multiple motorized movements of mechanical stages and electronic control hardware interfaced with a computer for real time monitoring during the fabrication. The fabrication of these devices requires an in-depth knowledge of the optical characteristics of the coupler and adequate control of the fabrication process to achieve target specifications. This chapter discusses the key control parameters for automated fabrication of fused couplers and the characteristic measurement parameters of couplers which include excess loss, insertion loss, directivity and spectral response. Finally the method to realize wavelength independent splitter is described.

2.1 Theory: 2x2 Waveguide Directional Coupler

A 2x2 waveguide directional coupler in its simplest form consists of two closely placed parallel single-mode optical waveguides. The basic operation of such a device involves a partial or complete transfer of power between the two waveguides. The exchange of power occurs due to optical coupling between the evanescent tail of the guided mode of one waveguide, in which light is launched and that of the natural mode of the second waveguide. This optical interaction can also be viewed as the beating between the symmetric and the anti-symmetric super modes of the composite structure. The uniformly spaced parallel interaction region plays the key role in the coupling process. The interaction region has a longitudinally invariant structure and the optical coupling that takes place in this region can be understood through the coupled mode analysis [6].
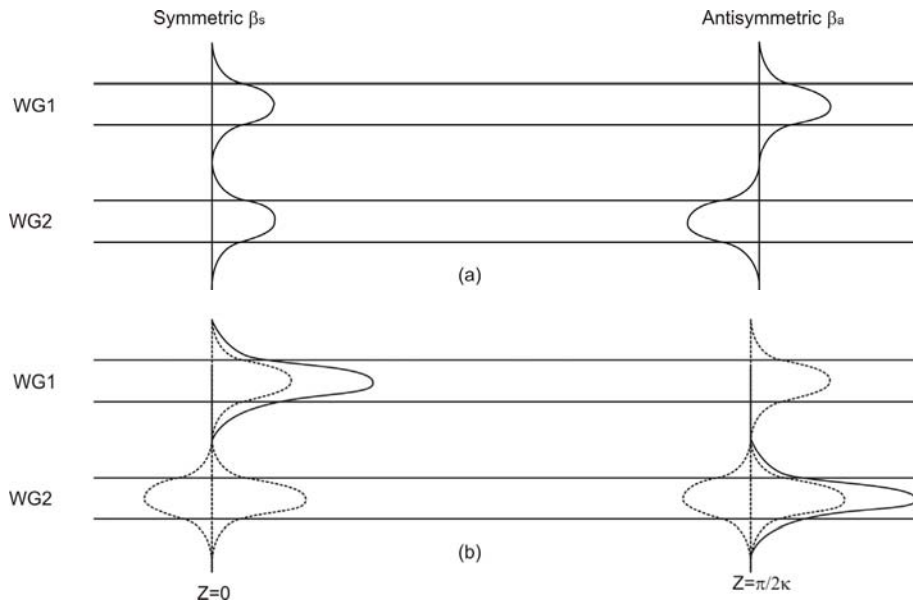
Figure 2.1 a: The symmetric and antisymmetric mode fields of the composite
structure formed by a pair of identical single mode waveguides

Figure 2.1b: The relative phase difference of the two modes propagating along *z* and
their superposition at *z*=π/2 cancel in waveguide-1 and add in waveguide-2

In the coupled mode analysis across the interaction region, the two uniform
waveguides lying parallel to each other are assumed as a composite structure [7]. The
composite system formed by the two single-mode waveguides can be shown to
support two modes, a symmetric (even) mode and an anti-symmetric (odd) mode.
These two modes called the normal modes or supermodes of the composite structure
have different propagation constants [8, 9, 10]. When light is coupled into one of the
waveguides, it excites a linear combination of the symmetric and the anti-symmetric
supermodes as shown in Figure 2.1. Due to the unequal propagation constants of the
two modes, the fields propagating down the system develop a relative phase
difference with the distance of propagation. For a certain length of interaction, if the
accumulated phase difference between these two modes becomes π, the superposition
of these two modal fields will result in the cancellation of the field amplitudes in the
input waveguide and an addition in the second waveguide. Such a situation is referred
to as coupled state, and the corresponding interaction length as the coupling length,
L_C. If the interaction length extends beyond L_C, reverse coupling takes place from the
second waveguide at the input waveguide. Thus, for propagation over a length of $2L_C$
will result in accumulation of a phase difference of 2π and hence power will be

27

restored back in the input waveguide. Thus a periodic exchange of power between the two waveguides takes place with propagation. If the two waveguides are identical, complete power can be transferred from one waveguide to the other and vice-versa, while for non-identical waveguides, only a certain maximum power transfer takes place.

For unit power launched in waveguide-1 at *z*=0, the power distribution between the throughput (P$_T$) and coupled (P$_C$) waveguides at any *z* [11], is derived in Appendix A and is given by

$$P_T(z) = 1 - \frac{\kappa^2}{\gamma^2} \sin^2 \gamma z \tag{2.1}$$

$$P_C(z) = \frac{\kappa^2}{\gamma^2} \sin^2 \gamma z \tag{2.2}$$

where
$$\gamma^2 = \kappa^2 + \frac{(\Delta\beta)^2}{4} \tag{2.3}$$

$$\Delta\beta = \beta_1 - \beta_2 \tag{2.4}$$

Here β_1 and β_2 are the propagation constants of the fundamental modes of the individual waveguides, and κ is called the coupling coefficient. κ is a measure of the strength of the coupling. It can be shown that:

$$\kappa = \sqrt{\frac{1}{1+A^2}} \left[\frac{\beta_s - \beta_a}{2} \right] \tag{2.5}$$

where $A = \dfrac{\Delta\beta}{2\kappa}$ is the asymmetry parameter, β_s and β_a represent the propagation

constants of the symmetric and antisymmetric supermodes and they are given by

$$\beta_s = \frac{\beta_1 + \beta_2}{2} + \sqrt{\frac{\Delta\beta^2}{4} + \kappa^2} \tag{2.6}$$

$$\beta_a = \frac{\beta_1 + \beta_2}{2} - \sqrt{\frac{\Delta\beta^2}{4} + \kappa^2} \tag{2.7}$$

For a symmetric coupler formed with two identical waveguides, $\Delta\beta$ =0 and hence,

$$\kappa = \left[\frac{\beta_s - \beta_a}{2} \right] \tag{2.8}$$

$$\beta_{s,a} = \beta \pm \kappa \tag{2.9}$$

28

Thus, the power distributions in a symmetric coupler are given by

$$P_T(z) = \cos^2 \kappa z \qquad\qquad (2.10)$$

$$P_C(z) = \sin^2 \kappa z \qquad\qquad (2.11)$$

These equations clearly demonstrate that for $z = \dfrac{\pi}{2\kappa}$, input power can be completely transferred to the coupled waveguide. Figure 2.2 depicts the variation of the throughput and coupled powers in the two waveguides as a function of the interaction length, z from which it is apparent that the periodicity of power exchange is $L = \dfrac{\pi}{\kappa}$.

The power remains in the input waveguide when the interaction length $z = 0$, $\dfrac{\pi}{\kappa}$, $\dfrac{2\pi}{\kappa} = \dfrac{m\pi}{\kappa}$; where $m = 0,1,2,3,...$ whereas the entire power is coupled to the second waveguide at $z = \left(m + \dfrac{1}{2}\right)\dfrac{\pi}{\kappa}$; $m = 0,1,2,3,....$. This suggests that by choosing a suitable interaction length, any arbitrary power distribution between the two interacting waveguides can be achieved. For a 50% distribution of power, the required interaction length is $z = \dfrac{\pi}{4\kappa}$. This is the basic principle underlying the operation of a 3dB coupler, used as signal splitters or combiners.

For an asymmetric coupler consisting of two non-identical waveguides, since $\Delta\beta \neq 0$, 100% transfer of power from one waveguide to the other is not possible. The efficiency (η_{max}) for maximum power transfer depends on the asymmetry parameter, A as

$$\eta_{max} = \left(\frac{\kappa^2}{\gamma^2} \sin^2 \gamma z\right)_{max} \qquad\qquad (2.12)$$

If $\dfrac{\Delta\beta}{2\kappa} = 1$, then $\eta_{max} = \dfrac{1}{2}$, i.e., a maximum of 50% power transfer is possible. The coupling coefficient κ quantifies the strength of coupling, which is the amount of power transfer that takes place per unit length of the coupler. κ is proportional to the difference between the propagation constants of the even and odd supermodes. Hence,

the value of κ is governed by the geometry and refractive index profile of the composite waveguide. Since the mode propagation constants vary with wavelength, κ is wavelength sensitive and also polarization dependent.
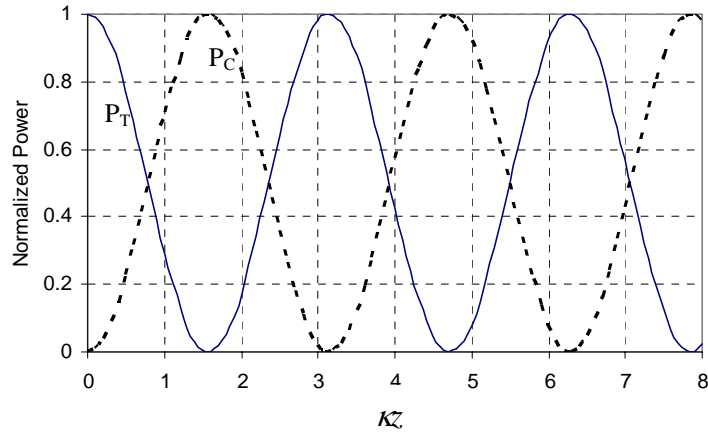

Figure 2.2: Estimated power variation in the throughput and coupled ports as a function of κz in a symmetric coupler

2.2 Fused Fiber Coupler

A fiber directional coupler, consisting of two closely spaced parallel fibers analogous to waveguide coupler discussed above, also functions on the basis of overlap between the modal fields of the guided modes of the constituent fibers through their evanescent tails [12] The two fibers are therefore required to be brought sufficiently close to each other such that they interact optically and function as a composite fiber directional coupler.

In the fused fiber coupler technology, where two or more fibers are fused and tapered together, the coupling substantially takes place through interaction between the cladding modes [8, 13, 14, 15]. In a fused tapered coupler the guided modal field gradually spreads more and more into the cladding with decreasing size of the core, eventually taking up the shape of a waveguide with original cladding as the core surrounded by air as the cladding. Naturally this waveguide will be characterized by relatively large Δn and hence, the waveguide in this region will effectively function as a multimode guide with its modes corresponding to cladding modes of the fiber. The distribution of launched power between the two output ports is dictated by coupling /

beating between the modes of multimode guide. This form of coupling is known as cladding mode coupling [16].

In the literature, coupling in Fused Biconical Taper (FBT) couplers is usually categorized on the basis of either strong fusion or weak fusion [13, 17, 18]. For a strongly fused coupler, the waist region can be approximated by a rectangular cladding-air waveguide, and the approximate analytical expression for the coupling coefficient is given by [8]

$$\kappa \approx \left[\frac{3\pi\lambda}{32a^2 n_2} \right] X \frac{1}{\left[1 + \left(\frac{1}{V} \right) \right]^2} \tag{2.13}$$

where a is the core radius, n_2 is the cladding refractive index , λ is the wavelength and V is the V-parameter.

For the weakly fused coupler, the waist region can be approximated by two touching cylinders in which case the coupling coefficient is approximately given by [19, 13]

$$\kappa \approx \frac{2^{\frac{1}{2}} (n_2^2 - n_3^2)^{\frac{1}{2}}}{n_2 a \sqrt{\pi} V^{\frac{5}{2}}} X (2.4048)^2 \tag{2.14}$$

where n_3 is the refractive index of the surrounding, which in most case is air.

For a coupler consisting of two parallel uniform axially invariant waveguides the coupling coefficient κ is a constant (depending on properties of the waveguide material, their core separation and operating wavelength) throughout the coupler length. In that case, the power transfer is a $\sin^2$ function of the product of coupling coefficient and interaction length, $\phi = \kappa.L$. Unlike parallel waveguide coupler, in an axially varying coupler structure (which is the case of FBT coupler), the transverse dimensions of the interacting fibers vary along the length, and therefore, the coupling coefficient also varies with z, i.e. it becomes $\kappa(z)$. The functional dependence of $\kappa(z)$ is determined by the longitudinal shape of the taper and by the dimension and refractive index profile of the coupler cross-section. Thus, the resultant coupling and the distribution of power between the output ports of a coupler depend on the effective length of interaction L and the effective coupling coefficient, κ. The coupled and throughput powers are expressed as [20].

$$P_T = \cos^2 \theta \tag{2.15}$$

$$P_T = \sin^2 \theta \tag{2.16}$$

where

$$\theta = \int_L \kappa(z)dz \tag{2.17}$$

2.3 Light Propagation through Tapered Fiber

The transmission through a single mode fiber is due to the fundamental core mode where the *V*-number is less than the cutoff *V*-value of the next higher order mode. While propagating down the taper, the wave encounters a gradually diminishing core and hence a gradually reducing local *V*-number [21]. This results in a progressive change in the field distribution of the local fundamental mode along the taper. The mode spreads into the cladding with decreasing *V*. For any given wavelength and core-cladding refractive index profile, there is a core diameter at which the light signal has effectively escaped from the core and is guided by the interface between the cladding and the external medium [22, 23]. This point is called the taper transition. Beyond the taper transition, the fiber is capable of supporting more than one mode since (i) the diameter of the cladding, which now forms the core, is much larger than the untapered core radius and (ii) the corresponding refractive index difference between the cladding and air is very large. These two effects lead to a large *V*-number and the structure becomes multimoded. The propagating light through such a structure can now be affected by external influences, which may perturb the evanescent field traveling outside the fiber.

As the light propagates beyond the point of minimum cross section of the taper, it eventually encounters the up-taper, where the size of the core progressively increases. The light enters the up-tapers guided by the cladding air-boundary and the structure is still capable of supporting more than one mode. When the signal reaches the taper transition point (symmetrically located on the other side of the waist), then the light begins to be guided again by the core-cladding interface and hence the lowest order mode becomes the only propagating mode in the untapered region of the fiber.

For a single mode tapered fiber with step profile, the core radius, $a_0(z)$ decreases along the *z*-axis and the ratio of the cladding radius, $a_1(z)$ to core radius, $a_0(z)$ remains constant.

$$a_1(z)/a_0(z) = a_1(0)/a_0(0) \tag{2.18}$$

The local *V* value for this kind of taper is given by:

$$V(z) = V(0)a_0(z)/a_0(0) \tag{2.19}$$

If the angle is sufficiently small to ensure negligible coupling between the fundamental and higher order modes, the taper is said to be adiabatic. In this case all the energy remains in the fundamental mode. If the taper angle is not small enough, the coupling energy loss is not negligible and the taper is non-adiabatic or lossy.

An infinite adiabatic taper with a parabolic profile defined at a length z from the input by:

$$n^2(R) = n_0^2(1 - 2\Delta R^2) \tag{2.20}$$

where $R(= r/a_0)$ is the normalized radial distance. The local spot size of $\omega(z)$ normalized to the initial radius $a_0(0)$ is given by:

$$\omega(z)/a_0(0) = [\omega(0)/a_0(0)][V(z)/V(0)]^{1/2} \tag{2.21}$$

It increases linearly with increasing a(*z*) or decreasing taper ratio. In the case of non adiabatic tapers the spot size is determined by the total field. It results from the superposition of the mode fields over the core cladding cross section, fundamental mode and higher-order cladding modes. In the case of finite clad step profile non-adiabatic taper with linear taper shape, we have:

$$a_0(z) = a_0(0)[1 - (z/L)] \tag{2.22}$$

where L is the length of the taper.

Consider a single mode fiber whose fundamental mode is excited. Fundamental mode power is coupled to the radiation field by any non-uniformity that alters the cylindrical symmetry. In the case of a finite clad fiber, the power is lost through coupling between the fundamental mode and cladding modes. The coupling length L_C is defined in terms of the propagation constants, β_1 of the fundamental mode and β_2 of the cladding mode:

$$L_C = 2\pi/(\beta_1 - \beta_2) \tag{2.23}$$

In the case of taper a length scale L' is defined in terms of the angle $\Omega(z)$ between the tangent to the core cladding interface and fiber axis. If $a(z)$ is the local radius, we have:

$$\tan \Omega(z) = a(z)/L' \tag{2.24}$$

where L' is the distance along the taper axis from the apex to the cone with half angle $\Omega(z)$. If the length scale L' of the non-uniformity is longer than the wavelength of the electromagnetic field, losses or scattering are observed, because the length scale of the field is small enough to detect the non-uniformity. If $n_1 \cong n_2 \cong n$ (weakly guiding approximation), losses are significant when ($\lambda/n < L'$). Significant loss will occur if the length scale of the non-uniformity (taper) is bounded approximately by:

$$\left(\lambda/n\right) < L' < L_C \tag{2.25}$$

Thus for an adiabatic taper, we have $\tan\Omega(z) \cong \Omega(z)$ and Equation 2.23 indicates that if $L' > L_C$ we have low or equivalent loss if:

$$\Omega(z) < a(\beta_1 - \beta_2)/2\pi \tag{2.26}$$

The taper angle must be sufficiently small and must satisfy the Equation 2.26 at each position along the taper. For a sufficiently slow taper, the wavefronts remain nearly practically plane. For a gradual taper, which can support multimode propagation at the enlarged portion, the conversion of the fundamental mode into higher order or radiation modes must be negligible.

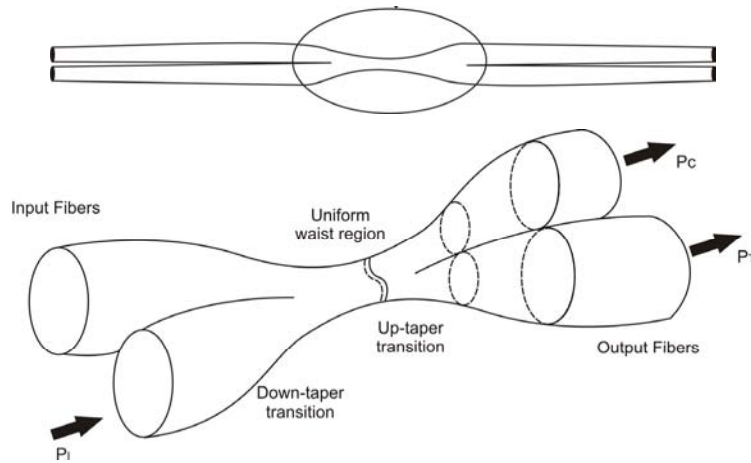## 2.4 Light Propagation in Fused Coupler

Figure 2.3 The basic structure of a fused biconical tapered (FBT) Coupler

In a FBT coupler, which consists of two laterally touching or coalesced tapered fibers as shown in Figure 2.3. The LP_{01} mode of the input fiber transforms into a cladding mode while traveling along the down-taper transition [24]. In the tapered waist, the

light guidance is provided by the large Δn between the cladding and air-interface. The original high-index cores play negligible role in the waveguidance. In the up-taper region while exiting the coupler waist, the mode is still guided by the air-cladding interface via the local modes of the multi-mode structure. These modes eventually, overlap with the natural LP_{01} modes of the output fibers. But since the composite structure has a low taper inclination, i.e the individual tapers being adiabatic [25], only two lowest order super modes (even and odd) are excited in this multimode region. Excitation of higher order cladding modes is negligible. One indicator of this is exemplified by the fact that the excess loss in the FBT couplers is typically less than 0.1 dB [26, 27].
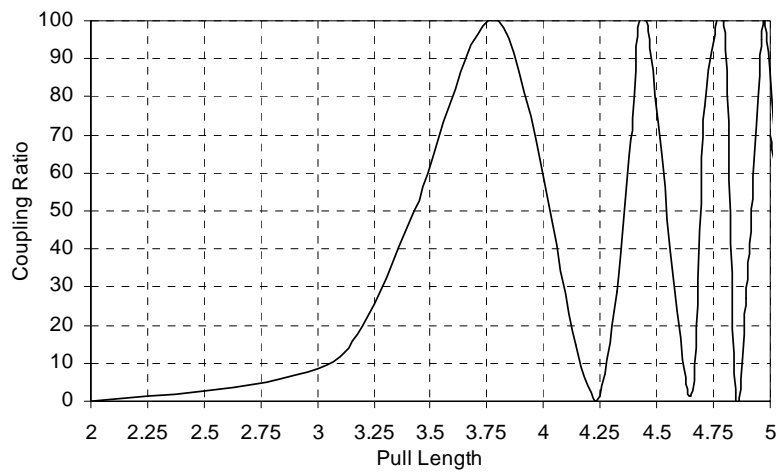

Figure 2.4: Power variation in the coupled port of a coupler with pull length during the fabrication process at a monitoring wavelength of 1550 nm.

The power in each of these supermodes experience a relative phase difference with propagation, the accumulated effect of this leads to the coupling and transfer of power between the fibers. This power-transfer takes place as a consequence of interference between the local modal fields. The light switches back and forth between the two constituent fibers with increase in interaction length as given in Figure 2.4, which shows corresponding experimentally recorded coupled power at 1550 nm, with increase in pull length during the fabrication of a symmetric 1x2 coupler.

2.5 Fabrication of Fused Coupler

Flame fusion technique has been employed for the fabrication of FBT couplers. This section describes our in-house designed, automated fabrication setup for realizing FBT couplers. The fused coupler station has axially moving mechanical stages that move over precision slides, driven by stepper motors. During the fusion process the power coupling behavior is online monitored by injecting power to the input fiber and monitoring the power at each outputs simultaneously. The process is stopped at that point where we get an equal coupling ratio over the required wavelength range. The electronic control circuitry is interfaced with PC for real time monitoring of status and instantaneous display.

For the fabrication of FBT couplers, a small section of an appropriately twisted pair of bare single mode fibers is fused laterally with a suitably designed high-temperature flame as sketched in Figure 2.5 [28]. The fiber-pair is simultaneously pulled at a slow pace along their length to form a uniform, smooth and slow taper, which is referred in the literature as a biconical, tapered structure. The fabrication process is implemented in two steps, fusion and elongation. The optical power of the monitoring signal, exiting from the two output fiber ports, is constantly recorded in real-time, throughout the process of fabrication. The status so provided is used to predict the time to stop and withdraw the flame from underneath the fibers in order to achieve a target coupling ratio. For a given pair of single-mode fibers, some of the important parameters for fusion and tapering are the pulling speed, flame temperature and flame brush width. These parameters dictate the performance of the fabricated couplers in terms of their optical characteristics.
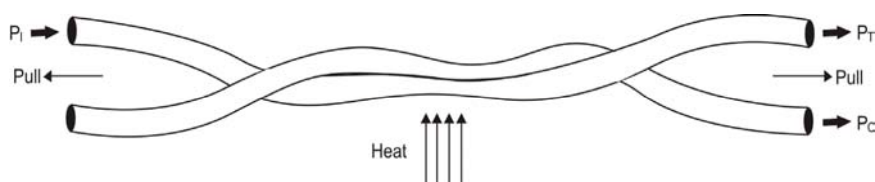
Figure 2.5: Fabrication of fused coupler: the basic fuse-pull-taper method

2.5.1 Automated Fabrication Set-up

Figure 2.6 shows the schematic of the fabrication station showing the electronic control and the mechanical stages. In the system, the fusion and elongation processes were carried out by computer control of the flame and the motors of the mechanical stages. The motor control cards (MCC) drive the motorized translational stages on

which the fibers are clamped during the fusion and tapering process. The PC does the real time monitor with all the status signals of the fabrication process and provides instructions for subsequent control operation.
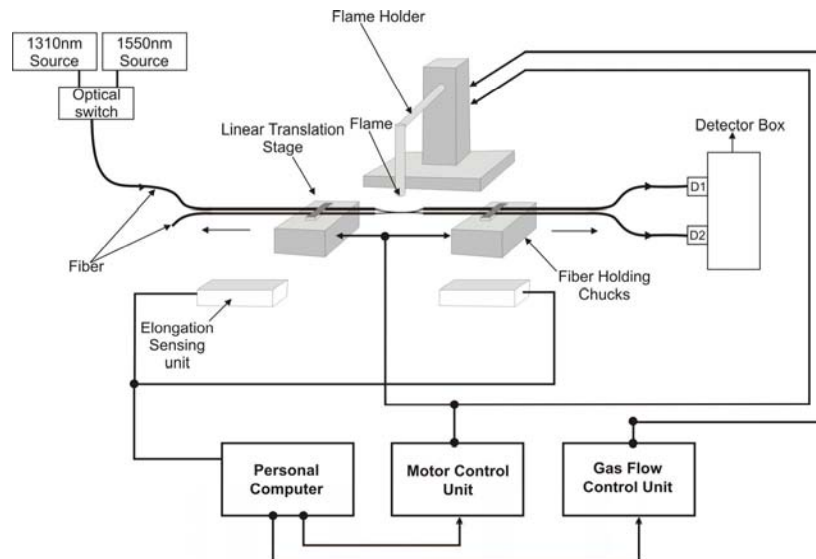

Figure 2.6: Schematic of the fabrication setup with motorized mechanical stages and a PC-based control system

The mechanical stages are the central part of the fabrication station that consists of a pair of fiber pulling linear translational stages and a flame holder assembly. All the movements are motorized, having electrical terminals, which are connected to the PC through suitable motor drive cards. A pair of motorized precision translational stages forms the fiber pulling mechanism by which the pair of fibers is pulled apart in a controlled manner during fusion. The twisted fibers are mounted on these stages with suitable mechanical clamps. The speed at which the stages move apart to pull the fibers can be precisely controlled through associated motors. Before every fabrication attempt, these stages are brought back to their "home" positions. These initial positions of the pulling stages are ensured by incorporating micro-switches, which enable stopping of the motor through a feedback circuit contained in the control hardware. A photograph of the fabrication is shown in Appendix B.

The flame holder assembly suitably positions the flame with respect to the twisted pair of fibers. The flame can be moved along the three axes, XYZ and is controlled in a prescribed manner. These movements are required for insertion and withdrawal of

the flame, to adjust the vertical position of the flame, and to provide flame-brush needed for a uniform distribution of heat over a selected length of fibers. The motorized movement employed for the insertion and withdrawal of the flame holder brings the flame underneath the fiber-pair at beginning of fabrication, the movement is also used to withdraw the flame at the end of the fabrication process. The two extreme positions of this movement are also kept fixed by a pair of micro-switches that ensures correct positioning of the flame with regard to the fiber pair. To realize the flame brush, which is required to uniformly heat a selected portion of the fibers, the flame holder is set into oscillation in a direction parallel to the length of the fibers. The flame brush also controls the taper profile [23, 29]. The heat source use either hydrogen or deuterium gas and the gas flow is regulated to the required level using a gas flow control card. The flame has a width of 6mm and is placed approximately 1cm away from the fiber. The temperature and the spatial extend of the flame together determine the shape of the taper in an FBT coupler and the required flame is coarsely identified by its typical fountain-type shape. Control the gas flow rates help to achieve the same flame condition.

The automation of the fabrication process has been achieved by an integrated real time monitoring system consisting of data acquisition card (DAC), processing, control and display module. PC acquires information regarding fabrication status with regard to target values from photo detector module and accordingly it controls the mechanical stages through motor drive unit. A pair of identical photodiodes followed by the respective signal amplifiers and DAC captures the power level exiting from the fiber output ports. The input data about the status of fabrication (i.e. coupling ratio and positions of the translational stages) are fed to the PC. The position limiting micro-switches for the various translational movements also generate different trigger signals. PC provides digital signals to activate the motors through respective current boost drive circuits. A set of three motors is activated for the movements of the flame holder in three mutually perpendicular directions for appropriate positioning of the flame with respect to fiber fusion zone. Another motor simultaneously controls the pulling stage for stretching the pair of fibers, with appropriate control of tension, during fusion and elongation.

In the fabrication process employing a real-time monitoring system, light is injected into one of the input ports and the light exiting at the two fiber output ports are measured. A loop of about 1 cm radius is introduced in the lay of the input fiber, which eliminates leaky and cladding modes that might have been excited during the

launching of light at the fiber input end. Before starting of the fabrication process, the total power exiting the input fiber appears at the transmitted port and is recorded (say, P_i). Once the fabrication gets over, the optical powers that appear at all the output ports are then recorded (say P_T, P_C for a 1x2 coupler). With no power fluctuation in the source output, the measured values of these three quantities are used to estimate the splitting ratio and the excess loss of the fabricated component. The coupling ratio is online monitored at two different wavelengths, to make sure that we get a equal coupling ratio over a wavelength range. For online monitoring at multiple wavelengths, light from two different sources (normally at 1310 nm and 1550 nm) at appropriate wavelengths are launched into the fiber through a 2x1 optical switch. By default, the monitoring will be at higher wavelength. After starting the fusion and elongation process, when the coupling ratio reaches at certain value, the optical switch is activated to select between the two wavelengths. The coupling ratio at two wavelengths is estimated in real time. For a wavelength insensitive coupler, the fusion process is stopped when the coupling ratio at both the wavelengths reaches the target value.

For on-line measurements the data corresponding to power appearing at all the output ports are recorded as a function of time and pulling length. The pulling length is calibrated in terms of the elapsed time and the speed of the translation motor. The real-time plot of power variation at the output ports versus time and pulling length obtained by this data, called pulling signature, is the most important fabrication parameter of a coupler [30, 19]. The pulling signature is used for analyzing coupling characteristics of the fabricated couplers and it provides the necessary feedback to the technology to tailor/modify the characteristics of a coupler.

The PC control program requires several initial inputs for the various target specifications (e.g.: coupling ratio) and process parameters (motor speeds, delay between activation and deactivation among different motors, etc). Once the process of fabrication is set to begin, the PC is updated with instantaneous fabrication status. This provides an excellent continuity of status information to the control program of the PC interface station back with the appropriate instantaneous data for motor controls. The monitor shows a real-time plot of power variations with the calibrated pulling length and displays all the instantaneous details of the status of fabrication process. In the PC-controlled fabrication, when the control system is switched on, which restores the flame-holder assembly and the pulling stages to their respective original positions. Control is achieved by recording the instantaneous coupling ratio

of the device in a feedback loop to regulate the speed of dc motors. Through an on-line monitoring of output powers from output ports, splitting ratio was computed instantaneously compared with the pre-set value. The difference between the two values is translated into an electrical signal in a feedback loop to control the different motor drives, and the whole fabrication is automated.
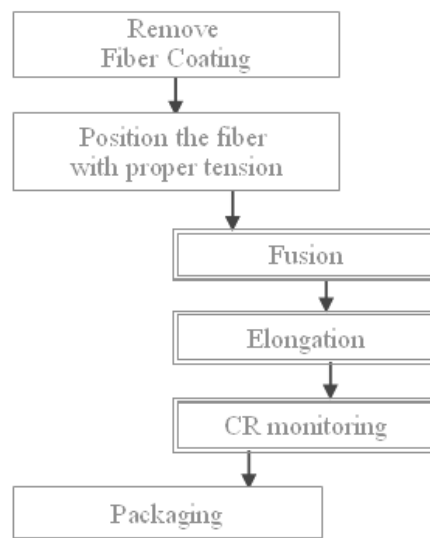
2.5.2 Process Flow

Figure 2.7: Processes for fiber coupler fabrication

The fiber coupler fabrication processes are shown in Figure 2.7. These include fiber coating removal, fiber setting, fusion, elongation, coupling ratio monitoring and packaging. These stages are described in the following section

1. **Fiber Coating Removal**

   The fiber carrying the monitoring signal and another piece of small length (approximately 2m) are placed laterally, after removing the acrylate coating using plastic strippers over a length of ~25mm. The resulting bare fiber region is then cleaned adequately. This is an important step because any microscopic impurity (dust or particles of plastic), if left on the fibers may result in scattering loss and degrade the overall performance of the device. For the same reason, usually the fabrication is carried out in a relatively dust-free environment. Plastic strippers are preferred since it does not create any micro-cracks in fibers.

2. Positioning fiber on the chucks

The pair of fibers are then twisted in order to make a close contact along the longitudinal direction over the bare stripped region and clamped at the two ends on the translational pulling stages with an appropriate tension. The twisting of the fibers should be localized and symmetric about the center of the stripped fiber lengths.

3. Fusion and pulling with online monitoring

Once the fibers are appropriately positioned, the light from the laser diode is switched on and the two fiber output ports are coupled to the photo detector unit. The system then reads the throughput and the coupled power and displays the same on the PC monitor in real-time. At this stage, the level of maximum power to be used as the monitoring signal may be adjusted appropriately. The value is recorded by the system as the total input power, P_i and is used to calculate the excess loss of the fabricated device for on-line measurements.

When the suitable level of the power at the through put port is recorded, the fabrication is started by pressing the start button. With this all the motors are sequentially activated – the flame holder is positioned underneath the bare twisted fiber-pair. A small tension is applied to the fibers through slow elongation to avoid any sagging of the softened fiber material due to gravity, which may lead to large loss of the fabricated couplers. Fusion and elongation results in the coupling of power, initially at a slower rate and eventually with a rapid exchange of power between the fibers. This can be easily observed in the status display of the PC monitor, which depicts on-line plots of the measured power at the two-fiber output ports with length of elongation. The coupling begins typically after about 6-7 minutes from the start of fabrication. At this point of time the PC program starts automatically recording of the data corresponding to the power-coupling. The PC-program constantly compares the instantaneous fabrication status with the pre-programmed parameters. When these two sets of data are identical or nearly identical, the control program generates a trigger signal to remove the flame-holder from underneath the fiber-pair, and the pulling motor is also simultaneously switched off. Once the fabrication is over, the device is then suitably packaged. During packaging, the monitor displays the instantaneous

splitting ratio, excess loss, insertion loss and absolute powers in the throughput and coupled ports.

4. **Packaging**

Packaging of the fabricated FBT couplers is an important step as the device can get easily damaged. Details of packaging of fused coupler devices have been discussed in detail in Chapter 7. The present method, takes about 10-15 minutes time to yield a completely packaged coupler.

2.5.3 Control Parameters

Fabrication of FBT coupler requires adequate control on the fabrication process to achieve target specifications [31]. This section discusses key fabrication control parameters to realize FBT couplers. The spectral splitting ratio of a coupler is a function of coupling coefficient, which is wavelength dependent and varies from point to point along a coupler length, being maximum at the waist and decreasing along either side across the biconical taper [17]. The exact magnitude of the coupling coefficient is determined by the geometry of coupler structure and taper shape. The longitudinal taper profile and the dimension of the waist effectively constitute the taper shape, which eventually dictate performance of the coupler at a given wavelength. The two parameters can be tailored by varying the pull speed, length of the hot zone, and the degree of fusion. Playing around these process variables to achieve different taper shapes, essentially implies variation in the core spacing, cross-section of the waist, the inclination of the up and down taper and the length of interaction. The taper transition transforms the local fundamental core mode of the untapered fiber to a cladding mode in the taper twist. In order to achieve a negligible loss due to conversion to the higher modes, the taper transitions are required to be adiabatic [32, 33].

Temperature Control: Heat source has a significant influence on the physical shape of the taper and hence its propagation characteristics. The heat source should provide a repeatable temperature profile, which can be controlled through gas flow rates. The length and shape of the flame are the most relevant control factors for tailoring the taper profile. All-fiber components based on the single-mode fiber tapers have been found to exhibit unique propagation characteristics according to the shape of the taper. In practice, any taper shape can be formed by appropriately controlling the temperature profile of the heat source, length of the hot zone and stretching tension applied to the heated pair of fibers during fusion.

Flame Brush width: The longitudinal profile of the taper is usually controlled by varying the length of hot zone during the elongation process. The length of the heated portion of the fibers can be varied by changing the oscillation of the flame during the flame brush. In the flame brush, a traversing flame heats a section of the fiber at a given time. The burner is made to travel across a fiber-length with a certain speed in a repeatable to-and-fro fashion. During each cycle of motion, the flame heats infinitesimally small element along the length of the fiber [34]. If the length over which the fiber is heated remains fixed with time, the resulting taper profile assumes an exponential shape. The condition of the fixed length of the hot zone can be achieved either by stationary flame or a traveling burner having constant brush length. Thus as the fibers are elongated, their diameters reduce across the heated section and the material is redistributed in the form of a taper. Since the length of the hot zone is the same, the volume of the softened silica is reduced due to tapering. This leads to an exponential taper of the form [23].

$$r(z) = r_0 e^{\frac{z}{\Delta z}} \tag{2.27}$$

where r (z) is the radius of the taper cross-section at any z, Δz is the flame width and r_0 is the radius of the coupler waist. If h is the length of the flame brush, length of the hot zone becomes h+Δz. Thus by varying the length of the flame-brush, it is possible to vary the length of the taper waist.

Pull Speed: The degree of fusion can be controlled by varying the temperature of the flame and the speed of the fiber elongation. The elongation speed, which induces tension in the two fibers, is adjusted by changing the drive power of the motors attached to the translational pulling stages. Minimum tension is required to be introduced during the fusion stage that should be sufficient to avoid any sagging of the softened pair of fibers due to gravity. By manipulating the temperature of the fibers, varying the fiber's location relative to the flame, the time of fusion phase, and the speed of elongation almost any degree of fusion can be achieved in practice. Degree of fusion together with the length of elongation determines the shape of the cross section.

The strength of coupling has a strong functional dependence on the center-to center separation between the constituent fibers and the resulting overall dimension of the coupler's waist cross section. The degree of fusion, f provides an analytical

expression, which to a good approximation quantifies these two parameters through a relation [35].

$$d = 2b\left\{1 - f\left(2 - \sqrt{2}\right)\right\}$$
(2.28)

where 2b is the diameter of the untapered fiber. The degree of fusion, f that satisfies the condition $0 \leq f \leq 1$ where f=0 corresponds to the case of "isolated" fiber and f=1 refers to the shape where two fibers have been fully fused to form a circular cross section.

For a given degree of fusion and for a given longitudinal profile, any required dimension of coupler cross section at the waist can be achieved by adjusting the pulled length of the coupler. The cross section of the waist, in practice is controlled through manipulation of taper profile by varying the flame brush width during coupler fabrication. For the same pulled length, a long flame brush width yields a relatively wide waist cross-section as compared to a short flame brush width. Narrow waist cross section with smaller length coupler results in a steep taper transition profile and of relatively higher loss usually [17]. In the PC-controlled fabrication system, pulled length is always decided by the preprogrammed splitting ratio. However the pulled length may be different for different degrees of fusion or different lengths of flame-brush, for a given coupler waist size.

2.6 Characterization of FBT Couplers

Passive optical splitters are required to conform to certain international standards set by Telcordia Technologies (formerly Bellcore) to qualify for its application. Also it is important that adequate characterization of the fabricated couplers is critical, for providing the necessary feedback to the fabrication process. The excess loss and spectral distribution of light in coupler are the two major features that decide the quality of a coupler-based device [33].

2.6.1 Performance Parameters of Couplers

The performance of the coupler components is quantified in terms of some important characteristic parameters [11]. The two most important characteristics of any generic coupler –based branching component are the splitting ratio and the excess loss.

Splitting ratio

Splitting ratio or coupling ratio is a measure of the distribution of power at the output ports of a coupler at a given wavelength of operation. Splitting ratio is defined as the ratio of power appearing a given output ports [11, 36]. The coupling ratio at the coupled port is defined as

$$\text{Coupling ratio (CR in \%)} = \left[\frac{P_C}{P_T + P_C} \right] \times 100\% \tag{2.28}$$

Similarly the coupling ratio in the through put port is,

$$\text{Coupling ratio (CR in \%)} = \left[\frac{P_T}{P_T + P_C} \right] \times 100\% \tag{2.29}$$

Splitting ratio describes how the input light to the coupler is split between the two output ports. CR% can vary from 0 to 100%. It is always quoted for a given wavelength. Naturally, it may be different at different wavelengths. It originates from the wavelength dependence of the coupling coefficient, κ.

Excess Loss

The excess loss of a coupler component is a measure of the fraction of the input power, which is not available at the output ports. This is usually expressed in dB. For an input power, P_i and output powers, P_C and P_T at the coupled and throughput ports respectively, the excess loss is expressed as

$$\text{Excess Loss (EL)} = -10 \log \left[\frac{P_T + P_C}{P_I} \right] \tag{2.30}$$

For a device with n output ports,

$$EL = -10 \log \left[\sum_{j=1}^{n} \frac{P_j}{P_i} \right] \tag{2.31}$$

The important figure of merit used to represent the overall efficiency of a coupler. It accounts for energy lost to the surroundings mainly through scattering [37]. EL in a good quality coupler is typically less than 0.1 dB.

Insertion Loss

The insertion loss of a device is the total throughput power loss suffered by the input light while propagating through the component along a particular path. Its is defined to be the ratio of the available power at a given output port to the launched power [11, 36]:

$$IL = -10 \log \left[\frac{P_C}{P_I} \right] \qquad (2.32)$$

 IL represents the total loss suffered by light in propagating from any specific input port through the coupler to the output port. It is the sum of the excess loss and the coupling ratio (expressed in dB) along a specific light path. Thus the IL of a 3 dB coupler would be more than 3 dB. IL is the key parameter of importance to a fiber optic system designer and it is expensively used while calculating power budget in link designs.

Directivity

Directivity of a coupler is a measure of the power reflected from the device. It describes how well the coupler transmits light to the output port(s) and quantifies the amount of light reflection inside the device. Expressed in dB, it is defined as the ratio of the power returned to any other input port to the injected input power [11, 36, 38].

$$Dir = -10 \log \left[\frac{P_R}{P_I} \right] \qquad (2.33)$$

For measurement of directivity, in actual practice, all the output ports are kept immersed in an index matching liquid. This procedure ensures that Fresnels reflections (due to index mismatch between the fiber terminals and air) do not contribute to the measured back reflected power. Directivity is also termed as near-end-isolation in literature.

2.6.2 Measurement of Coupler Characteristics

The measurement is essential to quantify the ultimate assured performance of the fabricated component after it is packaged. This is necessitated by the fact that during packaging, the adhesive (optical cement), which is used for fixing the coupler with the quartz substrate often introduces a small stretching tension during the course of its

curing. This often results in minute alteration of the characteristic optical parameters like splitting ratio and wavelength response.

The splitting ratio and the excess loss (as defined above) are measured both during and after fabrication [39]. In addition to measuring EL, CR, IL and Directivity, the characterization includes measurement of the wavelength response of all the components in general, and the wavelength isolation, in particular for WDM components. Figure 2.8 depicts a schematic of the measurement set up for coupling ratio, IL and polarization dependent loss. Light from a stack of sources is connected to an Nx1 optical switch, which in turn is connected to a polarization controller. The multiple wavelengths can be so selected that the wavelengths are evenly spaced in the required spectral range. The output of the polarization controller is spliced to the coupler under test. The output leads of the coupler are connected to the two channel detector using bare fiber adaptors. The InGaAs detectors are in turn connected to a PC through a DAC card.
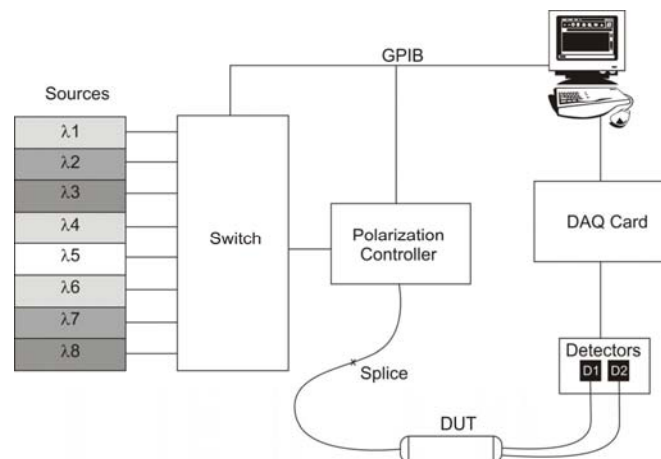

Figure 2.8: Schematic of the coupler measurement setup with a multiple laser sources.

For measuring the wavelength response of a coupler, light from broadband light source is launched to the input fiber and the output is connected to an Optical Spectrum Analyzer (OSA). The broadband white light sources used are either a tungsten halogen lamp or a multiple LED based source. The data from the measurement using multiple laser sources can also used to estimate the spectral response of the device, using curve fitting methods. For measurement of power exiting from the directivity port, which is usually carried out at the end of the

measurement cycle, the two output ports are immersed in an index matching liquid to avoid contribution to the measured power from Fresnel reflections. The optical return loss, which arises due to the back reflection to the same port, is measured using back reflection meter. In these devices, light is launched to the fiber and taken back to the photodetectors using optical circulators. Temperature Dependent Loss (TDL) is another important parameter, which shows the variation in insertion loss of a coupler, when the temperature of the coupler is varied between the maximum and minimum values of the operating temperature conditions. The temperature of the device is varied with a suitable ramp and the insertion loss is online monitored. The typical value of the temperature dependent loss is 0.2 dB.

2.6.3 Pull Signature

The real-time monitoring system records the instantaneous coupler output power, during the fabrication of couplers, and calculates the splitting ratio and excess loss of the coupler. The recorded data on output power with pull length constitutes the pull signature. Figure 2.9 shows the power variation at the coupled port of a coupler as a function of the pulled length at the monitoring wavelength of 1310 nm and 1550 nm. This clearly indicates that the rate of change of splitting ratio becomes faster with increase in the pull length (i.e., with decrease in size of the coupler waist). Compared with the case of elongation at 1310 nm, rate of change of power variation becomes still faster at higher wavelengths. Here the fiber used in the fabrication of couplers for the operation at 1310 nm and 1550 nm wavelength was SMF-28 from Corning USA (having a cut-off wavelength at 1270 nm).

The coupling behavior of a fused single mode coupler is a function of the interaction length and the operating wavelength. This fact has been readily exploited to modify the characteristics of an FBT coupler by tailoring the design parameters for realizing various application specific devices. Such a design process requires a thorough understanding of the wavelength dependence of the splitting ratio and its optimization by controlling the factors that influence it. The rate of change of spectral splitting ratio ie, how fast or slow the power transfer varies with wavelength determines the wavelength period of power-transfer oscillations. This is solely a characteristic property of the coupler structure and can be mapped to targeted requirement by controlling the shape of the taper during fabrication. A knowledge of the pulling signature (ie, coupling characteristics at the monitoring wavelength) for a given set of fabrication variables provides the necessary feedback for controlling the taper shape resulting in the desired wavelength periodicity [40]. The pulling signature obtained

from the real-time measurement leads to an estimate of the pulled length, required to fabricate a component of desired splitting ratio, this also establishes the nature of coupling during the fabrication process. Control and optimization of spectral splitting ratio of a fused coupler can yield a number of in-line components such as beam-splitter, wavelength division mux, wavelength flattened coupler, etc.
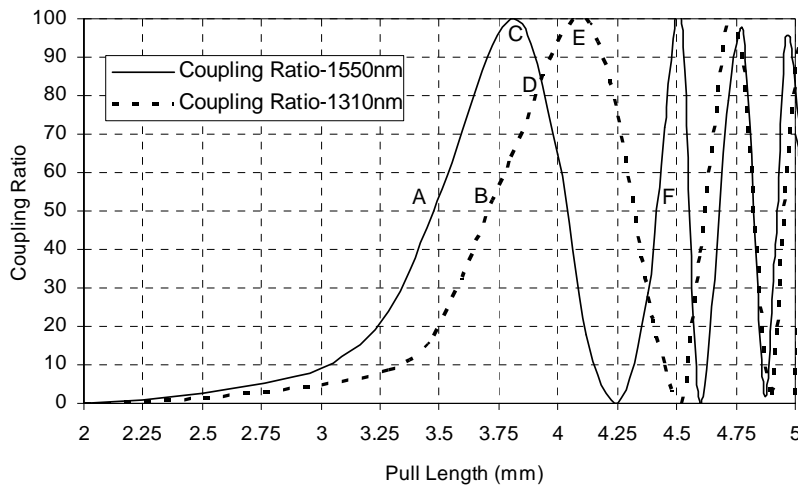

Figure 2.9: Variation in optical power with pulled length for fused biconical taper couplers at 1310 nm and 1550 nm

2.6.4 Wavelength Response of Couplers

A symmetric coupler is one in which the constituent fibers are identical, so as to achieve a 100% power transfer. A very common device required for a number of different systems is one that splits the light equally between the two output ports, a 3dB splitter. This equal splitting will occur at a point B for a wavelength of 1310 nm. Figure 2.10 shows the wavelength response of a typical 3-dB coupler at 1310 nm, measured using the setup described in section 2.6.2. It is evident that this coupler would function as a 3 dB splitter at the 1310 nm wavelength but the coupling ratio at 1550 nm is around 85%. Thus a device made in this way would make a good splitter at 1310 nm but not at 1550 nm.
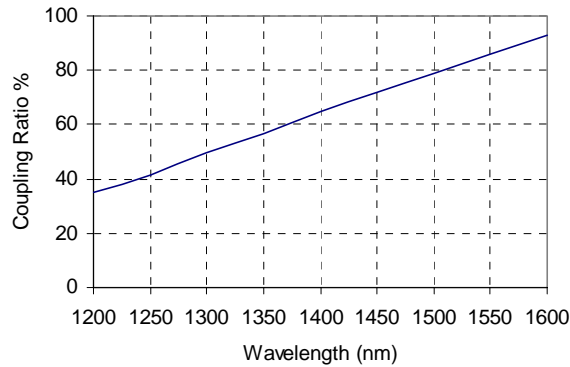
Fig 2.10: Wavelength dependence of coupling ratio of a 3 dB coupler at 1310 nm

The variation in coupling ratio with wavelength can be reduced, significantly in a single wavelength region, by stopping the pulling process at a point like C in Figure 2.9. The peak coupling ratio can be lowered for asymmetric couplers. Such couplers can be fabricated by forming a fused tapered coupling region between two fibers of slightly different propagation constants. This difference in propagation constant can be realized by using fiber of different diameter or profile, or by tapering one of the two identical fibers, more than the other [41].

2.7 Wavelength Insensitive Coupler

The wavelength dependence of coupling ratio can be reduced over the entire band from 1310 nm to 1550 nm by stopping the process at the point indicated by point D in Figure 2.9., where the two wavelengths have the same coupling ratio. The intersection point can be lowered to 50%, with two non-identical fibers, to realize a wavelength independent 3dB coupler. The devices reported here were made by pre-tapering one fiber. The pre-tapered fiber is twisted with a non-tapered fiber of constant diameter 125 μm, and the pairs heated and pulled in a similar manner of standard fused couplers. The coupling process was monitored throughout the pulling operation by launching 1310 nm and 1550 nm light into the input port and by measuring the power at these wavelengths in both output ports. The pull signature of the device when the pre-tapered fiber has a diameter of 122 μm is shown in Figure 2.11. The fibers were pulled beyond the normal stopping point to demonstrate the coupling behaviour in this region. As expected, the difference in propagation constants leads to incomplete power transfer between the fibers. The crossover point has now shifted to a coupling ratio of 50%.
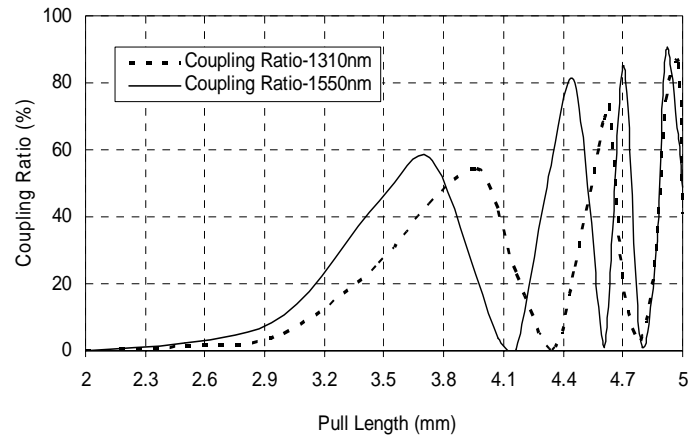
50

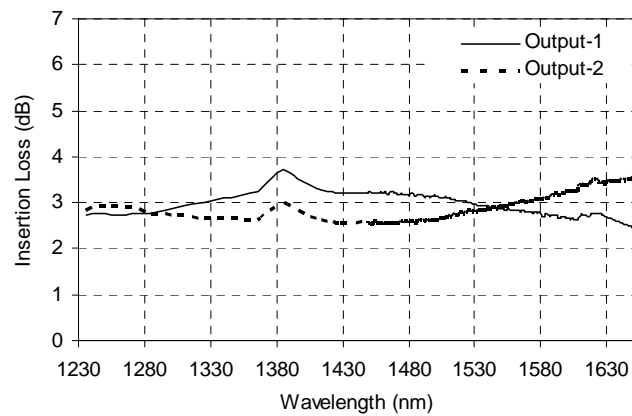Figure 2.11: Pull signature of a wavelength insensitive 3dB coupler

Figure 2.12: Spectral dependence of insertion loss of a wavelength insensitive 3 dB coupler

Figure 2.12 shows the wavelength dependence of the coupling ratio of a coupler, stopped at a point A as shown in Figure 2.11. The coupling ratio is 50% at both 1310 nm and 1550 nm. In addition, the coupling ratio is nearly independent of the wavelength over the entire band from 1200 to 1600 nm. Thus such a device offers a wavelength insensitive performance. The peak evident at 1380 nm corresponds to the water absorption peak.

2.8 Conclusions

The FBT coupler technology has been employed to realize important all-fiber branching components. The design of these components relies on the control of the process variables in the automated fabrication system. It has been possible to arrive at a set of suitable processes parameters in order to get a desired spectral response and excess loss with reasonable repeatability.

References

1. K. O. Hill, D. C. Johnson and R. G. Lamont, "Optical fiber directional couplers: Biconical taper technology and device applications", in Proc. SPIE – Fiber Optic Couplers, Connectors and Splice Technology II (San Diego, CA), Aug. 20-21, Vol. 574, pp.92-99, 1985.

2. C. M. Lawson, P. M. Kopera, T. Y. Hsu and V. J. Tekippe, "In-line single mode wavelength division multiplexer/demultiplexer", Electron. Letters, Vol. 20, pp.963-964, 1984

3. K. O. Hill, D. C. Johnson, F. Bilodeau and S. Faucher, "Narrow-bandwidth optical waveguide transmission filters: A new design concept and applications to optical fiber communications", Electron. Letters, Vol. 23, pp 465-466, 1987.

4. A. W. Snyder, "Polarizing beamsplitter from fused fiber couplers", Electron. Letters, Vol. 21, pp. 623-625, 1985.

5. J. D. Minelly and C. D. Hussey, "Single-mode fiber Y-junction beam splitter", Electron. Letters, Vol. 27, pp 1087-1088, 1987.

6.   A. Ghatak and K. Thyagarajan, Optical Electronics, Cambridge University Press, Appendix.G, pp.609-612, 1991

7. A. Ghatak and K. Thygarajan, Optical Electronics, Cambridge University Press, Ch.14, pp.447, 1991.

8. F. P. Payne, C. D. Hussey and M. S. Yataki, "Modeling fused single-mode fiber couplers", Electron. Letters, Vol.21, pp.461-463, 1985.

9. S. K. Sheem and T. G. Giallorenzi, "Single-mode fiber optical power divider: encapsulated etching technique, Optics Letters, Vol.4, pp.29-31, 1979.

10. S. K. Sheem, H. F. Taylor, R. P. Moeller and W. K. Burns, "Propagation characteristics of single-mode evanescent field couplers", Applied Optics, Vol.20, pp.1056-1062, 1981.

11. A. Ghatak and K. Thyagarajan, Introduction to Fiber Optics, Cambridge University Press, Ch.17, pp.369, 1999

12. A. W. Snyder and J. D. Love, Optical Waveguide Theory, Chapman and Hall, Ch.18, pp.387, 1983

13. F. P. Payne, C. D. Hussey and M. S. Yataki, "Polarisation Analysis of strongly fused and weakly fused tapered couplers", Electron. Letters, Vol.21, pp.561-563, 1985.

14. A. W. Synder and X. H. Zheng, "Fused couplers of arbitrary cross section", Electron. Letters, Vol.21, pp.1079 -1081, 1985.

15. F. P. Payne, "Fused single mode optical fiber couplers", Journal for the Institution of Electronics and Telecommunications Engineers (India), Vol. 32, pp.319-324, 1986.

16. M. S. Yataki, "Fused taper single-mode fiber couplers", Ph. D. Thesis, University of Southampton, Ch. 2, August 1988.

17. J. V. Wright, "Wavelength dependence of fused couplers", Electron. Letters, Vol.22, pp. 320-321, 1986.

18. H. C. Chang, T. H. Lin, and T. L. Wu, "Accurate coupling coefficients for fiber couplers with weakly fused cross-sections" Applied Optics, Vol.34, p.6168-6172, 1995.

19. F. De Fornel, C. M. Ragdale and R.J. Mears, "Analysis of single-mode fused tapered couplers", Journal of Optoelectronics, Vol.131, pp.221-227, 1984.

20. B. P. Pal (Ed), "Fundamentals of fiber optics in Telecommunications and Sensor systems", Wiley Eastern Limited, New Delhi , Ch.25, pp.606, 1992,

21. A. C. Boucouvalas and G. Georgiou, "Tapering single mode optical fibers", IEE Proceedings Pt. Journal, Vol.133, pp. 385-390, 1986.

22. S. E. Moore, W. F. Gasco and D. W. Stove, "Mass production of fused couples and couples based devices" SPIE proceedings, 574, Fiber Optic Couplers, Connectors and Splice Technology 2, pp.135 - 140, 1985.

23. W. K. Burns, M.Abebe, C. A. Villarruel and R. P. Moeller, "Loss mechanisms in single-mode fiber tapers", Journal of Lightwave Technology, LT-4, pp.608 -612, 1986.

24. K. Okamoto, "Theoretical investigation of light coupling phenomena in wavelength flattened couplers", Journal of Lightwave Technology, Vol.8, pp.678-683, 1990.

25. J. D. Love, "Spot size adiabaticity and diffraction in tapered fibers", Electron. Letters, Vol.23, pp.993-995, 1987.

26. K. Okamoto, "Fundamentals of optical waveguides, Academic Press (San Diego, USA), Ch.8, pp.323, 2000.

27. I. Yokahama, J. Node and K.Okamoto, "Fiber coupler fabrication with automatic fusion-elongation process for low excess loss and high coupling ratio accuracy", IEEE Journal of Lightwave Technology, LT-5, pp.910-915, 1987.

28. B. S. Kawasaki, K. O. Hill, and R. G.Lamont, "Biconical-taper single-mode fiber coupler", Optic Letters, Vol. 6, pp.327 -330, 1981.

29. R. P. Kenny, T. A. Birks, K. P. Oakley, "Control of optical fiber taper shape", Electronic Letters, Vol. 27, pp. 1654 - 1655, 1991.

30. M. Eiesenmann and E. Weidel, "Single-mode fused biconical couplers for wavelength division multiplexing with channel spacing between 100 and 300 nm", Journal of Lightwave Technology, Vol. 6, p. 113-115, 1988.

31. P. Roy Chaudhuri, "Technology and modeling of fused single-mode fiber coupler components", PhD Thesis, Ch. 5, pp. 67-80, 2000.

32. W. J. Stewart and J. D. Love, "Design limitation on tapers and couplers in single mode fibers", Proceedings of ECOC' 85 (Venice), pp. 559-562, 1985.

33. J. D. Love and W. M. Henry, "Quantifying loss minimization in single-mode fiber tapers", Electron. Letters, Vol. 22, pp. 912-914, 1986.

34. F. Bilodeau, K. O. Hill, S. Faucher and D. C. Johnson, "Low-loss highly over coupled fused couplers: fabrication and sensitivity to external pressure", Journal of Lightwave Technology, Vol. 6, pp. 1476-1480, 1991.

35. S. Larcoix, F. Gonthier, J. Bures, "Modeling of symmetric 2x2 fused-fiber coupler", Applied Physics, Vol. 33, pp. 8361 - 8364, 1994.

36. B. P. Pal, "Electromagnetics of all-fiber components", in Electromagnetic fields in unconventional structures and materials by A. Lakhotia, and O. N. Singh (Eds.), John Wiley, New York, 2000.

37. A. K. Ghatak, B. Culshaw, V. Nagarajan and B. D. Khurana, "trends in fiber optics and Optical Communications", Viva Books Pvt. Ltd. (New Delhi), Ch. 4, pp. 45,1995.

38. F. J. Liao and J. T. Boyd, "Single mode fiber coupler", Applied Optics, Vol. 20, pp. 2731-2734,1981.

39. F. Bilodeau, K. O. Hill, D. C. Johnson and S. Faucher, "Compact, low-loss, fused biconical taper couplers: over coupled operation and antisymmetric supermode cutoff", Optic Letters, Vol.12, pp. 634-635, 1987.

40. P. Roy Chaudhuri, B. P. Pal, and M. R. Shenoy, "Modeling fused 2x2 coupler components", Proceedings of National Symposium of Advances in microwave and Lightwave, New Delhi, pp. 57-63, March 24-28, 2000.

41. D. B. Mortimore, "Wavelength flattened fused couplers", Electronics Letters, Vol.21, pp. 742-743, 1985

Wavelength Independent Monolithic 1x4 Couplers: Fabrication and Characterization

A new method for the fabrication of monolithic 1x4 singlemode fused coupler is described along with details of its performance in terms of coupling ratio, spectral response and polarization sensitivity. The device thus fabricated exhibits ultra-broadband performance with low polarization dependent loss. The signature pattern exhibits identical coupling to all interacting fibers, enabling an easy control on fabrication parameters of the device. The effect of different process parameters on the performance of the device is studied. The device performance is also analyzed for bi-directional transmission.

Wavelength independent splitters are essential components in triple play Passive Optical Network (PON) deployments. Passive optical networks employ a multi-wavelength transmission scheme namely 1310, 1490, 1550 and 1625 nm wavelengths for upward and downward transmission as well as for physical layer monitoring [1, 2]. Hence the signal splitters installed in such networks must handle the signals faithfully and evenly at these wavelengths. Also these splitters shall be able to handle sufficiently high power levels for analog video overlay. High power handling splitters now find application in other areas also such as Erbium Doped Fiber Amplifiers and Fiber Lasers [3, 4, 5]. Integrated planar splitters are less advisable in high power applications due to epoxy in optical path, used to bond the fiber array and splitter chip, which can degrade in a long run. Thus fused biconical taper coupler offers distinctive advantage for broadband high power applications [6].

In fused couplers, coupling ratio is wavelength dependent [7, 8]. But it is well known that by controlling the propagation characteristics of interacting individual fibers and controlling the degree of fusion between the fibers it is possible to control the wavelength dependence [9-12]. The propagation constants can be altered by pre-tapering, pre-etching or pre-polishing one fiber prior to coupler fabrication. Though such technique has been well established for fabricating 1x2 wavelength independent couplers, it has not been explored in the case of truly fused 1xN couplers, where N is greater than 3. This chapter focuses on the theory and fabrication process of 1x4 monolithic couplers and suggests a new easy method for building wavelength independent 1x4 couplers.

3.1 All-Fiber 1xN Splitters

1xN Splitters are fabricated using Planar Lightwave Circuit technology or by fused coupler technology [13]. Fused coupler technology helps in realizing all-fiber 1xN splitters, with no epoxy in optical path. All-fiber 1xN splitters are fabricated by cascading 1x2 fused couplers [14, 15] as shown in Figure 3.1. Couplers are spliced one after another and are routed inside a metallic box enclosure. Here the reliability of the 1xN splitter depends on the reliability of the individual 1x2 couplers as well as on the reliability of each of the splices. Moreover, uniformity of the cascaded 1xN splitter depends on the performance of each of the selected device. Arbitrary selection of the couplers may result in a high uniformity value: careful selection of the couplers from a batch is essential to achieve good performance. The throughput and coupled ports of fused couplers have different behavior as discussed in the previous

Chapter. When we cascade the 1x2 couplers, the wavelength dependence become prominent in the path where only odd and even ports are spliced. For the paths in which odd and even ports are spliced, the wavelength dependence does not get added, since odd and even ports have different spectral characteristics. The cascaded 1xN splitter has large form factor, since we have to take care of the bend radius constraints and the typical size is 100x80x10 mm^3 [16].

In Gigabit PON, a single fiber line is normally distributed among 32 homes. Centralized splitting is not preferred in cases where home clusters are randomly distributed from the Central Office (CO). Splitting in such a situation is shared between the central office splitting cabinet and outside field fiber distribution hub. For instance, the central office splitting cabinet does a 1x8 splitting followed by 1x4 splitting near the premises of customer cluster. Hence in this work, we focus on the fabrication of wavelength insensitive 1x4 couplers. A typical application diagram of such device is shown in Figure 3.2.
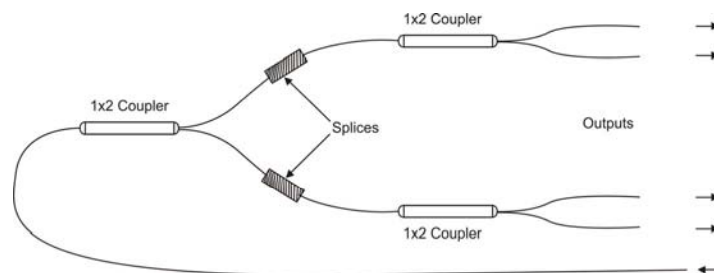

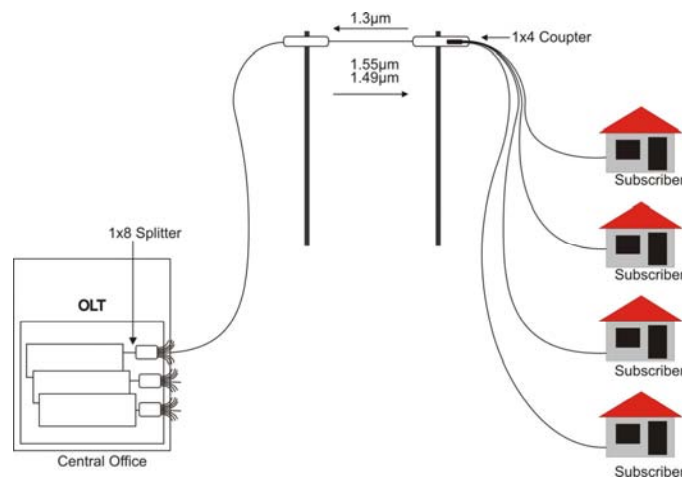Figure 3.1: 1x4 splitter formed by cascading 1x2 couplers

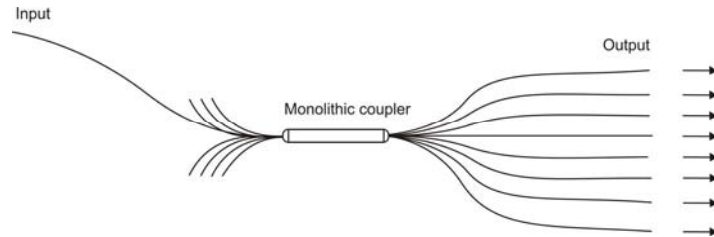Figure 3.2: Application diagram of 1x4 coupler in a GPON network

57

Figure 3.3: Schematic of Monolithic 1xN coupler

Monolithic Couplers are devices where more than two fibers are fused together as shown in Figure 3.3. Monolithic 1xN couplers are used both as a simple power splitter as well as a building block for larger port-count splitters. Thus singly fused 1xN coupler helps to reduce the footprint as well as the component density of large port count devices. A monolithic 1x4 coupler can replace three 1x2 couplers and two splices in a cascaded 1x4 coupler as shown in Figure 3.1. Less number of components is preferred from a long term reliability perspective. The schematic of a 1xN monolithic coupler is shown in Figure 3.3.

3.2 Monolithic 1x4 Coupler: Fabrication Methods

There are different methods, reported in literature, for the fabrication of fused monolithic singlemode 1x4 couplers. It is important to keep the geometry of fibers correctly at the fusion region; different approaches have been suggested for the same. In one approach, four bare fibers are inserted into a Vycor capillary tube having an internal diameter just large enough for the fibers to fit [17-19]. The use of capillary tube helps to keep the relative positioning of the individual fibers. The Vycor material is chosen because its refractive index is lower than that of the silica cladding of the fibers. Leakage of the optical field into the tube will therefore be minimized. In another method, use of dummy fibers is suggested to achieve relative positioning of fiber [20]. In fiber braiding method, fibers are twisted in such a way that, four identical fibers are positioned at the vertices of a square with a void space at the center [21, 22].

3.2.1 Coupling Behaviour

The waist structure of monolithic 1x4 a coupler is shown in the inset of Figure 3.4. It consists of four identical fibers centered at the vertices of a square. If this structure is reduced in size, so that the modal fields of each fiber expand, then coupling between the fibers will occur. The coupling constants C_s and C_w represent the strong coupling

between adjacent fibers and weak coupling between diagonal fibers respectively. If unit power is launched into fiber-1 of this *z*-invariant structure, then the power P_n carried by each fiber after a propagation distance *z* is [17],

$$P_1(z) = \frac{1}{4}[1 + 2\cos(2C_s z)\cos(2C_w z) + \cos^2(2C_s z)] \tag{3.1}$$

$$P_2(z) = P_4(z) = \frac{1}{4}\sin^2(2C_s z) \tag{3.2}$$

$$P_3(z) = \frac{1}{4}[1 - 2\cos(2C_s z)\cos(2C_w z) + \cos^2(2C_s z)] \tag{3.3}$$

The coupling behaviour as a function of the propagation distance z is shown in Figure 3.4. Figure shows the power coupling at 1550nm. The coupling constants C_s and C_w are chosen to give sensible coupling over distances observed in practice. This profile, where there is strong interaction between the diagonal fibers, is similar to the power coupling profile in a quadruple core fiber [23, 24]. This complex coupling profile is attributed to different types of interactions among the interacting fibers in the structure, namely the coupling between the through-put and coupled fiber, coupling between coupled fiber and coupled fiber etc.
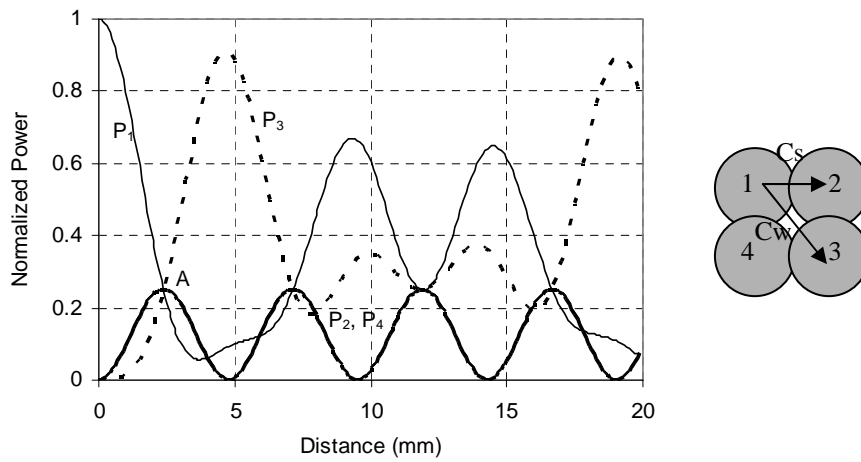

Figure 3.4: Theoretically calculated power in each fiber as a function of the propagation distance *z* with C_s=0.33 mm^{-1} and C_w=0.065 mm^{-1} at 1550nm

It can be seen clearly from this graph that the power guided by the fibers adjacent to the input fiber never carry more than 25% of the total power. At $z = \dfrac{n\pi}{4C_s}$ (n=1, 3, 5…), each fiber carries the same power 25%. Hence, at a point A, as shown in the graph, all fibers carry 25% of the total power and it is possible to fabricate an equal split coupler operating at 1550nm. The propagation distance at which this equal coupling condition occurs only depends on the coupling coefficient C_s. The effect of C_w is to modulate the power transferred between the diagonal fibers. The wavelength response of such device is more flattened in port 2 and 4, owing to the reduced power coupling to adjacent fibers, where the maximum power coupling is only 25%.

3.2.2 Pull Signature

Four fibers are twisted and tapered using the fused fiber coupler fabrication station described in Chapter 2. The power coming out of each of the fibers during fusion is monitored in real time at both 1310nm and 1550nm. The pull signature is shown in Figure 3.5, where the coupling at 1550nm is faster compared to 1310nm. At a distance of 8.25mm (point A), the power at 1550nm is equal in all fibers and a 1x4 coupler operating at 1550nm can be realized by stopping the pulling at this point. Similarly, 1x4 coupler operating at 1310nm can be realized at a pull length of 8.45mm (point B). The photograph of the cross-section of the coupler's waist is shown in Figure 3.6.

Here all the fibers are identical, but the coupling to different fibers is not identical. The coupling ratio exhibits strong dependence on the wavelength. But there is a requirement for fabricating couplers with identical performance at 1310nm and 1550nm wavelength bands. Such broadband couplers are essential for passive optical networks, owing to the multi-wavelength transmission scheme. It is possible to fabricate wavelength insensitive couplers only if we can precisely control the fabrication process. Practically, it is observed that we need to control the propagation characteristics of individual fibers to realize a wavelength insensitive coupler [21]. Such requirements on the control of propagation characteristics of the individual fibers make the process complicated and yields less repeatable results.
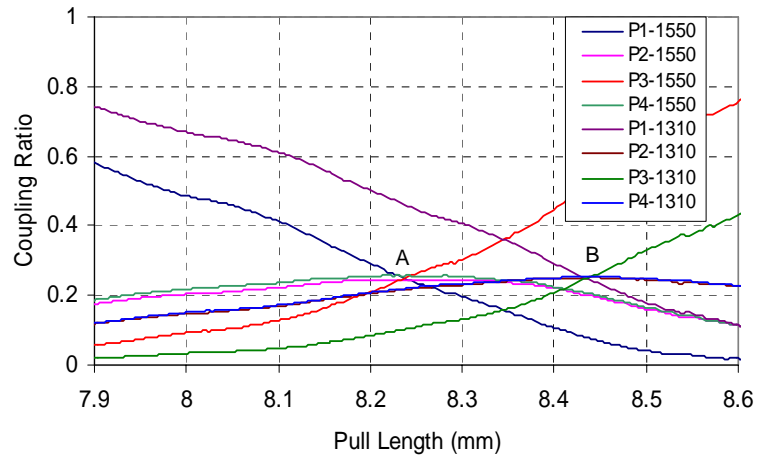
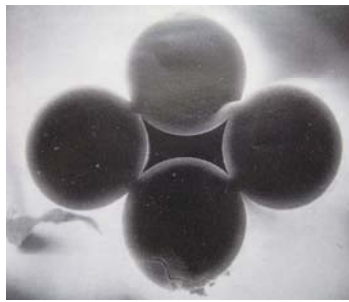Figure 3.5: Pull Signature of a Monolithic 1x4 coupler

Figure 3.6: Photograph of the cross-section of the coupler's waist

Theoretical models have been reported where the power carried by a central fiber is equally coupled among identical fibers surrounding it within an infinite cladding medium [25]. This type of interaction demands the positioning of fibers at the corners of an equilateral triangle with the central fiber placed at the vertex. However, it is difficult to achieve the relative positioning of the fibers and we have to depend on special methods.

3.3 Wavelength Insensitive Monolithic 1x4 Coupler: Theory

The operating principle of wavelength insensitive monolithic couplers can be understood by considering the coupling between an array of electromagnetically well separated fiber cores in an infinite cladding medium. Figure 3.7 shows a central core region, labeled 1, surrounded by 4 identical cores with their centers lying on a circle

of radius r. The radius and refractive index of each core is denoted by ρ and n_{co} respectively. The infinite cladding medium has refractive index, n_{cl}.
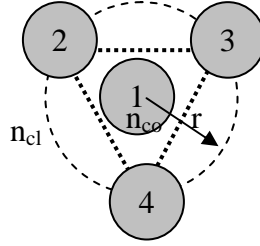

Figure 3.7: Central core region surrounded by a ring of
identical cores in an infinite cladding medium

Coupling between the array of fiber cores is described by the following set of equations [26]

$$\frac{da_k}{dz} + i\beta a_k = -i\sum_{s\neq k} a_s C_{ks} \qquad (3.4)$$

where a_k is the fundamental mode amplitude of fiber k, and β represents the propagation constant of the identical fibers. C_{ks} is the coupling coefficient between cores k and s, which may be represented by [27]

$$C_{ks} = \frac{(2\Delta)^{1/2}U^2}{\rho V^3}\frac{K_0(Wd_{ks}/\rho)}{K_1^2(W)} \qquad (3.5)$$

where U, V and W are the usual modal parameters, $\Delta = \frac{(n_{co}^2 - n_{cl}^2)}{2n_{co}^2}$, d_{ks} is the distance between the cores k and s and K_n are the modified Bessel function of the second kind.

Due to the illumination of the central core alone and the geometrical arrangement of the cores as shown in Figure 3.7, Equation 3.4 can be simplified. By considering nearest neighbor interaction only, two coupling constants C_0 and C_1 are defined. C_0 represent the coupling between the central fiber and any identical fibers in the ring. C_1 represents the coupling between nearest adjacent fibers on the ring. Considering the modal amplitude of the fibers in the ring are identical and the amplitude is a_r; i.e $a_r = a_k$

(k=1,2,3), coupling of power between the fibers is reduced to a two mode problem and the equations can be written as

$$\frac{da_0}{dz} + i\beta a_0 = -inC_0 a_r \qquad (3.6)$$

$$\frac{da_r}{dz} + i\beta a_r = -i\left(C_0 a_0 + 2C_1 a_r\right) \qquad (3.7)$$

These equations can be solved for the coupled power as a function of the propagation distance z. If unit power is launched into the central fiber then the power carried by each fiber as a function of the propagation distance z can be written as

$$P_1(z) = \left[\cos^2(Cz) + \frac{C_1^2}{C^2}\sin^2(Cz)\right] \qquad (3.8)$$

$$P_2(z) = P_3(z) = P_4(z) = \frac{C_0^2}{C^2}\sin^2(Cz)P_0 \qquad (3.9)$$

where $C = \sqrt{C_1^2 + 4C_0^2}$. The maximum power transferred to each fiber in the ring is therefore $\dfrac{C_0^2}{C^2}$. In terms of the parameter F used by Snyder [28], which describes the total power fraction coupled out of the central fiber

$$F = n\frac{C_0^2}{C^2} = \left[1 + \frac{C_1^2}{nC_0^2}\right]^{-1} \qquad (3.10)$$

The maximum coupled fraction depends on the number of fibers in the ring and the relative degree of coupling between them.

In a fused structure as shown in Figure 3.7, there exists no interaction between the fibers and hence there exists only one coupling and thus the power coupling equations for such a structure can be written as

$$P_1(z) = \cos^2(\sqrt{3}Cz) \qquad (3.11)$$

$$P_2(z) = P_3(z) = P_4(z) = \frac{1}{3}\sin^2(\sqrt{3}Cz) \qquad (3.12)$$

where P_1 is the power carried by the central fiber and $P_{2,3,4}$ is the power carried by each fiber at the corners of the equilateral triangle. The coupling between the central fiber and each surrounding fiber are identical and hence only one coupling constant, C

appears in the equations. The coupling coefficient will depend upon the usual large range of parameters such as fiber specification, array geometry, array size and wavelength.

The coupled power as a function of the propagation distance is plotted in Figure 3.8. The C values taken are 0.1mm^{-1} and 0.13mm^{-1} at $1.3\mu m$ and $1.53\mu m$ respectively. From this graph it can be seen that at a propagation distance marked A, the power in each fiber is equally distributed at both wavelengths. Therefore by stopping at this equal coupling point when fabricating a device, a wavelength insensitive response can be realized.
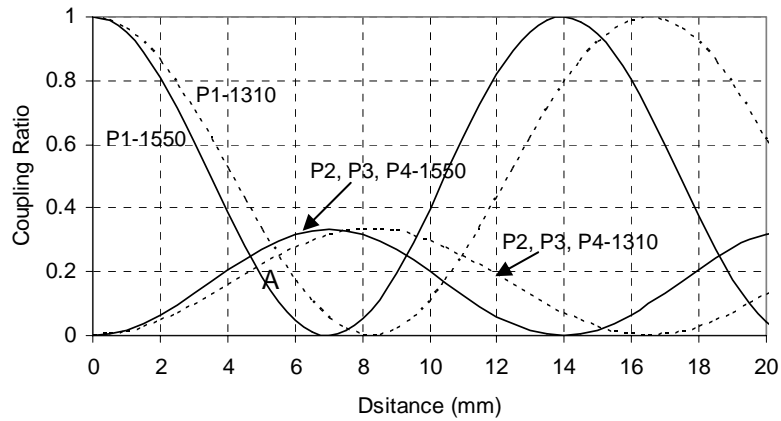

Figure 3.8: Theoretical estimation of power carried by each fiber as a function of the propagation distance z with C=0.11mm^{-1} and at 1310 nm and C=0.13mm^{-1} at 1550nm

Compared to the coupling profile described in Figure 3.4, the new profile described in Figure 3.8 is simpler because of the identical and synchronous coupling to the interacting fibers. In the former case, separate control on the propagation characteristics of the interacting fibers is required to get a wavelength insensitive response. However in the latter case such individual processing of fibers is not required. It can be seen that the maximum coupling to each of the fibers is 25% only and no further processing is required to get wavelength insensitive couplers.

3.4 Fabrication and Characterization

The device is fabricated from an array of four fibers using fused bi-conical taper technology [29-31]. Standard fused coupler fabrication equipment is used to fabricate

the device. The fiber holding chucks of the fused coupler fabrication station is modified to accommodate four fibers. The fibers are kept in a plane in the holding chuck and are braided suitably to get the required cross-section at the fusion point. The braiding is a skilful job which needs patience.

3.4.1 Fabrication Steps

Four pieces of required length (~2m) of bare single mode fiber is cut from the spool and is centre stripped along a length of ~25mm.The stripped area is cleaned so that there is no dust or residues of the removed buffer. The output end of the fibers are cleaved and connected to a 4-channel detector system. At first 3 fibers are placed in the order as primary, secondary and tertiary fiber and the fibers are clamped at the output side. Hold the fibers between our thumb and forefinger of one hand and using the other hand, separate out one of the end fibers and carefully cross it over the other two without twisting the fiber itself. Repeat this with the next two fibers until the fiber sequence is the same as at the start. Using plastic tweezers adjust the crosses into center of stripped area, looking through the microscope, by flattening and pinching the buffered region of both sides of fibers until crosses are uniformly put. When properly centered, add slight tension to the fibers by firmly grasping the fiber leads and pulling simultaneously. Care must be taken not to touch the tweezers in the stripped region of the fibers. The view of the fiber cross after this step is illustrated in the Figure 3.9 below:
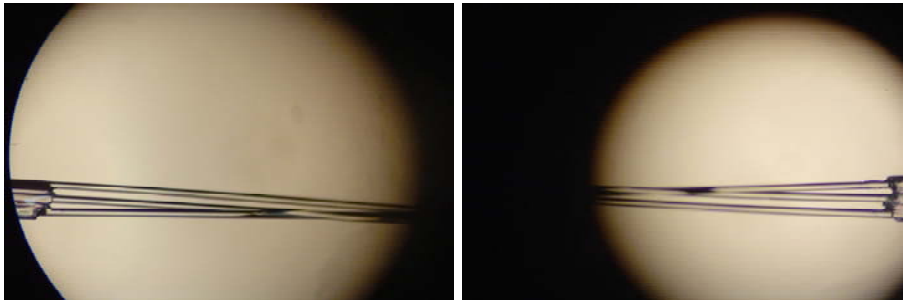

Figure 3.9: Photograph of the fiber pattern after the first step a) Left side b) Right side

The position of the cross shall be ensured with respect to the torch orifice as indicated in Figure 3.10. If the crosses are not at the correct position, adjust it slightly. Once the adjustment is over, unclamp the fiber chuck at the input side and apply proper tension, by holding the fibers together. This helps to remove the slack on the fibers, that may have occurred during the cross adjustments. Apply a very small drop of epoxy on the

buffer-stripped fiber interface at both ends of the stripped area, just to hold the crosses and cure it. The epoxy layer should not be thick, as it may induce problems in the primary packaging.
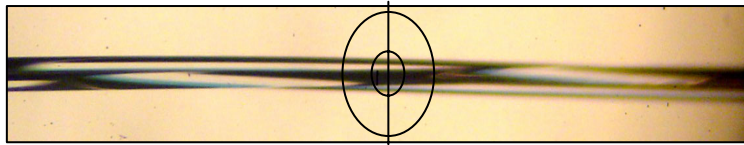

Figure 3.10: Position of torch orifice with respect to the crosses

Figure 3.11: Photograph of the fiber pattern after four fibers are twisted

Now the fourth fiber is placed close to the primary fiber, such that its stripped region is centralized between the fiber holding chucks. Glue the output side of the buffer-stripped fiber interface with very small drop of epoxy and cure it. Hold the fibers together at input side and unclamp the fibers from left holder, looking through the microscope cross the fourth fiber over the crossed bundle. Cross the twisted 3-fiber bundle over the fourth fiber. While doing this cross, ensure that the fourth fiber is passing through the torch orifice center point. Make the buffers parallel on both sides. Now check the twist pattern, which should be similar to the pattern shown in Figure 3.11. A closer view of the twist patterns on the left hand side and right hand side is shown in Figure 3.12.

The center of the torch orifice has to be at the point as shown in Figure 3.13. If the position of the torch is not at the said point, adjust the crosses. Once the cross adjustment is over unclamp the outer clamp on input side and slightly pull the four fibers holding them together so that equal tension is being transferred to all the fibers. Apply a very small drop of epoxy on the buffer-stripped fiber interface at both ends of the stripped area, just to hold the crosses and cure it.
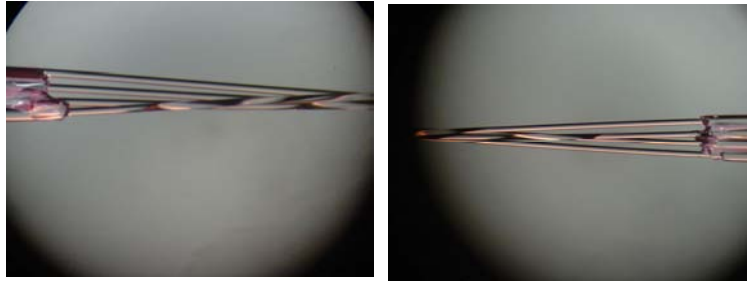
Figure 3.12: Twist position on the left hand side and right hand side
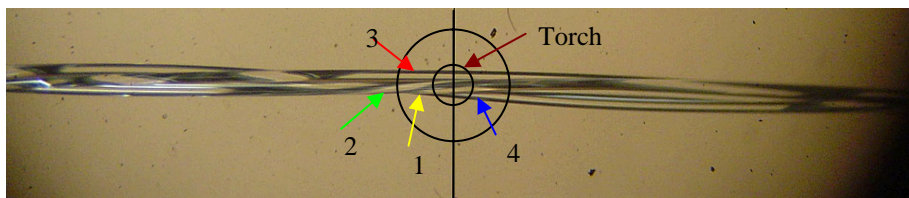of the four fiber structure

Figure 3.13: Torch position w.r.t the four fiber braided structure

The fiber bundle is then heated and pulled in the usual manner to form a tapered structure. During the pulling process, light carried by the central fiber and the surrounding fibers are monitored at both 1.3 μm and 1.5 μm. Each fiber is fed to independent detectors and the power coupled to each fiber and coupling ratios are online monitored. When the coupling at the two wavelengths become equal the elongation process is stopped and the device is packaged. A photograph of the typical waist cross-section of the fabricated device is shown in Figure 3.14.
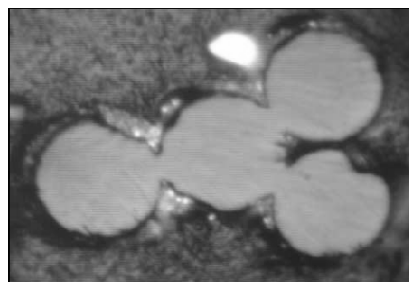

Figure 3.14: Photograph of the waist cross-section of the
fabricated 1x4 monolithic fused coupler

The fused region is protected inside quartz substrate, whose thermal expansion is similar to that of fiber. The substrate is selected in such a way that the fiber is fully protected inside the substrate even at all the regions. The width of quartz substrate groove is designed in such a way that it is sufficient to accommodate four parallel fibers. The depth is so designed that the braided structure is fully with in the groove at all positions of the bundle. The structure is fixed to the substrate using suitable epoxies so that the fused region is safeguarded from external perturbations. The surface of the quartz groove at both the ends of the substrate is roughened to make the epoxy adhesive bonding stronger. The material used for the quartz substrate is GE214. The typical range of groove roughness is 80 μm. Also the epoxies is mixed with quartz powder to minimize its thermal expansion, as explained in Chapter 7. The unutilized fibers at the input side of the coupler are terminated suitably as in the case of 1x2 couplers with an index matching epoxy. The summary of performance parameters according to the new method is

        Maximum Insertion Loss: 7.2 dB

        Uniformity over a range of 1250-1650 nm: 1.2 dB

        Excess Loss: 0.2 dB

        Polarization Dependent Loss: 0.15 dB

        Back Reflection: 60 dB
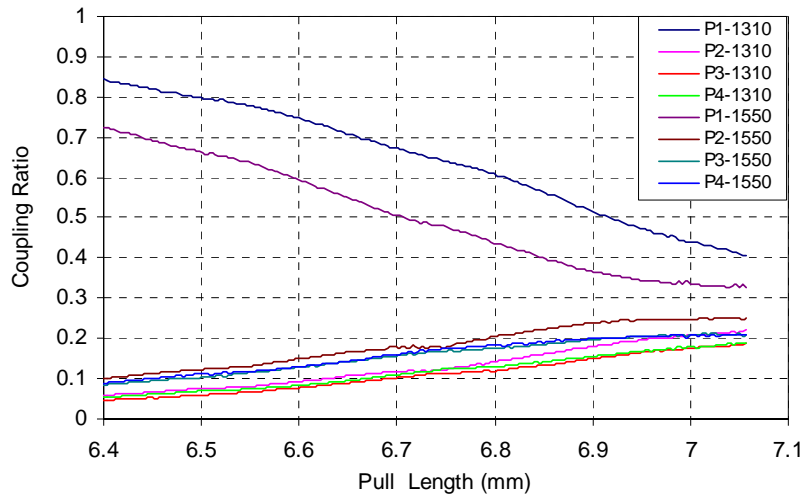
3.4.2 Pull Signature

Figure 3.15: Variation in coupled power with elongation length, when all the fibers have same propagation constants

Figure 3.15 shows the variation in coupled power with elongation length. Here all the fibers are identical and the maximum coupled power at 1310 nm is around 60%, when the propagation constants are same. The primary fiber is pretapered to a level where the maximum of the oscillatory response coincide to get the 25% coupling ratio as well as the ultra broadband spectral response. Figure 3.16 shows the variation of coupled power against coupler elongation, with the throughput fiber pre-tapered. As predicted, the power coupling from the central fiber is identical to the surrounding fibers. This power coupling behaviour helps a straightforward determination of the pulling algorithm and easy control on the fabrication process. It can be seen that at a distance of about 6.6mm, the power at both the wavelengths is shared among all the fibers. At this equal coupling point pulling is stopped and the device is packaged.
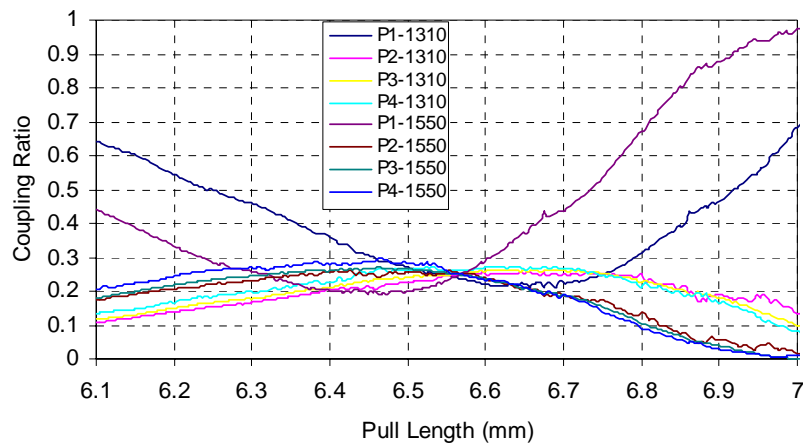

Figure 3.16: Power coupling profile of the fabricated 1x4 coupler

Power coupling profile of the device with extended length is shown in Figure 3.17, which is similar to the results as in the case of typical fused biconical taper coupler [32]. The profile shows beating, the frequency of which becomes higher with the pulling length. The coupling performance of the devise is almost independent to the state of polarization of the input light, due to the rotational symmetry of the structure. This process leads to a device, which has low loss, all-fiber, is smaller (similar in size to a standard 1x2 coupler). The device offers the same degree of performance and ruggedness as normally demonstrated by fused fiber components.
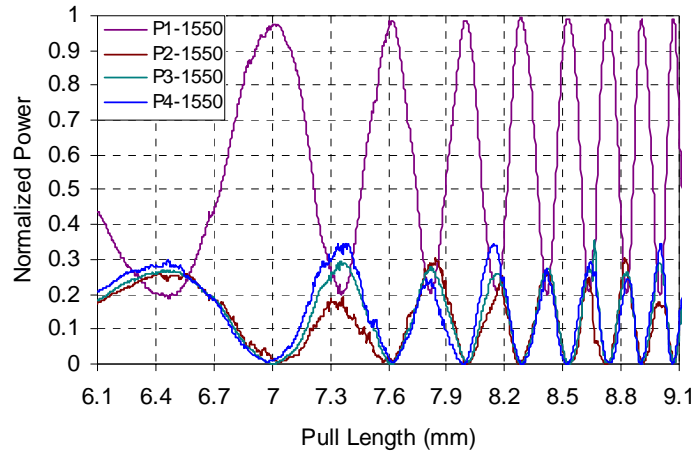
Figure 3.17: Power coupling characteristics of a 1x4 coupler, for extended pull length

3.4.3 Measurement of 1x4 Monolithic Coupler Characteristics

The splitting ratio and the excess loss are measured after packaging the device. To characterize a coupler, the devise measurement is taken up first followed by the "cut-back" of input fiber for reference measurement. Light from a series of pigtailed laser diodes connected to a Nx1 optical switch is launched into the input port of a coupler by splicing the input fiber with a fiber pigtail FC/APC connector at one end. Optical outputs from all the ports of the coupler namely P_1, P_2, P_3 and P_4 are measured using a 4-channel detector system. The input power P_i at the launching end is measured by cleaving the input fiber after the splice by taking care that the input light coupling condition is not disturbed during this step [33]. This is often referred to as the "cut-back" method in the literature, analogous to conventional cut-back method employed to measure the loss spectrum of an optical fiber [33]. For measurement of power exiting from the directivity port, which is usually carried out at the end of the measurement cycle, the output ports are immersed in an index matching liquid to avoid contribution to the measured power from Fresnel reflections.

Using cutback method the coupling related to the total output power, from the central fiber to each of the output fiber is measured at wavelengths 1310, 1490 and 1550 nm. The mean coupling ratio at 1.55 µm is 24%. The maximum insertion loss is 6.86 dB. At the operating wavelengths of 1310 nm, 1490 nm and 1550 nm the maximum insertion losses are 6.30 dB, 6.86 dB and 6.77 dB respectively. The maximum loss at 1625 nm is 6.57 dB. The above mentioned insertion losses include the polarization

sensitivity also. The excess loss of the device is less than 0.2 dB. Table 3.1 shows the measured insertion loss values of a typical 1x4 coupler.

Output	Insertion Loss (dB)			
	1310	1490	1550	1625
Port 1	6.30	6.86	6.77	6.57
Port 2	6.25	6.26	6.22	6.31
Port 3	5.79	5.69	5.75	5.87
Port 4	6.24	6.09	6.14	6.20

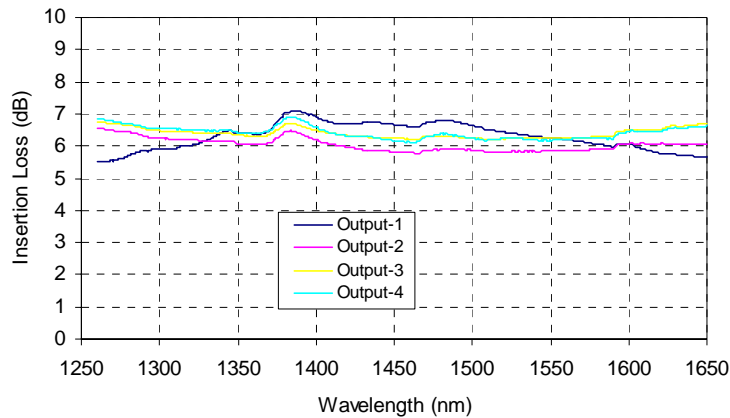Table 3.1: Measured Insertion Loss of a 1x4 Coupler

Figure 3.18: Measured wavelength response of 1x4 coupler from 1250nm to 1650 nm.

In addition to measuring CR, IL and Directivity, characterization includes measurement of wavelength response. The wavelength response of the coupler is measured by launching a broadband source into the coupler and recording the response using an optical spectrum analyzer. A broadband light source from HP, which gives wideband output from 800 to 1650 nm has been used. The spectrum analyzer is from Agilent (Model No. 6410B). The spectral response of the fabricated device from input fiber to each output is shown in Figure 3.18. All the coupled fibers have the same wavelength response. The small peak in the wavelength response of all the fibers at 1380nm corresponds to the water absorption peak. The three-coupled ports have more flattened wavelength response compared to the throughput fiber. This is owing to the incomplete transfer of power from the throughput fiber to the coupled fiber, the technique used in 1x2 couplers. Thus the fabrication method explained in

section 3.5.1 is simple method to realize 1x4 wavelength insensitive monolithic coupler. However, in the previously reported method, careful control of processing of individual fibers was required to achieve wavelength independent performance.

To measure the polarization sensitivity of the device a laser was spliced to an input fiber via a polarization controller. While monitoring the power output from each fiber in turn, the polarization controller was adjusted so that all polarization states were launched into the coupler. The maximum and minimum power readings were recorded. The results show that the power in the coupled fibers varies by 0.08 dB while the power in the throughput fiber varies by 0.15 dB. Among the coupled fibers, the polarization sensitivity is more in throughput fiber. The spectral dependence of the polarization dependent loss is shown in Figure 3.19. The structure at coupling region makes the process less sensitive to changes in the polarization states, because of the low degree of fusion and the symmetry being preserved.
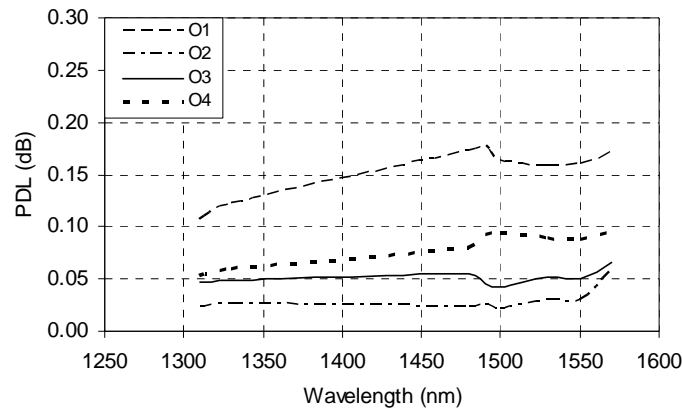
Figure 3.19: Wavelength dependence of PDL

3.4.4 Histograms of IL, Uniformity and PDL

Figure 3.20, 3.21 and 3.22 shows the histograms of the insertion loss, polarization dependent loss and uniformity of 30 number 1x4 monolithic couplers respectively, measured as described in section 3.5.3. The maximum insertion loss is 7.2 dB, but 90% of the couplers have an insertion loss less than 6.8 dB. The uniformity of the couplers is below 1.2 dB. The polarization dependent loss is below 0.16 dB as shown in Figure 3.22.

Figure 3.20: Insertion loss histogram of 1x4 monolithic coupler

Figure 3.21: Uniformity histogram of 1x4 monolithic coupler

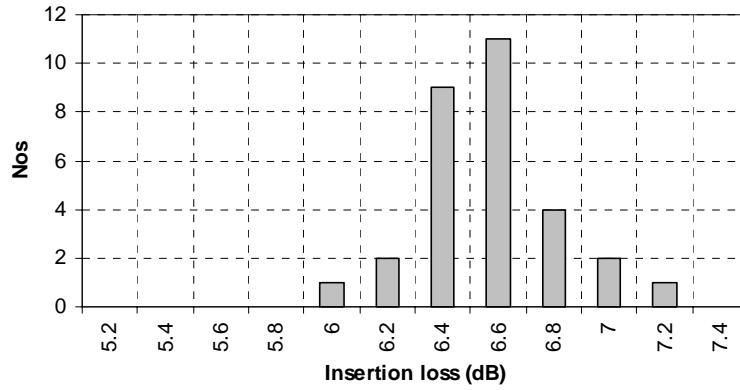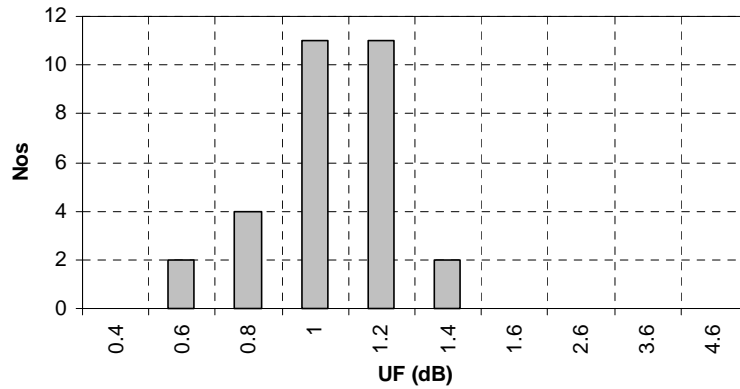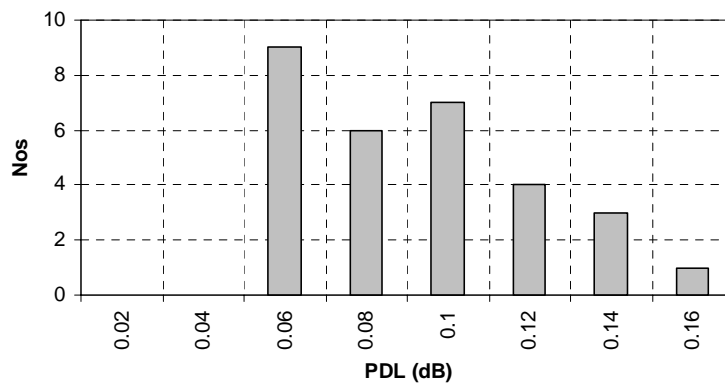Figure 3.22: Histogram of polarization dependent loss of 1x4 monolithic coupler

3.4.5 Stability of Array Geometry

The cross-section of the braided pattern, after fusion, at five different locations is shown in Figure 3.23. From the figure, it is clear that the secondary fibers are disposed around the central fiber, but not symmetrical with respect to each of the secondary fibers. It is observed that the cross-section pattern gets slightly rotated around the central fiber. The cross-section is taken by cleaving the fused region and is inspected with a microscope of suitable magnification. As shown in the cross-section, there exists an acute angle between the two secondary fibers 1&2. Both these fibers make an obtuse angle with the other secondary fiber 3. At the end of the coupling region, the four fibers will again be in the same parallel plane. We have analyzed the cross-sectional pattern of a number of devises and it is observed that the relative positioning of the fibers are not so critical, as it affects the final optical performance of the devise very little. However the twist related residual strains can affect the long term reliability of the product. It is important to make sure that there is no interaction among the surrounding fibers. As soon as there is physical interaction between the fibers, the cross-coupling coefficients comes into picture and the pull signature is no longer a simple one.

To get identical coupling profile, it is not necessary that each of the secondary fibers shall be symmetrically disposed over the primary fiber, but it is necessary that secondary fibers be separated by at least a distance to avoid the interaction between them. The braided pattern helps to maintain the secondary fibers in close proximity to the primary fiber, along the coupling region, with a waist cross-section as shown in the Figure 3.23. We have tried two different ways for braiding. In the first type, three such fibers are singly twisted three times, among which one fiber is the primary fiber. After that the fourth fiber is twisted over the three-fiber bundle with full turn, so that the relative positions of the four fibers at both ends are 1, 2, 3, 4 and 1, 2, 3, 4. This structure is sufficient to get an identical coupling profile. However, there may be a chance that a small deviation in the relative tension can contribute to the interaction among a pair of fibers, thus slightly affecting the uniformity and repeatability of the process. In the second braiding pattern, three fibers are singly twisted three times, among which one fiber is the primary fiber. Then the fourth fiber is full twisted, followed by a half turn over this bundle. In this case the relative positions of the fibers are 1, 2, 3, 4 and 4, 1, 2, 3 at the ends. Coupling in structures with the latter twist pattern are found to be more efficient than the former twist and offers good repeatability and better uniformity. The four-fiber bundle is properly secured to keep the structure during the fusion and elongation. For the above described fiber braiding patterns no special jigs is required and can be done manually. Thus the same platform

used for the manufacturing of basic FBT coupler can be used for the fabrication of 1x4 couplers.
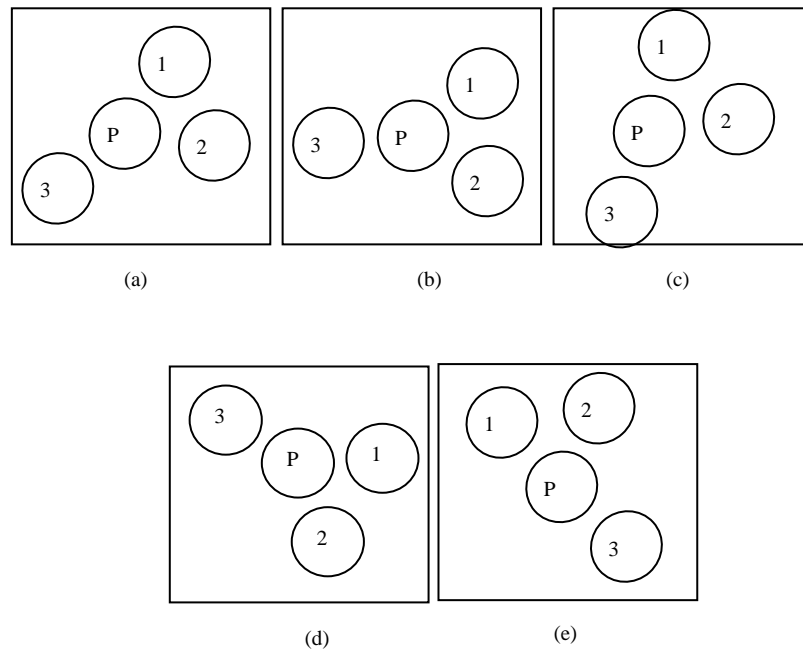
Figure 3.23: Cross-section drawings of the 1x4 coupler as per the new method, at five different locations (a) cross-section at waist (b) cross-section at 2mm right to the waist (c) cross-section at 2mm left to the waist (d) cross-section at 6mm right to the waist.(e) cross-section at 6mm left to the waist.

At the waist of the fused region, the distance between the fiber cores of each of the secondary fiber and the primary fiber typically ranges from 35 ± 3 μm, where the primary fiber is having a slightly reduced diameter (of the order of 1 μm) compared to the secondary fibers. There exists physical separation between the secondary fibers and the minimum separation is between the secondary fibers 1 & 2 as shown in the Figure 3.23, which is typically in the range of 40 ± 7 μm. At the waist, the lateral area of contact is typically around 10μm.

3.5 Fabrication Parameter Tuning

There are several important process parameters that control the performance of monolithic fused couplers. The important parameters are pull speed, gas flow and the brush width. This section details the effect of different process parameters on the performance of 1x4 couplers. Different couplers were fabricated at different pull speeds, by keeping the gas flow conditions and the brush width unchanged. The pull speed is varied from 0.5 mm/min to 2.5 mm/min and it is observed that the excess loss of the device is minimum at a pull speed of 1mm/min and it increases thereafter as shown in Figure 3.24.a. However the polarization dependent loss of the device increases linearly with pull speed as shown in Figure 3.24.b. The polarization dependent loss is 0.1 dB at a pull speed of 1mm/min. The port-to-port uniformity value remains unchanged, irrespective of the pull speed as shown in Figure 3.25. Here we have fabricated 20 samples at each condition and the average value is plotted.
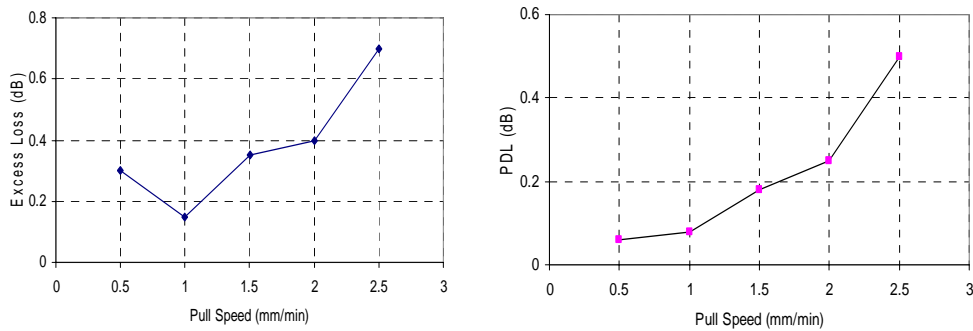

Figure 3.24: a) Relationship between pull speed and excess loss b) Variation in polarization dependent loss with pull speed
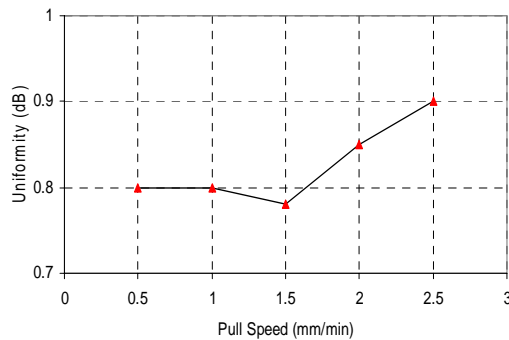
Figure 3.25: Variation in uniformity with pull speed

Brushwidth is the length of over which the flame is oscillated to get a distribution of the heating zone during the fusion process. The brush speed is kept at 36mm/min. The pull speed and gas flow conditions are kept unaltered and the brush width is varied from 4 to 7.5mm. The variation in insertion loss with brush width is plotted in Figure 3.26.a. The insertion loss decreases first and then increases rapidly. This rapid increase is due to the fact that the flame comes to the twisted region of the coupler. The relationship between polarization dependent loss and brush width is shown in Figure 3.26.b and wavelength dependent loss vs. brush width is plotted in the Figure 3.27. The polarization dependent loss and wavelength dependent loss improves with increase in brush width. The optimum brush width is found to be at ~6mm.

Figure 3.26: a) Relationship between insertion loss and brush width b) Variation in polarization dependent loss with brush width

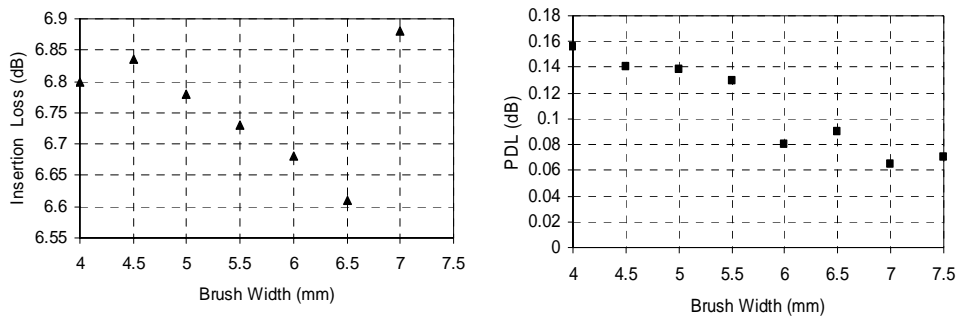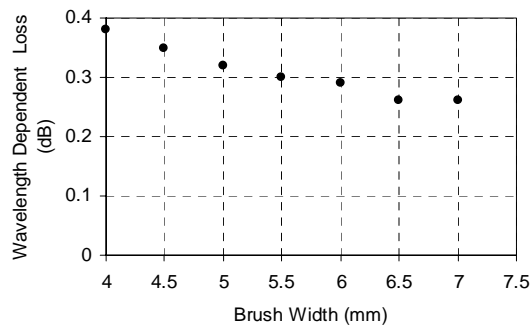Figure 3.27: Variation in wavelength dependent loss with brush width

Thus the optimum parameters of the suggested process are :

    H_2 Flow Rate: 215 sccm

Stage Separation: 40 mm

Torch Velocity: 36 mm/min

Flame Brush Width: 6.5 mm

Left stage Velocity: 2.5 mm/min

Right stage Velocity: 2.5 mm/min

Torch Height: 10 mm

3.6 Directionality Analysis

In passive optical networks, the signals are transmitted in both upstream and downstream directions. Hence the splitter performance needs to be analyzed in both directions. The measurement data of the coupler performance at 1310nm and 1550nm, when different inputs ports are excited is summarized in Table 3.2. It is to be noted that the coupling coefficient is not identical when any fiber other than the central fiber is illuminated. From Table 3.2, it is clear that the coupling ratios are same when light is coupled from central fiber (Input-1) to the surrounding fibers (Output-2, Output-3 and Output-4). But the coupling ratios vary when light is launched to the any of the surrounding fibers (Input-2, Input-3, Input-4). In any case, the coupling ratio between the launched fiber and the central fiber remains at 25%, but the coupling ratio with other fibers significantly reduces; up to 0.06% at 1310 nm and 0.12% at 1550 nm. Hence to use this device as a 1x4 coupler, the central fiber must always be excited.

Light launched to	Coupling Ratio							
	Output							
	1	2	3	4	1	2	3	4
	1310nm				1550nm			
Input-1	0.24	0.24	0.24	0.24	0.24	0.24	0.24	0.24
Input-2	0.24	0.60	0.06	0.06	0.24	0.52	0.12	0.12
Input-3	0.24	0.06	0.61	0.06	0.24	0.12	0.51	0.12
Input-4	0.24	0.06	0.06	0.60	0.24	0.12	0.12	0.52

Table 3.2: Coupling Ratios at 1310nm and 1550nm,
when different fibers are illuminated

This coupling ratio will remain true when the product is measured from output side to the input side. Thus 25% of light launched to any fiber will get coupled to the input port. Thus this product will work as a combiner with 6dB loss in the reverse direction. This confirms the suitability of the product for bi-directional PON applications. However, it is to be noted that for light applied to any port other than the throughput port, more than 25% of the light (60% at 1310 nm and 52% at 1550 nm) is coming to

the corresponding port. At the input side, fibers at the unused ports are terminated, without affecting the twist region. The termination is done either with an index matching material or with angled cleaving of fiber end. Thus the termination efficiency of the port become critical. Thus this devise can effectively work as a 1x4 coupler in both the directions. However, this configuration is not suitable for 2x4 and 4x4 configurations.

3.7 Estimation of Back Reflection

Back Reflection (BR) is a major performance deciding factor for all passive optical components [34]. In fused couplers, back reflection is directly related to the termination effectiveness of the unused input ports. In the present case, three input fibers are terminated to make it a 1x4 coupler; the unused ports are terminated inside the coupler package itself. The factors which contribute to the back reflection are inherent defects in the fused region and the reflection from the terminated optical leads. The former case is usually negligible, unless there is a discontinuity in the path. For the latter case, to eliminate Fresnel reflection from the terminated optical leads, the end surface is prepared and index matching epoxy is applied. The performance of the termination is highly dependant on the end preparation and refractive index matching. For a flat endface, the reflection will be around -14 dB at 1550 nm.

Back reflection is measured by connecting a light source to each of the output port and by measuring the light reflected to the same port. In 1x4 coupler, when light is launched from one of the output ports, it gets branched into the four input ports. The splitting ratio will depend on excited port, as shown in Table 3.2. Light will be reflected back from all the input ports. The reflected light will couple from each of the input ports to all the output ports, depending on the coupling ratio. Thus the back reflected power measured at each port will be a combined effect of the reflection from all the input ports and can be expressed as,

$$P_R = P_0 \sum_{i=1}^{4} b_i c_i^2 \qquad (3.13)$$

where b_i is the reflection coefficient and c_i is the coupling coefficient

When light is input from the throughput port, it will be equally split into the four input ports. In the reverse direction, 25% of the light reflected from each of the input ports will be coupled back to this port. Denoting the reflection coefficient from input fibers as b_1, b_2, b_3, b_4 and considering the typical power coupling coefficients given in Table

3.2, the light reflected back to each of the ports can be estimated. Considering the excitation of the port-1, each input port will receive ~25% of the light and will get reflected back depending on the reflection coefficient. This reflected light will again coupled to the throughput port in accordance with the coupling coefficients. Thus the power reflected back to the port-1 at 1310nm can be expressed as,

$$P_{R1} = 0.0576P_0(b_1 + b_2 + b_3 + b_4) \qquad (3.14)$$

Similarly, we can workout the reflected power to the second port at 1310nm as,

$$P_{R2} = P_0(0.0576b_1 + 0.36b_2 + 0.0036b_3 + 0.0036b_4) \qquad (3.15)$$

When b_2 has worst termination and when b_3 and b_4 are zero, the back reflected power measured at port-2 will be 7.96 dB higher than the value measured at port-1. If back reflection measured from port-2 is 50 dB, then the reading at port-1 will show 57.96 dB. In another case, when all the termination coefficients b_2, b_3 and b_4 have equal performance, the back reflected power measured at port-1 will be 3.27 dB higher than that measured from port-2. i.e, if the value measured from port-2 is 50 dB, the reading at port 1 will be 53.27 dB.

The power reflected back to port-1 at 1550nm can be estimated as.

$$P_{R1} = 0.0576P_0(b_1 + b_2 + b_3 + b_4) \qquad (3.16)$$

Similarly, we can workout the reflected power to the second port at 1550nm as,

$$P_{R2} = P_0(0.0576b_1 + 0.2704b_2 + 0.0144b_3 + 0.0144b_4) \qquad (3.17)$$

Hence, if all other ports except port-2 are having the best termination, the power measured at port-1 will be 6.71 dB higher than the value measured at port-2. Thus port-1 will show a value of 56.71 dB, if the value at port-2 is 50 dB. If the ports 2, 3 and 4 have the same reflection coefficient, the back reflected power measured at port-1 will be 2.38 dB higher than that measured from port-2. i.e, if the value measured from port-2 is 50 dB, the reading at port -1 will be 52.38 dB.

The coupling ratio when light is launched from port-3 or port-4 is similar to that when light is input from port-2. Thus the estimation done for port-2 is valid for port-3 and port-4 also. For marginal performance of ports 2, 3 and 4, the BR measured at port-1 will have a value in the range of 3.27 dB to 7.96 dB higher. Hence the product performance can be judged to be good if the back reflection at port-1 is 7.96 dB higher than the specification limit. However, if the BR at port-1 shows a value in the

range of 3.27 to 7.96 dB, it shall be tested from all ports. The product will be a fail, if the BR at port-1 is less than 3.27 dB.

Since the PON systems need to have a minimum back reflection limit of 40dB, the back reflection value of the coupler should not go below 40dB, even if all the four output ports are lightened. So if the ports have marginal performance at 40dB, when tested with only one port illuminated; the back reflection coming to each port will be high, when all ports are lightened. Considering a reflection of 40dB from each port, and all port is lightened with equal optical power, the BR measured at port-1 will differ by 2.7 dB to the measurement with only one port lightened. If only one port is having marginal performance, say port-2, the BR measured at port-1 will be 10dB higher to the measurement with only one port lightened. Thus by adding a margin of 10 dB to the product specification, one can judge the product as good or bad, by measuring the BR at only one port.
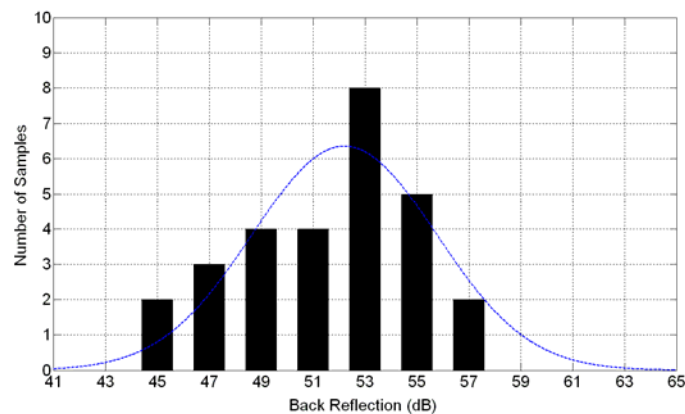
Figure 3.28: Distribution of the BR failed couplers, Port 1 at 1310nm

This model helps in predicting the termination efficiency of the 1xN coupler, by just measuring from a single output port. This model has been validated by testing the back reflection performance of 100 couplers. This helps in saving the time. The BR value of the failed couplers (26#) are analyzed; Figure 3.28 shows the distribution of the values measured at port-1 at 1310 nm. All the failed devices have a value less than 58 dB.

3.8 Fabrication of 1x5 Couplers

1x5 couplers are fabricated based on the new method of 1x4 coupler. As described in section 3.5.1, five single mode optical fibers are prepared and fused. The braiding pattern is adapted to get the required cross-section at the fusion point, i.e four fibers symmetrically positioned around the central fiber. The braiding of the first four fibers is done in a similar way as done for the 1x4 coupler. The fifth fiber is placed in a way such that it comes at the mirrored position of the fourth fiber. The pull signature of the 1x5 coupler is shown in Figure 3.29. Here also the coupling to the interacting fibers is identical. The insertion loss performance of 1x5 coupler is summarized in Table 3.3.
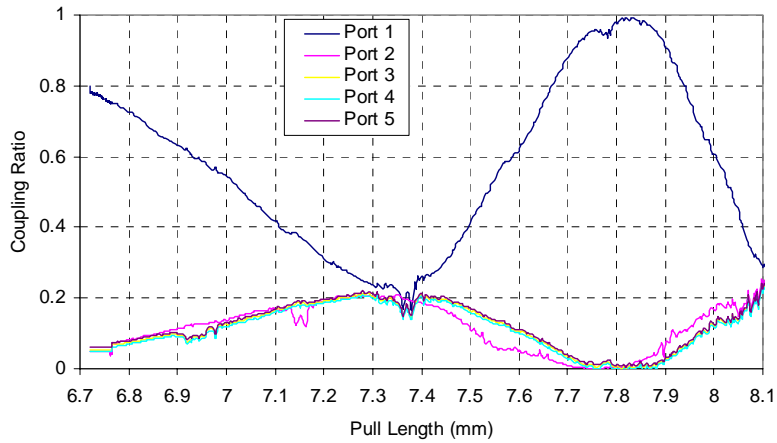
Figure 3.29: Pull signature of the 1x5 coupler

Output	Insertion Loss (dB)		
	1310	1490	1550
Port 1	7.40	8.02	7.50
Port 2	7.20	7.10	7.16
Port 3	7.05	6.9	7.01
Port 4	6.95	6.75	7.01
Port 5	7.10	7.02	7.15

Table 3.3: Measured Insertion Loss of a 1x5 Coupler

Here a method is reported to achieve wavelength independent coupling in fused 1x5 coupler, where the fabrication control is much easier due to the synchronous and identical coupling between the identical fibers. Even though, the fabrication of 1x5 couplers is described, the same principle can be easily extended to build 1x6 couplers.

But this technique may not be applicable for monolithically fused couplers where N is greater than 7.

3.9 Conclusions

A repeatable and easy method for the fabrication of monolithic, wavelength independent 1x4 single mode fused coupler has been developed. In conventional 1x4 couplers, the coupling profile is complex due to asymmetric coupling among the fibers. However, the new method provides symmetric coupling to all the coupled fibers. The fabricated device offers wideband performance from 1250 to 1650 nm. There is no need to pre-process the individual fibers before fusion, which makes the manufacturing process simple. Moreover, the new structure is formed by braiding the fibers and no special jigs are required. The broadband coupler exhibits low excess loss (<0.2 dB) as well as low polarization dependent loss (0.15dB). Compared to cascaded 1x4 couplers, monolithic 1x4 coupler offers a reliable and compact solution. The uniformity of the device is around 1.2 dB, which is almost double compared to the planar splitters. Monolithic 1x4 coupler can provide an economical solution for passive optical networks based on distributed splitting architecture. Other applications include high Splitter Array Sub Assemblies (SASAs) and multi output erbium doped fiber amplifiers and fiber lasers.

Many samples were fabricated to establish the device and process reliability. The stability of the array geometry on the performance of the device is studied and it is found that minute differences in the relative positions of the fused fibers are not critical, as long as there is no interaction between the coupled fibers. The effect of different process parameters on the performance on monolithic coupler is analyzed and optimum values were found out. The structure is suitable for bidirectional applications such as power splitting PONs. However, this structure is not useful as a 4x4 coupler, since it yields different coupling ratios depending on the input fiber being illuminated. Based on the coupling analysis a simple way of judging the back reflection performance of the device is suggested. It is shown that the reported method can be extended to make 1x5 couplers.

References

1. International Telecommunication Union (ITU-T) Recommendations G.984.1, "Gigabit-capable passive optical networks (G-PON): General characteristics", 2008

2. International Telecommunication Union (ITU-T) Recommendations G.984.5, "Enhancement band for gigabit capable optical access networks", 2008

3. P. C. Becker, N. A. Olsson, J. R. Simpson, "Chapter 3: Erbium Doped Fiber Amplifiers: Fundamentals and Technology", Academic Press, 1997

4. P. Even, D. Pureur, "High power double clad fiber lasers: a review", Proc. SPIE – Int. Soc. Opt. Eng., Vol. 4638, pp.1-12, 2002

5. François Gonthier, Lilian Martineau, Nawfel Azami, Mathieu Faucher, François Séguin, Damien Stryckman, Alain Villeneuve, "High-power All-Fiber components: The missing link for high power fiber lasers", Proc. SPIE - Fiber Lasers: Technology, Systems, and Applications, Vol. 5335, pp. 266-276, 2004.

6. Samuel Varghese, Muhammed Iqbal, Baiju C. B, Hari. K, Abraham Thomas and Suresh Nair, "Design Improvements of fused couplers for PON Applications", Proceedings of Seventh International Conference on Optoelectronics, Fiber Optics and Photonics, PHOTONICS-2004, Cochin, 2004.

7. J. V. Wright, "Wavelength dependence of fused couplers", Electronics Letters, Vol. 22, pp 320-322, 1986.

8. B. S. Kawasaki, K. O. Hill and R. G. Lamont, "Biconical Taper Single-Mode Fiber Coupler", Optics Letters, Vol.6, pp. 327-329, 1981.

9. D. B. Mortimore, "Wavelength Flattened fused couplers", Electron. Letters, Vol. 21, pp. 742-743, 1985

10. R. G. Lamont, K. O. Hill and D. C. Johnson, "Fabrication of fused twin biconical taper single mode fiber splitters: effect of unequal cladding diameters", OFC Tech Digest, pp. 78-79, 1985

11. T. A. Birks and C. D. Hussey, "Wavelength-flattened Couplers: Performance Optimization by twist tuning", Electronics Letters, Vol.25, pp. 407-408, 1989.

12. D. B. Mortimore, "Optical Fused Couplers", US Patent 4,798,436, 1989

13. "Passive Splitters for FTTH PON Applications" FTTH Council, www.ftthcouncil.org, 2004

14. Shigehito Yodo, Akio Hasemi and Masanobu Shimizu, "Single mode 1x8 Fused Couplers", Proc. Conference on Optical/Hybrid Access Networks, Canada, pp. 4.05/01 - 4.05/06, September, 1993

15. D. B. Mortimore, "Wavelength flattened 8x8 single mode star coupler", Electronics Letters, Vol.22, pp.1205-1206, 1991

16. Michael Besendhal and Piero Bruno, "Planar Splitter (PLC) *vs.* Fused Biconic Taper (FBT)", White paper from Teem Photonics, www.teemphotonics.com, 2004

17. D. B. Mortimore, "Monolithic 4x4 single mode fused coupler", Electronics Letters, Vol. 25, pp. 682-683, 1989.

18. J. W. Arkwright and D. B. Mortimore, "Monolithic MxN single mode fused fibre couplers using capillary tube technology", EFOC/LAN, London, UK, pp. 246-253, 1991.

19. J.W. Arkwright, "Novel structure for monolithic fused fiber 1x4 couplers", Electronics Letters, Vol.27, pp.1767-1768, 1991.

20. D. B. Mortimore, J. W. Arkwright and R. M. Adnams, "Monolithic wavelength flattened 1x4 single mode fused coupler", Electronics Letters, Vol.27, pp. 2252-2253, 1991.

21. Hani S. Daniel, Douglas R. Moore and Vincent J Tekippe, "Broadband MxN optical fiber couplers and method of making", US patent 5355426, October, 1994.

22. David B. Mortimore, "Theory and Fabrication of 4x4 single-mode fused optical fiber couplers", Applied Optics, Vol.29, No.3, pp. 371- 374, 1990.

23. S. Bethuys, L. Lablonde, L. Rivoallan and P. Auvray, "1x4 fused multicore fiber coupler: theory, fabrication and analysis", Electronics Letters, Vol.34, pp. 1516-1517, 1998

24. Naoto Kishi, Eikichi Yamashita, and Kazuhiko Atsuki, "Modal and Coupling Field of Optical Fibers with circularly distributed multiple cores and a central core", Journal of Lightwave Technology, Vol. LT-4, pp.991-996, 1986.

25. D. B. Mortimore, and J. W. Arkwright, "Theory and fabrication of wavelength flattened 1xN single mode couplers", Applied Optics, Vol.29, pp. 1814-1818, 1990.

26. Allan W. Snyder, "Coupled mode theory of optical fibers", J. of Optical Society of America, Vol. 62, pp. 1267-1277, 1972.

27. A. W. Snyder and J. D. Love, "Optical Waveguide Theory", Chapman and Hall, pp. 392-400, 1983.

28. A. W. Snyder, "Optical Fibre Coupler – Optimum Solution for unequal cores", J. Lightwave Technology, Vol.36, pp. 463-474, 1988

29. David Salazar, Marco Antonio Felix, Jessica Angel-Valenzuela and Heriberto Marquez, "A simple technique to obtain fused fiber optics couplers", Journal of the Mexican Society of Instrumentation, Vol.5, pp. 170-174, 2001

30. R. J. Black, S. Lacroix, F. Gonthier, and J. D. Love, "Tapered singlemode fiber and devices, part 2: Experimental and theoretical qualification", IEE Proc., Vol. 38, pp. 355-364, 1991.

31. D. B. Mortimore and J. W. Arkwright, "Performance tuning of 1x7 wavelength flattened fused fibre couplers", Electronics Letters, Vol. 26, pp. 1442-1443, 1990

32. D. Uttamchandani, "Single-mode all-fibre components", Chapter 26: Fundamentals of Fibre Optics in telecommunication and sensor systems, Edited by B. P. Pal, Wiley Eastern Limited, 1992.

33. A. K. Ghatak and M. R. Shenoy, "Fiber Optics through experiments", Viva Books Pvt. Ltd., New Delhi, Sec.13.3, Ch.13, pp.150, 1994

34. P. Bohn and S. Das, ''Return loss requirements for optical duplex transmission,'' J. Lightwave Tech., Vol.5, pp. 234–254, 1987.

Chapter 4
High Uniformity 1x4 Monolithic Couplers

A method for the fabrication of high uniformity monolithic 1x4 coupler is described. The new technique utilizes a five fiber structure instead of four fiber structure. The fabricated device exhibits good uniformity from 1250nm to 1650nm. Port-to-port uniformity ~ 0.4 dB is achieved, which is similar to the performance of planar lightwave circuit based splitters. The reliability of such couplers is also evaluated. By controlling the process parameters it is possible to control the power remaining in the through put port, which can be used for in-situ network health monitoring.

Passive Optical Networks (PON) is one of the hottest broadband access technologies today [1-3]. Triple-play Fiber-To-The-Home (FTTH) services based on PON architecture uses a multi-wavelength transmission scheme for carrying data, voice and analog video [4-7]. The network content is shared among several users using passive splitters with wavelength independent performance and good branching uniformity. The difference in uniformity of a splitter at different wavelengths can translate into different reach conditions at different wavelengths and can cause reduction in effective reach conditions. Good branching uniformity over the entire operating band is essential to get optimum reach conditions in Fiber-To-The-Home network deployments.

Fused couplers are ideal for signal splitting in PON because of wavelength independent performance and high power handling capability. Wavelength insensitive 1xN splitters are formed by cascading arrays of 1x2 couplers; uniformity of the final device depends on uniformity of the individual coupler [8]. Monolithic 1xN fused couplers are attractive as a simple power splitter and as a building block for high port-count splitters. The spectral dependence of uniformity arises from difference in spectral characteristics of the throughput and coupled ports of fused couplers. This chapter investigates on uniformity performance of 1x4 couplers over the entire PON operating band and reports an efficient and simple method to improve the branching uniformity of monolithic fused 1x4 couplers.

4.1 Splitter Uniformity and Passive Optical Networks

Uniformity is defined as the difference between maximum and minimum insertion losses of different output ports of a splitter, at a specific wavelength. The uniformity of a splitter with two output ports j and k are defined as [9]:

$$U = \left| 10 \log_{10} \left(\frac{t_{ij}}{t_{ik}} \right) \right| \ \text{dB} \tag{4.1}$$

where t_{ij} and t_{ik} are the transfer coefficients from input to each of the output ports. All of a passive optical component characteristics can be defined in terms its transfer coefficients. The power at an output port, P_j can be found by multiplying the power at any input port, P_i by the transfer coefficient, t_{ij}. Uniformity is measured over the pass band, depending on the application. In an ideally uniform passive optical component, all passive optical ports are equally coupled and hence uniformity is zero. For passive optical components intended for use in digital systems at bit rates up to 10Gbps shall have uniformity $\leq 0.6 \log_2 N$ for 1xN and $\leq 0.7 \log_2 N$ for 2xN [9].

Passive Optical Network operates at different wavelengths such as 1310, 1490, 1550 and 1625 nm [7]. Hence the port-to-port uniformity at all these wavelengths is equally important. The uneven port-to-port uniformity of the splitters translates into different reach conditions for different ports of the splitter. Also the spectral dependence of the port-to-port uniformity causes different coverage area for different wavelengths. Thus the guaranteed reach condition can be specified by considering loss at the wavelength having the worst uniformity value. The effect of uneven uniformity on reach conditions is sketched in Figure 4.1, where L_1 shows the minimum guaranteed distance at λ_1 and L_2 is the distance at λ_2. Moreover, in point-to-multipoint systems, passive optical component non-uniformity tends to increase the uncertainty in power at the receiver. This effect widens the required receiver dynamic range and reduces sensitivity. For receivers that are sensitive to excessive power, it is necessary to specify the minimum loss of a passive optical component, which can be expressed in terms of uniformity and number of ports as [9]:

$$IL_{\min} = -10\log\left(1 - \frac{N-1}{10^{0.1U} + N - 1}\right) \quad \text{dB} \qquad (4.2)$$

In fused couplers the coupling ratio is wavelength dependent [10]. Wavelength insensitive fused couplers are realized by modifying the propagation characteristics of one of the fused fibers prior to coupler fabrication [11-12]. The throughput and coupled ports have different spectral insertion loss characteristics and the wavelength dependence of uniformity originates from this. The uniformity at all wavelengths is measured and greater of these values is specified as the uniformity of the splitter.
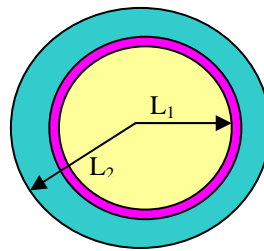

Figure 4.1: Effective reach conditions due to uneven uniformity

4.2 Uniformity of Monolithic 1x4 Coupler

Monolithic 1x4 couplers [13-16] are ideal for distributed splitting in passive optical networks [13-16]. The waist cross-section of a typical wideband 1x4 coupler is shown

in Figure 3.14; there exists identical coupling between central fiber and surrounding fibers [17]. Such a structure exhibits identical coupling to surrounding fibers, due to the symmetric waist cross-section and no cross coupling between the coupled fibers. The spectral response of a 1x4 coupler measured from input fiber to each of the output fibers is shown in Chapter 3 (Figure 3.18), where all coupled fibers exhibit same wavelength response. The three-coupled ports have more flattened wavelength response compared to the throughput fiber (Output 1), owing to the incomplete transfer of power from central fiber to the coupled fiber. The spectral dependence of the port-to-port uniformity of such a coupler is shown in Figure 4.2. The uniformity values vary from 0.3 to 1.2 dB over a spectral range of 1250 to 1650 nm. The uniformity is low at 0.6 dB from 1320 nm to 1360 nm and 1560 to 1600 nm. The uniformity is high at 1490 and 1625 nm bands, which is undesirable for FTTH networks. The highest contribution to the variations in uniformity comes from the central fiber, owing to its largest spectral dependence. The uneven port-to-port uniformity causes worst reach conditions for data transmission at 1490 nm. Thus it is essential to look for new techniques to improve the uniformity over the entire operating band.

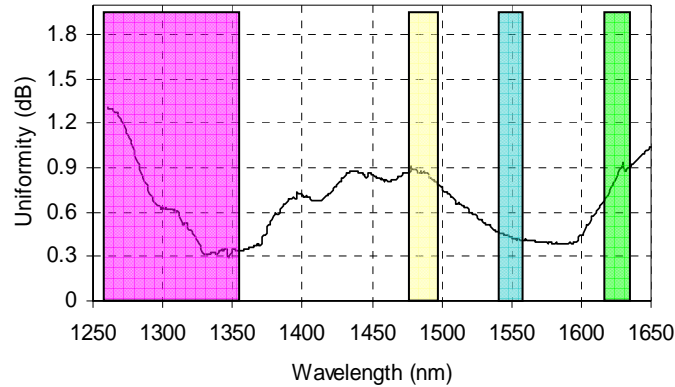Figure 4.2: Spectral dependence of uniformity of a fused 1x4 coupler

It is possible to improve port-to-port uniformity over wide operating range of a monolithic 1x4 coupler, if all output fibers have the same spectral response. This is achieved by fusing 5 identical fibers, where power from the throughput fiber is completely coupled to four surrounding fibers positioned symmetrically around the central fiber.

4.3 High Uniformity Monolithic 1x4 Coupler

The schematic in Figure 4.3 shows a 1x4 coupler with high uniformity, where O1 is the throughput fiber, O2, O3, O4 and O5 represent the coupled fibers. Here all the launched power couples entirely to the four coupled ports. Thus the four output ports exhibit the same wavelength dependence of coupling ratio. Here five fibers are arranged so that four fibers surround a central fiber symmetrically like a face centered square structure. The five fibers are elongated to induce the desired coupling. By controlling the process parameters, it is possible to retain a small amount of power in central fiber, which can be used for in-situ health monitoring of the networks.
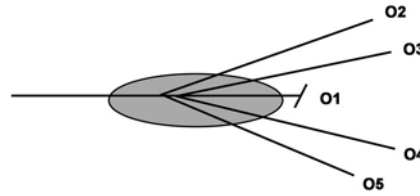

Figure 4.3: Schematic of high uniformity 1x4 coupler

4.3.1 Theoretical Background

Consider an array of 5 fibers, where four fibers surround a central fiber in a symmetric manner. If this structure is reduced in size, such that mode coupling between the fibers can occur, then light launched into the center fiber will completely get transferred to the surrounding fibers, equally. By considering nearest neighbour interaction only, the equations, which describe the evolution of power with propagation distance z are [18],

$$P_1 = 1 - \sin^2[\sqrt{4C}z] \qquad (4.3)$$

and

$$P_C = \frac{1}{4}\sin^2[\sqrt{4C}z] \qquad (4.4)$$

where P_1 is the power carried by central fiber and P_c is the power carried by each of the surrounding fibers. The coupling between the central fiber and each surrounding fiber are identical and hence only one coupling constant appears in the equations. The coupling coefficient depends upon a range of parameters such as fiber specification, array geometry, array size and wavelength. *C* around the waist region of the 1x4 coupler is taken as 0.11mm^{-1} and 0.13mm^{-1} at 1310nm and 1550nm respectively. The power carried by each fiber as a propagation distance *z* is shown in Figure 4.4, P_1

represents power in the central fiber while P_2, P_3, P_4 and P_5 represents the power carried by surrounding fibers.
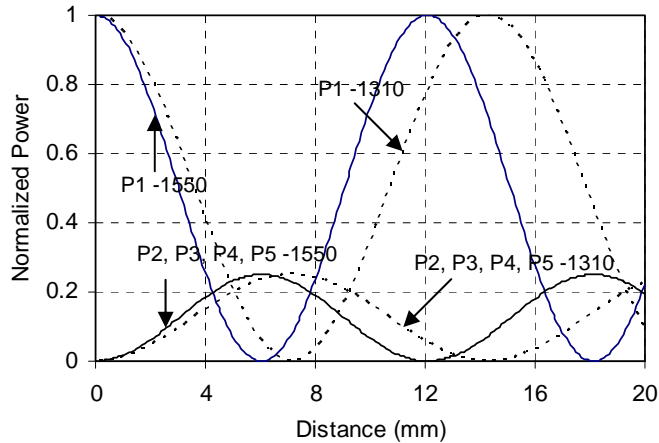

Figure 4.4: Theoretical estimation of power carried by each fiber as a function of the propagation distance z with C=0.11mm^{-1} at 1310nm and C=0.13mm^{-1} at 1550nm

4.3.2 Fabrication

The device is fabricated from an array of five fibers using fused tapered fiber technology [19-22]. The fiber holding chucks of the fused coupler fabrication station is modified to accommodate five fibers. The fibers are kept in a plane and braided carefully to get the required symmetric cross-section, at the fusion point. Five pieces of required length (~2m) of bare single mode fiber is cut from the spool and is centre stripped along a length of ~25mm.The stripped area is cleaned so that there is no dust or residues of the removed buffer. Cleave the output end of fiber pieces and connect to the 5-channel detector system. At first 3 fibers are placed in the chuck and clamped. Hold the fibers between the thumb and forefinger of one hand and using the other hand, separate out one of the end fibers and carefully cross it over the other two, without twisting the fiber itself. Repeat this with the next two fibers until the fiber sequence is the same as at the start. Using the tweezers adjust the crosses into center of stripped area, looking through the microscope, by flattening and pinching the buffered region of both sides of fibers until crosses are uniformly put. When properly centered, add slight tension to the fibers by firmly grasping the fiber leads and pulling simultaneously. Care must be taken not to touch the tweezers in the stripped region of the fibers. Apply a very small drop of epoxy on the buffer-stripped fiber interface at both ends of the stripped area, just to hold the crosses and cure it. Now the fourth

fiber is placed close to the first fiber, such that its stripped region is centralized between the fiber holding chucks. Glue the output side of the buffer-stripped fiber interface with very small drop of epoxy and cure it. Hold the fibers together at input side and unclamp the fibers from left holder, looking through the microscope cross the fourth fiber over the crossed bundle. Cross the twisted 3-fiber bundle over the fourth fiber. While doing this cross, ensure that the fourth fiber is passing through the torch orifice center point. Make the buffers parallel on both sides. Adjust the twists and apply a small amount of epoxy to fix the twists. Now place the fifth fiber at the mirror position of the forth fiber and do the twisting as done for the fourth fiber. Clamp the fibers in the chuck and apply a small tension in the horizontal direction.

Using equipment designed for the fabrication of standard fused couplers, the fiber array is heated and pulled to form a tapered structure. During the pulling, power carried by the central fiber and surrounding fibers is monitored at both 1.3μm and 1.5μm. Each fiber is fed to independent detectors and the power coupled to each fiber and coupling ratios are online monitored. When coupling to each of the coupled fibers become equal and the power remaining in central fiber become zero, the elongation process is stopped and the device is packaged. A photograph of the typical waist cross-section of the fabricated device is shown in Figure 4.5.
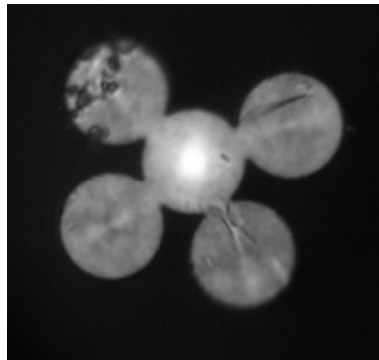
Figure 4.5: Photograph of the waist cross-section of fabricated
High Uniformity 1x4 monolithic fused coupler

Figure 4.6 shows the measured variation of coupled power with elongation length. The power coupling at 1550nm is plotted in the figure; coupling from the central fiber is identical to the surrounding fibers, as predicted. This power coupling profile helps in straight forward implementation of the pulling algorithm and easy control of fabrication parameters. It can be seen that at a distance of about 7.5mm, the power at

both wavelengths is equally shared among all surrounding fibers and the power in the throughput fiber is very small. At this point the pulling is stopped and the device is packaged. The throughput fiber with nominal power is angle terminated for low back reflection and protected with an index matching epoxy. The coupling performance of the coupler is almost independent to the state of polarization of the input light, because of the rotational symmetry of the structure. This process leads to a monolithic 1x4 coupler, which has low loss, high port-to-port uniformity and smaller size (similar in size to a standard 1x2 coupler).
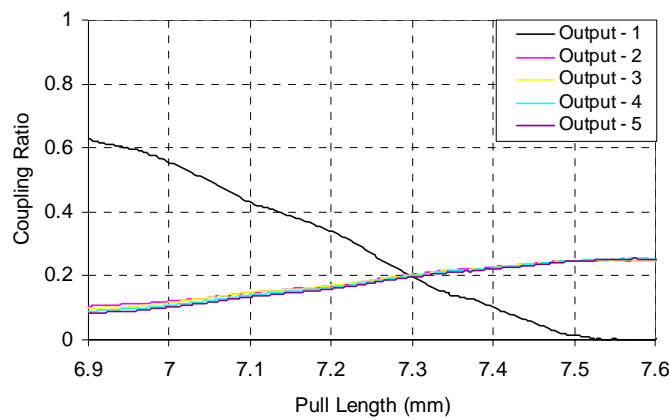

Figure 4.6: Typical power coupling data of the fabricated 1x4 coupler

The power remaining in throughput fiber is controlled by optimizing the diameter of central fiber and fusion parameters. Devices were fabricated with power in central fiber in the range of 1 to 3%, when the preprocessed diameter of the central fiber was around 121 μm. The power in the central fiber can be used for monitoring power flowing through the splitter, without disturbing the communication path in which splitter module is installed. The spectral dependence of this monitoring port is relatively poor compared to other coupled fibers. However, this spectral dependence doesn't affect the branching uniformity of splitter, as it is used only for monitoring purpose.

4.3.3 Characterization

The coupled power related to total output power, from the central fiber to each of the output fiber is measured at wavelengths 1310, 1490 and 1550 nm. The mean coupling ratio at 1.55μm is 24%. At the operating wavelengths of 1310 nm, 1490 nm and 1550

nm the maximum insertion losses are 6.4 dB, 6.39 dB and 6.42 dB respectively. The excess loss of the device is less than 0.25 dB, which is due to the uncoupled power remaining in the throughput fiber. Table 1 shows the measured insertion loss values of a typical monolithic 1x4 coupler, with high uniformity. The polarization dependence loss is also tabulated in Table 4.1.

Output	Insertion Loss (dB)			Polarization Dependent Loss (dB)		
	1310	1490	1550	1310	1490	1550
Port 2	6.25	6.19	6.3	0.09	0.08	0.12
Port 3	6.4	6.39	6.42	0.08	0.10	0.11
Port 4	6.17	5.92	6.05	0.12	0.14	0.15
Port 5	6.1	6.04	6.28	0.09	0.11	0.14

Table 4.1: Measured Insertion Loss and PDL of a High Uniformity 1x4 Coupler

The spectral response of the fabricated device measured from input fiber to each output is shown in Figure 4.7. All the coupled fibers show identical wavelength response. The slight variation in the insertion loss among different outputs is due to the small difference in the average coupling coefficients, arising from the relative fiber positioning and fusion depth variations. The spectral uniformity or wavelength dependent insertion loss in each of the output fiber is less than 0.5 dB and the peak in the response at 1380nm corresponds to the water absorption peak of standard single mode fiber. Here the spectral response of the throughput fiber is not considered, since it is not used for power splitting. The back reflection of the device is better than –50 dB.
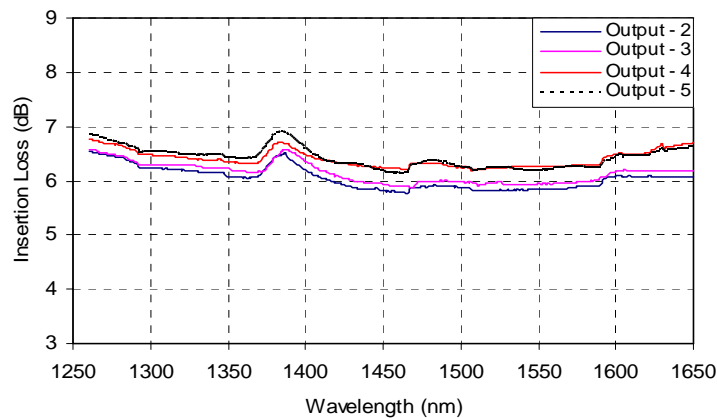

Figure 4.7: Measured wavelength response of high uniformity 1x4 coupler

The polarization sensitivity of the device is measured by splicing the input fiber of the coupler to laser through a polarization controller. While monitoring the power output from each fiber in turn, the polarization controller was adjusted so that all polarization states were launched into the coupler. The maximum and minimum power readings were recorded. Polarization dependent loss of the device is tabulated in Table 4.1 and the maximum value among all the ports is 0.15 dB. The polarization sensitivity is more at higher wavelengths, and can be controlled by changing the degree of fusion of the fibers and by carefully positioning of fibers around the central fiber.

4.3.4 Uniformity Analysis

The branching uniformity of the fabricated devise over the entire range from 1250nm to 1600nm is shown in Figure 4.8. The average branching uniformity is less than 0.5 dB. The branching uniformity performance is better at lower wavelengths and increases slightly towards the 1600nm wavelength region. This increase is attributed to the slight bending stress in the fibers due to the special braiding pattern employed to achieve the waist cross-section. Thus couplers made with new technique offers a three fold improvement in branching uniformity performance compared to the other monolithic 1x4 couplers. Also this value is comparable to the uniformity performance of splitters made using planar lightwave circuit technology.
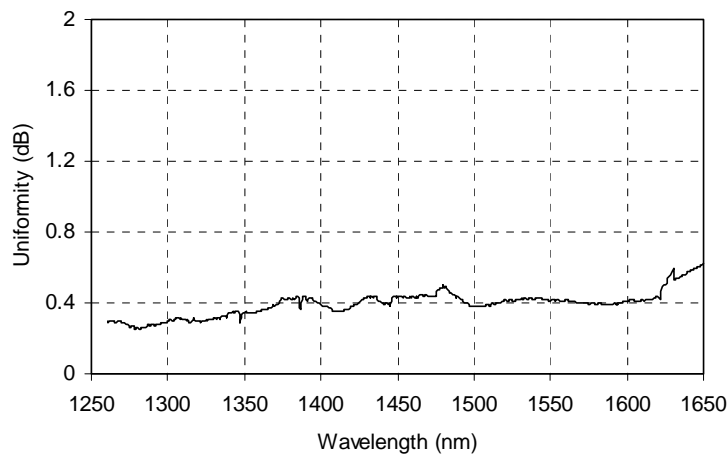

Figure 4.8: Spectral dependence of uniformity of High Uniformity 1x4 coupler

4.4 In-situ Monitoring Coupler

Tap couplers, where the coupling ratio is typically less than 10%, play a critical role in monitoring optical networks [23, 24]. Such monitoring helps to determine the presence of different optical channels and its strength. Thus integrating a monitoring coupler with a passive splitter offers an added feature. This can be realized by controlling the power remaining in the through put port of the high uniformity 1x4 monolithic couplers described in the previous sections.

We tried to fabricate couplers with 1% to 5% power remaining in the through put port. For this the central fiber in which the light is launched, is reduced in diameter to expand the mode field of the propagating light. The central fiber is pre-tapered to have a diameter around 122µm. Table 4.2 shows the measured insertion loss of a high uniformity monolithic 1x4 coupler integrated with a 2% tap port. The excess loss of the devise is less than 0.15 dB.

Output	Insertion Loss (dB)			Polarization Dependent Loss (dB)		
	1310	1490	1550	1310	1490	1550
Port 1	15.5	16.9	15.8	0.16	0.15	0.14
Port 2	6.3	6.25	6.34	0.09	0.10	0.11
Port 3	6.4	6.38	6.35	0.10	0.08	0.11
Port 4	6.1	6.05	6.12	0.10	0.11	0.12
Port 5	6.15	6.2	6.3	0.13	0.12	0.15

Table 4.2: Measured Insertion Loss and PDL of

High Uniformity 1x4 Coupler with monitoring port

4.5 Reliability Evaluation

Fused couplers are generally sensitive to mechanical and environmental stresses, causing long term splitting ratio drifts. Hence packaging of the coupler, to keep the integrity of the fused region, is very critical to maintain the performance in field over a period of time. In typical approach of fused coupler packaging [24], the fused region is protected inside a quartz substrate, using a thermally cured adhesive. The adhesive is filled with quartz powder to match its thermal coefficient with substrate and fiber. This primary packaged structure is attached inside an invar tube and end sealed. The end sealing prevents the penetration of water molecules and doesn't allow degradation of epoxy and refractive index variations at fused region.

We subjected 11 samples of the couplers for temperature cycling and temperature humidity aging [25]. For cycling test, the temperature is varied from -40^0C to $+90^0$C in 2.4hours. For humidity aging test, samples are kept at 85^0C and 85RH. A failure is defined as a change in the insertion loss above 0.5 dB in the operating regime around 1310, 1490 and 1550nm. The maximum insertion losses before and after each of the above tests are plotted in Figure 4.9 and Figure 4.10.
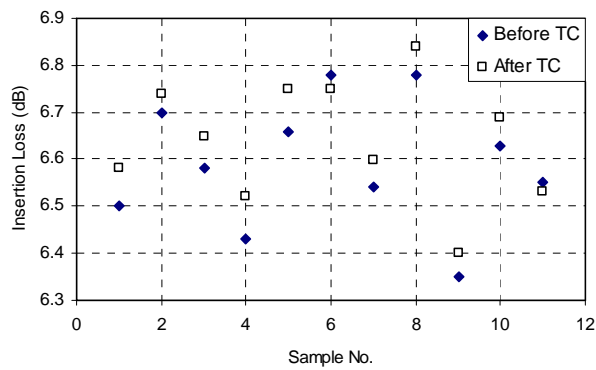
Figure 4.9: Insertion Loss before and after Temperature Cycling
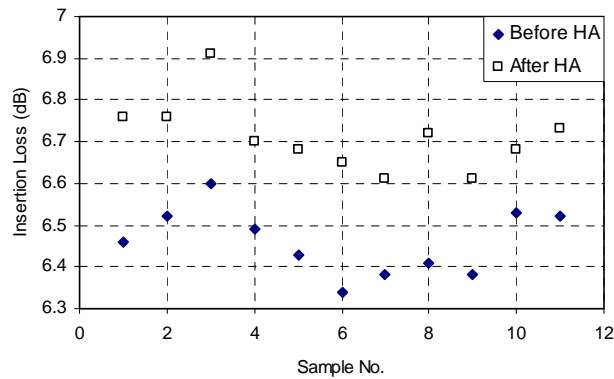
Figure 4.10: Insertion Loss before and after Humidity Aging

The result shows the stability of insertion loss and hence branching uniformity of the couplers, after the accelerated tests. The average increase in Insertion Loss in all the ports is less than 0.25 dB. In order to analyze the performance of the device at high power, it is exposed to optical power from +23dBm using in-house built erbium doped fiber amplifier. The devices showed no degradation even after a continuous

exposure of 4000hrs, at this power level. To test the performance further, we varied the temperature and humidity conditions in which the device is kept, while exposing to high power levels. However the device doesn't show any degradation in performance.

4.6 Conclusions

A simple method for the fabrication of monolithic, wavelength independent 1x4 coupler, with high uniformity has been discussed. This is realized by fusing five fibers together and transferring the entire power to the coupled fibers. The insertion loss of the device is slightly increased (by <0.1 dB), due to uncoupled power remaining in central fiber. But the spectral flatness of port-to-port uniformity is improved by three times. The device exhibits good uniformity (<0.5 dB) and low polarization dependent loss (0.15 dB) over the entire operating range. The performance is identical to planar lightwave circuit splitters. The device offers the same degree of performance and ruggedness as normally demonstrated by fused fiber components. Monolithic 1x4 couplers find applications in splitter assemblies, high port count fiber amplifiers and fiber lasers. Moreover, by controlling the process parameters it is possible to control the power remaining in the through put port of the device, which can be used for dedicated non-intrusive network health monitoring.

References

1. N.J. Frigo, ''A Survey of Fiber Optics in Local Access Architectures,'' in Optical Fiber Telecommunications, IIIA, edited by I.P. Kaminow and T.L. Koch, Academic Press, pp. 461–522, 1997.
2. E. Edmon, K.G. McCammon, R. Estes, J. Lorentzen, ''Chapter 2: Today's broadband fiber access technologies and deployment considerations at SBC,'' Broadband Optical Access Networks and Fiber-to-the-Home: Systems Technologies and Deployment Strategies, ed. Chin-Lon Lin, pp. 17-40, John Wiley & Sons, 2006.
3. N.J. Frigo, P.P. Iannone, and K.C. Reichmann, ''A view of fiber to the home economics,'' IEEE Opt. Communications, Vol.2, pp. S16–S23, Aug., 2004.
4. ITU-T Recommendation G.983.1, "Broadband Optical Access Systems Based on Passive Optical Networks (PON)", 2005.

5. ITU-T G.984.1, "Gigabit-capable Passive Optical Networks (GPON): General Characteristics", 2003.

6. ITU-T G.984.2, "Gigabit-capable Passive Optical Networks (GPON): Physical Media Dependent (PMD) layer specification", 2003.

7. ITU-T G.983.3, "A broadband optical access system with increased service capability by wavelength allocation", 2001.

8. Shigehito Yodo, Akio Hasemi and Masanobu Shimizu, "Single mode 1x8 Fused Couplers", Proceedings of 5th Conference on Optical/Hybrid Access Networks, Canada, pp. 4.05/01 - 4.05/06, September, 1993

9. Telcordia GR-1209-CORE, "Generic requirements for passive optical components", Issue 3, March 2001.

10. D. B. Mortimore, "Wavelength flattened fused couplers", Electron. Letters, Vol.21, pp. 742-743, 1985.

11. R. G. Lamont, K. O. Hill and D. C. Johnson, "Fabrication of fused twin biconical taper single mode fiber splitters: effect of unequal cladding diameters", OFC Tech Digest, pp. 78-79, 1985.

12. T. A. Birks and C. D. Hussey, "Control of power splitting ratio in asymmetric fused-tapered single mode fiber couplers", Optics Letters, Vol.13, pp 681-683, 1988.

13. Hani S. Daniel, Douglas R. Moore, Vincent J Tekippe, "Broadband MxN optical fiber couplers and method of making", US patent 5355426, October, 1994.

14. D. B. Mortimore, Monolithic 4x4 single mode fused coupler, Electron. Letters, Vol. 25, pp. 682-683, 1989

15. D. B. Mortimore, J. W. Arkwright, R. M. Adnams, "Monolithic wavelength flattened 1x4 single mode fused coupler", Electron. Letters, Vol.27, pp 2252-2253, 1991.

16. J.W. Arkwright, Novel structure for monolithic fused fiber 1x4 couplers, Electron. Letters, Vol.27, pp.1767-1768, 1991

17. Samuel Varghese, Muhammed Iqbal, Suresh Nair, V. P. N. Nampoori and C. P. G. Vallabhan, "Fabrication and characterization of monolithically fused wavelength independent 1x4 couplers" Fiber and Integrated Optics, 26, pp.245-254, 2007

18. Allan W. Snyder, "Coupled mode theory of optical fibers", J. of Optical Society of America, Vol. 62, pp. 1267-1277, 1972.

19. David Salazar, Marco Antonio Felix, Jessica Angel-Valenzuela, Heriberto Marquez, "A simple technique to obtain fused fiber optics couplers", Vol.5, Journal of the Mexican Society of Instrumentation, pp. 170-174, 2001.

20. F. Bilodeau, K. O. Hill, S. Faucher and D. C. Johnson, "Low-loss highly over coupled fused couplers: fabrication and sensitivity to external pressure", Journal of Lightwave Technology, Vol.6, pp 1476-1479, 1991

21. S. E. Moore, W. F. Gasco and D. W. Stove, "Mass production of fused couplers and couplers based devices", SPIE Proceedings, 574, Fiber Optic Couplers, Connectors and Splice Technology II, pp. 135-137, 1985.

22. P. Roy Chaudhari, M. R. Shenoy and B. P. Pal, "Fused fiber coupler components: software driven fabrication, characterization and packaging", Proceedings of the International Conference on Fiber Optics and Photonics: PHOTONICS-98, 2, pp.752- 755, 1998.

23. D. R. Moore, Z. X. Jiang and V. J. Tekippe, "Optimization of Tap Couplers made by the FBT process", Proc. SPIE, International Conference on Fiber Optics and Photonics: Photonics India '96, Vol. 3211, pp. 243 -247, 1998

24. V. J. Tekippe, "Passive fiber optic components made by fused biconical process", Fiber and Integrated Optics, Vol. 9, pp. 97-123, 1990

25. Telcordia GR-1221-CORE, "Reliability requirements for passive optical components", Issue 2, January 1999.

Chapter 5
Isolation Improvement in Fused WDMs

Isolation in fused WDMs is limited by wavelength dependence of coupling ratio and deviation from ideal coupling characteristics. All-fiber methods to improve the isolation are not compact and economical. A method is proposed to improve the isolation in fused-fiber wavelength division multiplexers, through the inscription of long period gratings fabricated by electric arc technique. This method offers a simple and compact all-fiber solution with good control of isolation over the required spectral band.

Wavelength Division Multiplexers (WDMs) are essential components in high capacity optical networks [1] and also in fiber amplifiers. WDMs are realized using various techniques like thin film filter, micro-optic and fused biconically tapered technology [2, 3]. Among these fused fiber WDMs are attractive because of the all-fiber nature, low insertion loss, stable optical performance and its compactness. Isolation is one of the key performance parameters of these devices when used as a de-multiplexer. In fused fiber devices, the wavelength dependence of the coupling ratio and deviations from ideal coupling cause the light of wrong wavelength to exit the ports of the WDM. Also, it is observed that the isolation of the fused fiber Wavelength Division De-Multiplexers (WDDM) decreases as the separation between the channel wavelengths decrease [4, 5]. These effects are undesirable, as the two wavelengths constitute two completely independent communication channels and hence contribute to the degradation in service quality.

This chapter explains the fabrication and performance parameters of fused WDMs and analyzes the factors affecting the isolation in WDMs. Different all-fiber approaches for improving the isolation in fused WDMs are discussed. Long period grating, which acts as spectrally sensitive filters are fabricated on standard single mode fibers, based on electric arc technique [6, 7]. Such long period gratings are integrated with fused WDM, demonstrating a simple and compact all-fiber method for isolation improvement.

5.1 WDM Technology: An Introduction

WDM technology enables the capacity upgradation of fiber optic links as per demand, through transmission of signals at multiple wavelengths over the same fiber as shown in Figure 5.1 [8]. At the transmitting end, a multiplexer is required to combine signals from independently modulated laser sources, to a single fiber. At the receiving end, a de-multiplexer is required to separate the optical signals into appropriate detection channels for signal processing [9]. Wavelength Division Multiplexer (WDM) / Demultiplexer is a passive component which combines / splits signals, atleast at two different wavelengths [10]. Both 1310 nm and 1550 nm wavelengths are used for long distance optical transmission. Single mode fibers available today have very low loss (typically 0.2 dB/km) and they also have very low dispersion at these wavelengths. The 1310/1550 nm WDM, with a channel spacing of 240nm is used to multiplex those telecom transmission bands. In passive optical networks, analog video signal is transmitted at 1550 nm wavelength [11], because of the low loss and the availability of erbium doped fiber amplifiers in this band.
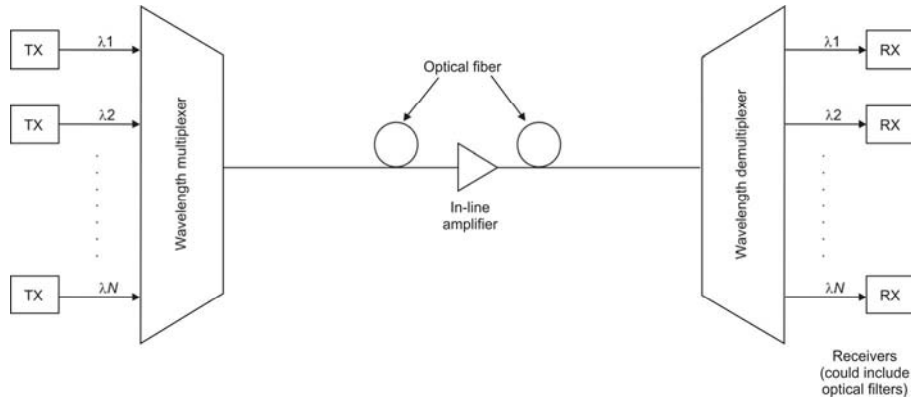
Figure 5.1: Implementation of a typical WDM network

Based on the channel spacing, WDMs are classified as narrow channel spacing and wide channel spacing (>100nm). The literature often uses the term dense WDM (DWDM) in contrast to regular WDM, where the channel spacing is less than 2nm, as specified by ITU-T G.692. WDMs can be realized by various methods as mentioned in Chapter 1. Wavelength multiplexers can also be made using Mach-Zehnder interferometry techniques. Such devices are configured with individual 2x2 couplers or using integrated optics. Arrayed Waveguide Grating (AWG), Fiber Bragg Grating etc is other technologies used for multiplexing [8]. Interleavers are used to separate a multiplexed stream to two different streams, with double the channel spacing [12]

The performance of WDM coupler is measured in terms of several characteristics such as insertion loss, isolation and directivity. Insertion loss and directivity are generic measurement indexes for any type of couplers, while isolation is specific to WDM. Isolation is a measure of how well light of an undesired wavelength is eliminated with respect to the desired wavelength at a particular port. Wavelength isolation is the key performance parameter of a WDM [13]. It is determined by measuring the power available at the output ports of a coupler at an operating wavelength and is a measure of the fracture of power blocked from input port to output port at the specified wavelength [14]. Mathematically,

$$\text{Wavelength Isolation} = 10\log\frac{P_T}{P_I}\bigg|_{\lambda 1} \tag{5.1}$$

where P_T is the power available at the throughput port and P_I is the input power, respectively at the wavelength λ_1.

105

Isolation bandwidth is another important parameter, which is a measure of the spread of wavelengths around the desired branching wavelengths. Isolation is usually quoted over a finite wavelength spread due to deviations from the specified nominal operating wavelength and finite spectral width of practical optical sources. The isolation bandwidth of a WDM is defined as the range of wavelength around the operating central wavelength, where the value of isolation is above a certain acceptable level. Passive optical components intended for use in digital systems at bit rates up to 10Gbps shall have a wavelength isolation of at least 25 dB [14]. Digital systems can operate with less isolation, but if one transmitter fails and the receive sensitivity is high or the span is short then the receiver may lock into the wrong signal. An isolation greater than 25 dB will avert this type of failure in most of the applications.

5.2 Fused Fiber WDM: Operating Principle and Fabrication

A fused WDM is a symmetric 2x2 FBT coupler, which can take two inputs at two different wavelengths, say λ_1 and λ_2, from the two input ports and combines them at one output port. Alternately, if these two wavelengths are injected into the same input port, they will get separated out at the two output ports. Such a design owes its origin to the fact that for a given coupler, the coupling coefficients and the effective length of interaction at two different wavelengths, say 1310 nm and 1550 nm, are different. Therefore the splitting ratios at these wavelengths are usually different. For a coupler to function as WDM at these two operating wavelengths, the fabrication parameters has to be optimized such that the coupling ratio at one wavelength is maximum and minimum at the other wavelength [13]. This implies that all of the input power at λ_1 will emerge at one output port, and all the input power at λ_2 will emerge at the other output, as sketched in Figure 5.2.

It is seen in Chapter 2 that the coupling characteristics of fused couplers are wavelength dependent [15]. Since the coupling coefficient is wavelength dependent, the interaction length will vary with λ[16, 17]. The coupling behaviour in fused coupler has an oscillatory response as seen in Figure 2.9. If the interaction length of a coupler is such that it is a multiple of coupling length L_c at the desired wavelengths λ_1 and λ_2, then the entire power at one wavelength will remain in one fiber and the other wavelength will come out at the second fiber. Such a coupler will act as a WDM for these two wavelengths λ_1 and λ_2. Referring to the pull signature shown in Figure 2.9, if the process is stopped at point F, the coupling ratio is 100% for 1550 nm and 0% for 1310 nm. This is the ideal point for making the wavelength division multiplexer.

Under this condition, if P_1 is the power at 1550 nm and P_2 is the power at 1310 nm, then both the wavelengths will appear without loss at the output. i.e, they will be multiplexed onto the same fiber. As a de-multiplexer, the situation is reversed and the two wavelengths are separated by the same device.
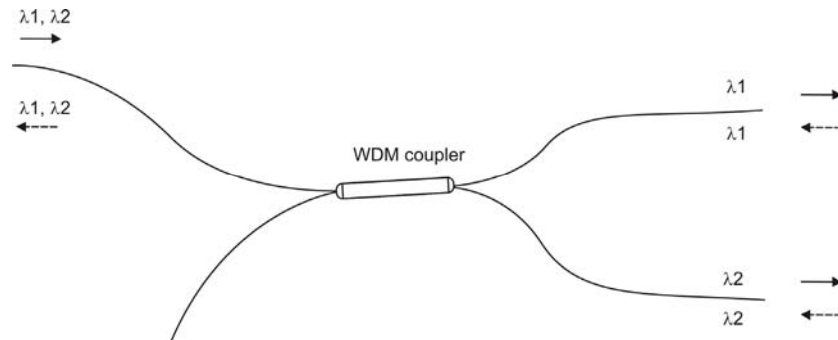

Figure 5.2: Schematic showing the operation of a fused WDM.

For a FBT coupler to function as a WDM, two conditions shall be precisely controlled. First, the channel spacing of the required WDM must be exactly identical to the wavelength separation between a maximum and a minimum in the wavelength response curve. Secondly, the wavelength corresponding to maximum and minimum splitting ratio must be precisely located in the wavelength response curve at the desired wavelengths [18]. In the actual fabrication process, the splitting ratio curve moves to the shorter wavelength side and the wavelength period decreases in successive coupling cycles [19]. The tuning of the fabrication process may be required to position the maximum and minimum coupling ratio at the desired wavelength. The fine tuning requires the control over elongation of the FBT coupler during fabrication.

1310/1550nm WDM coupler is fabricated in the same way as that of a standard coupler. Here SMF-28 single mode fiber, made by Corning, is used. In the automated fabrication process, elongation is stopped at the precise location by monitoring the maximum and minimum of the coupling ratio at one of the required wavelengths. The important item for realizing a WDM is to determine the appropriate number of coupling cycles at the monitoring wavelength. This helps in getting a channel spacing, close to the required one around the WDM wavelength. For a specific set of fabrication parameters, the central wavelength separation can be controlled by adjusting the pull length or the gas flow. Our experiments show that both of these

parameters have an inverse relationship with the channel wavelength separation. That is increasing either of these parameters will decrease the wavelength separation. The central wavelength can be set to the desired value by adjusting the preset coupling ratio in the control program. Figure 5.3 shows the wavelength response of 1310/1550nm WDM.
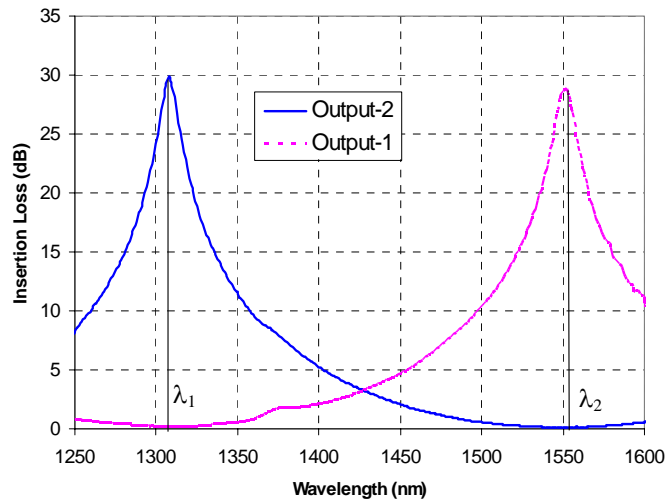

Figure 5.3: Wavelength response of a 1310/1550 WDM coupler

The same process can be extended to make WDMs such as 980/1550 and 1480/1550 etc, which are useful in the assembly of erbium doped fiber amplifiers. Corning Flexcore 1060 fiber has been used, for making 980/1550 WDMs. WDMs with narrow channel spacing (~50 nm) can be realized with fused biconical process. These couplers may exhibit a slightly higher excess loss and low sensitivity to polarization [5, 20]. To realize a narrow WDM with narrow channel spacing, large number of power coupling cycles are required. The typical half cycles observed in practice for a 1480/1550nm WDM is 20 cycles. The polarization dependence of such WDMs can be reduced by imparting a small rotation in the fused region, and devices with PDL less than 0.3dB are fabricated.

5.3 Isolation in Fused Fiber WDMs

Figure 5.4 shows the wavelength dependence of the coupling ratio for a WDM coupler fabricated with stop point at F as shown in Figure 2.9. In ideal case the coupling ratio is 100% at 1550 nm and 0% at 1310nm. As one moves away from

these wavelength, the coupling ratios are no longer ideal for a WDM. In addition, in practical, it is difficult to achieve ideal coupling even at λ_1 and λ_2 and the typical values observed in practice are 99% and 1%, respectively. These effects have a significant impact on the insertion loss and isolation made by fused taper process.
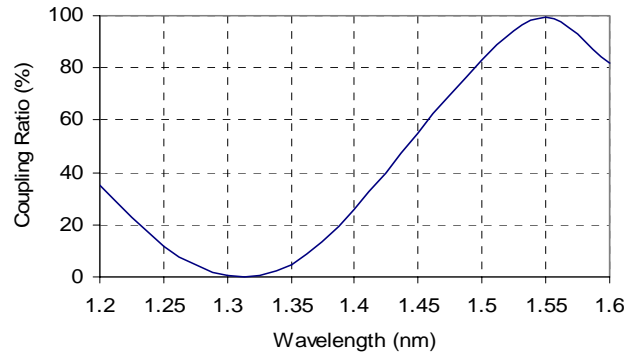

Figure 5.4: Wavelength dependence of coupling ratio of a 1310/1550 WDM coupler

For the best isolation characteristics, it is desirable that the maximum and minimum coupling ratio should occur exactly at the branching wavelengths. Isolation is of great importance, when the WDM is used as a demultiplexer. The wavelength dependence of the coupling ratio and the deviation from ideal coupling cause poor isolation performance [21]. The isolation of a WDM is shown in Figure 5.5, which shows the wavelength dependence of the isolation for a 1% deviation from the ideal. The isolation can reach 20dB near 1310nm, when the coupling ratio is ideal, but falls off rapidly as one moves away from 1310nm. Typical demultipelxers are specified at 20 dB over a ±10nm bandwidth or 16dB over a ±20nm bandwidth. This isolation bandwidth is significant because the central wavelength of single mode sources usually varies over a 20 to 30nm band.

The insertion loss of the WDM is the amount of light that is lost in the device and is determined by comparing the useful output light to the input light. This is a key parameter for both multiplexers and de-multiplexers, because it affects the overall system power budget. The fusion process itself contributes a small loss called excess loss. In addition, for a WDM, losses can occur because of the wavelength dependence of the coupling ratio and the non ideal coupling. Thus the total insertion loss of WDM consists of the excess loss and the wavelength dependence / non-ideal coupling.
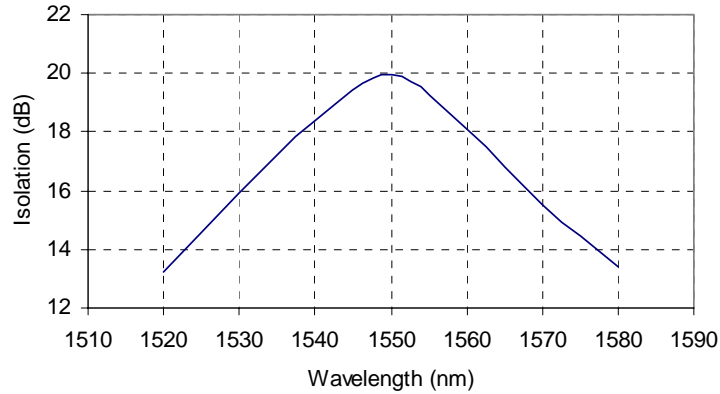
Figure 5.5: Wavelength dependence of the isolation of a fused 1310/1550 WDM, with a coupling ratio of 1% at 1550nm.

5.4 All-Fiber Methods for High Isolation WDMs

The isolation offered by a single fused WDM is usually not sufficient for most telecommunication applications, where the requirement is as much as 30 - 35 dB isolation. One simple way to improve the isolation is to add bulk component band pass filters at the appropriate wavelengths just before the receivers, an efficient way without increasing the complexity and insertion loss. But, as data rate increase, however, it gets more difficult to insert filters and many systems now require single mode fiber right up to the detector. Also all-fiber components will have increased component stability over bulk optic counterparts.

Typical isolation achieved using fused fiber technology is around 20-24 dB. For 1310/1550 nm WDM, for a coupling ratio variation of 1%, the achievable isolation is around 22 dB, more than such accuracy of 1% is very difficult to achieve in FBT process. Various methods are used to improve the isolation of fused fiber WDMs. A simple way to increase the isolation in fused WDMs is by concatenating multiple WDMs [22], additional WDMs serve as filters to clean up the outputs of the WDM as shown in Figure 5.6. Of course the complexity and cost of the resulting device is increased, but it offers an all-fiber method for obtaining higher isolation.

If identical WDMs centered at 1310nm is used to make the concatenated WDM, then the insertion loss will be less than 1 dB and the peak isolation will be 40 dB at the centre wavelength. But the isolation varies rapidly as one moves away from the

central wavelength. Since individual components are used to make concatenated WDM, there exists some flexibility in choosing the components and hence trade-offs can be made between peak isolation and the isolation bandwidth. Figure 5.7 shows the isolation of a device made of WDMs whose peak positions are symmetrically displaced about 1300nm by ±20nm. The upper curve shows the isolation of the concatenated WDM made from the two WDMs. Clearly, the useful bandwidth has been improved with some decrease in isolation at the centre wavelength.
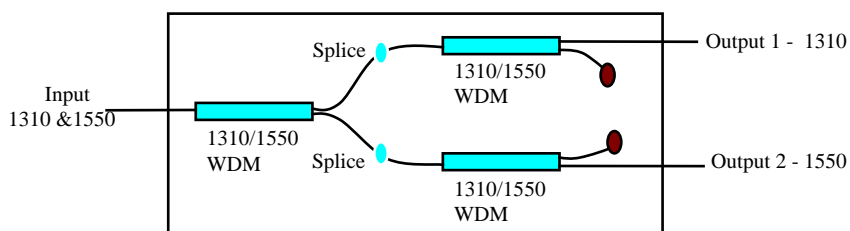
Figure 5.6: Concatenated WDMs in demultiplexing configuration
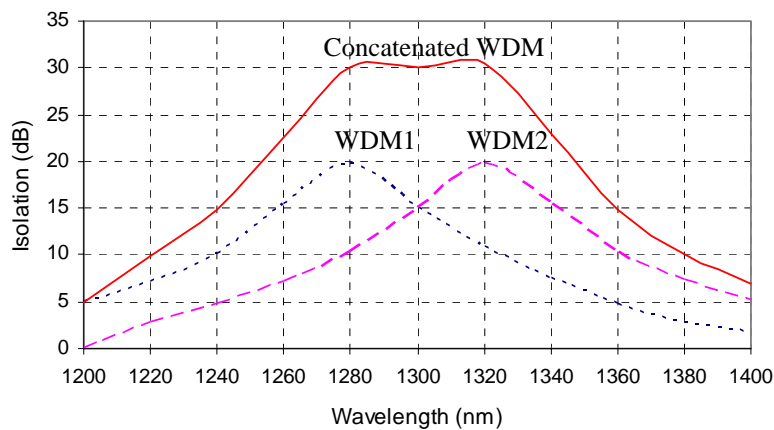
Figure 5.7: Isolation curve of a concatenated WDM, whose peak positions are separated by 40nm around 1300nm.

Another all-fiber solution to improve isolation comes from inline spectral filters such as tapered fiber filters [23]. The tapered fiber filters are ideal where high isolation bandwidth is required and hence is not suitable for devices that operate in the Coarse Wavelength Division Multiplexing domain. Although it is possible to achieve narrow

band isolation by concatenating tapered filters, but the process gets complicated and device become very lengthy. However long period gratings, which acts as spectrally sensitive loss elements with narrow bandwidth [24], are compact and can be integrated into the same fiber [25] in which WDMs are fabricated.

5.5 Long Period Gratings: An Overview of Fabrication Methods

Fiber gratings are increasingly being used in optical networks, for variety of applications. The devices are typically fabricated by exposing photosensitive fiber to a spatially periodic pattern of UV radiation. This periodic perturbation in the fiber core causes power to couple between the modes of the fiber. Fiber gratings in general are classified according to the grating period into Fiber Bragg Grating (FBG) with grating period of about 1 μm and Long Period Grating (LPG) having a grating period of about 100 μm [24]. In FBG, the diffracted light travels contra-directionally to the light launched and in an LPG, that diffracted light is co-directional with the launched light as shown in Figure 5.8. FBGs find applications as laser diode stabilizers, mode converters, fiber lasers, band-pass filters, add-drop filters, dispersion compensators, optical sensors [26, 27, 28] etc, whereas LPGs are generally used as non-reflecting band-rejection filters and source-noise suppressors [24] and, more importantly, as gain-equalising or gain-flattening filters for erbium-doped fiber amplifiers (EDFAs) [29, 30, 31]. Other communications applications include LPGs employed as comb filters [32], wavelength-selective optical fiber polarisers [33, 34, 35, 36], add-drop couplers [37], components in wavelength division multiplexing (WDM) systems [38, 39, 40] or in all-optical switching [41], and for chromatic dispersion compensation [42].
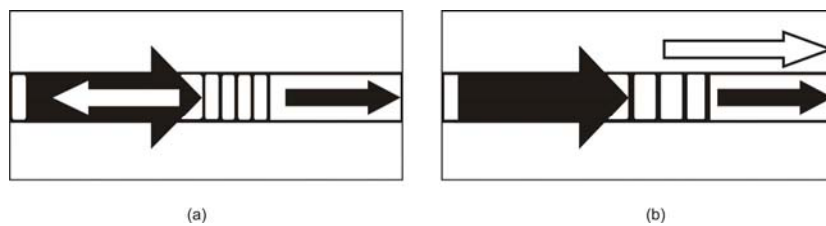

Figure 5.8: Light propagation in FBG (a) and LPG (b)

Sensitivity of doped-glass to UV light has been reported in literature for a number of years. The use of photo-sensitivity to obtain a periodic refractive index modulation in a germano-silicate optical fiber was discovered by Hill in 1978 [43]. These fiber gratings became prominent in their application areas after the side-wring technique

was invented in 1989 [44] and till researchers increased the photo-sensitivity of telecommunication grade fiber by hydrogen-loading. When an optical fiber is irradiated by ultraviolet (UV) light the refractive index of the fiber changes permanently; a phenomena termed as photosensitivity [45]. The change in refractive index is permanent if the optical waveguide after exposure is annealed appropriately. The magnitude of refractive index change (Δn) obtained depends on several factors such as the irradiation conditions, the composition of glassy material forming the fiber core and any processing of the fiber prior to irradiation. The refractive index change can be enhanced (photosensitization) by processing the fiber prior to irradiation using techniques such as hydrogen loading or flame brushing.

Fiber gratings can be fabricated by a variety of techniques. The more versatile and widely used techniques such as interferometric, phase masks, amplitude masks, and point-by-point technique, employ UV writing procedure by single-photon absorption. In the Holographic (interferometric) technique UV light from a laser is split into two and allowed to interfere to form a standing wave pattern of periodic spatial light intensity that writes a corresponding periodic index grating in the core of the fiber [44]. This method known as the transverse holographic technique is possible because the fiber is transparent to the UV light where the fiber core is highly absorbing. In the phase mask technique, the ultraviolet light which is incident normal to a phase mask, is diffracted by its periodic corrugations [46]. The phase mask is made from flat slab of silica glass, which is transparent to ultraviolet light. On one of the flat surfaces, a one dimensional periodic surface relief structure is etched using photolithographic techniques. The shape of the periodic pattern approximates a square wave in profile. The optical fiber is placed almost in contact with the corrugations of the phase mask. A drawback of the phase mask technique is that a separate phase mask is required for each Bragg wavelength. The phase mask technique not only yields high performance devices but also flexible in that it can be used to fabricate gratings with controlled spectral response characteristics. The phase mask technique has also been extended to the fabrication of chirped or aperiodic fiber gratings.

A simple, yet efficient way of fabricating LPGs is the amplitude mask technique where an amplitude mask with variable transmittance is used to modulate the UV light falling on the optical fiber. Point-by-point technique bypasses the need of a master phase mask and fabricates the grating directly on the fiber, period by period, by exposing short sections of the fiber to a high energy pulse. The fiber is translated

by a distance before the next pulse arrives, resulting in a periodic index pattern such that only a fraction of each period has a higher refractive index. The method is referred to as point-to-point fabrication. The technique works by focusing an ultraviolet laser beam so tightly that only a short section is exposed to it.

Besides illumination of the fiber by UV light, there are a number of ways to manufacture LPGs by altering the refractive index of the core. These include [47] irradiation from a carbon-dioxide laser, radiation with femtosecond pulses, writing by electric discharge, ion implantation, and dopant diffusion into the fiber core. Fibre deformation is less commonly used for fabricating LPGs, but various novel methods have been reported, such as: modification of the fiber core by periodic ablation and annealing [48], corrugation of the cladding [49, 50], and micro-structuring of tapered fibers [51].

The continued investigation of methods for LPG manufacture that do not require photosensitization and UV-irradiation has led to the use of electric arcs from a commercial fiber fusion splice machine [52]. The greatest advantage of this method is the simplicity of the procedure; there is also no need to use expensive laser equipment. Furthermore [53], any type of fiber can be used for writing gratings in this way without prior photosensitising, since it is predominantly the local heating of silica that creates the modulation in the fiber.

The fabrication process of LPGs by electrical discharge is very simple. The coating of the fiber is removed before fixing it to a translation stage controlled by a motor that allows the straightened fiber to move past the electrodes of a fusion splicer at predetermined intervals (this motion stipulates the grating period) [54]. An electric arc discharge is applied to the fiber situated between the electrodes, and the electric current (which determines intensity of the discharge) and duration of exposure is typically user defined. [31, 52-54]. Point-by-point writing occurs by advancing the fiber after each discharge has occurred, and the strength of the grating is increased to its desired level by repeating the entire process a specific number of times. Several mechanisms have been proposed as reasons for grating formation by electric arc discharge Investigations have provided evidence that it is mainly the relaxation of internal residual stresses that ensure LPGs can be manufactured with this method [53]. The discharges applied to specific points along the fiber cause rapid variations in temperature at these locations, which serve to anneal the fiber locally, thereby providing periodic changes in the residual stress distributions that facilitate mode

coupling. It has also been suggested that local cooling rates in excess of 1000 degrees Celsius per second can lead to a localised change in the density, viscosity and index of refraction of the glass, as well as Rayleigh scattering – all contributing to mode coupling subsequent to application of the electric discharge [53].

These gratings are also less sensitive to temperature fluctuations in the low temperature range (30-160°C) than LPGs written by UV-irradiation, as can be seen by the smaller spectral shift of the resonant wavelengths. Another advantage of gratings formed with the electric arc discharge method is that they are very stable at high temperatures. If the temperature is kept below the strain point of the fiber (i.e. the point at which residual stresses are annealed and stress relaxation begins), the spectral characteristics due to temperature are linear, but further heating may even cause plastic deformation of the fiber [53]. Fabrication methods with electric arc are attractive as they can provide a simple and flexible means of producing LPGs of relatively good performance. Such LPGs can be written on any type of optical fiber as their characteristics are mainly defined by intrinsic properties of silica glass itself. The LPGs act as a spectrally sensitive loss element by rejecting a narrow band signal and hence can be integrated with fused WDMs to improve the isolation at required ports.

5.6 Theoretical Background

A perfect dielectric waveguide can transmit optical energy by any of its guided modes without converting the energy to any other possible guided modes or to the non-guided modes which consists of a discrete set of cladding modes and a continuous spectrum of radiation modes. Any imperfection in the guide, such as a local change of its index of refractive or a deviation from perfect straightness or an imperfection of the interface between two regions with refractive indices, couples the power in a particular guided mode among other guided modes as well as unguided modes. Coupled mode theory describes the energy exchange, and serves as the primary tool for designing optical couplers and filters.

5.6.1 Coupled Mode Equation for Periodic Coupling

Consider a waveguide with a refractive index profile $n^2(x, y)$ in which there is an z-dependent perturbation given by $\Delta n^2(x, y, z)$. Let $\psi_1(x, y)$ and $\psi_2(x, y)$ be the two modes of the waveguide in the absence of perturbation. The total field at any value of z is given by:

$$\psi(x, y, z) = A(z)\psi_1(x, y)e^{-i\beta_1 z} + B(z)\psi_2(x, y)e^{-i\beta_2 z} \tag{5.2}$$

β_1 and β_2 are the propagation constants in the absence of perturbation and *A(z)* and *B(z)* are the corresponding amplitudes. Here, the modes with propagation constants, β_1 and β_2 are propagating in the +z direction. In the absence of perturbation *A* and *B* are constants; the perturbation, however couples power among the modes and hence *A* and *B* are z-dependent. Since ψ_1 and ψ_2 are modes of the fiber in the absence of any perturbation, they must satisfy the following equations:

$$\nabla_t^2 \psi_1 + \left(k_0^2 n^2(x, y) - \beta_1^2\right)\psi_2 = 0 \tag{5.3}$$

$$\nabla_t^2 \psi_2 + \left(k_0^2 n^2(x, y) - \beta_1^2\right)\psi_1 = 0 \tag{5.4}$$

where
$$\nabla_t^2 = \nabla^2 - \frac{\partial^2}{\partial z^2} \tag{5.5}$$

They also satisfy the orthogonality condition:

$$\int\limits_{-\infty}^{\infty}\int\limits_{-\infty}^{\infty} \psi_1^*(x, y)\psi_2(x, y)dxdy = 0 \tag{5.6}$$

In the presence of a perturbation in refractive index, the wave equation to be satisfied by $\psi(x, y, z)$ is

$$\nabla_t^2 \psi + \frac{\partial^2 \psi}{\partial z^2} + k_0^2 \left[n^2(x, y) + \Delta n^2(x, y, z)\right]\psi = 0 \tag{5.7}$$

Substituting for ψ from Equation 5.2, and neglecting double derivatives of *A* and *B* w.r.t *z* (under slowly varying approximation),

$$-2i\beta_1 \frac{dA}{dz}\psi_1 - 2i\beta_2 \frac{dB}{dz}\psi_2 e^{-i\Delta\beta z} + k_0^2 \Delta n^2(x, y, z)\left[A\psi_1 + B\psi_2 e^{-i\Delta\beta z}\right] = 0 \tag{5.8}$$

where
$$\Delta\beta = \beta_1 - \beta_2 \tag{5.9}$$

Multiplying Equation 5.8 by ψ_1^* and integrating and then further multiplying by ψ_2^* and integrating, we get after simplifications:

$$\frac{dA}{dz} = -iC_{11}A - iC_{12}Be^{i\Delta\beta_z} \tag{5.10}$$

$$\frac{dB}{dz} = -iC_{22}B - iC_{21}Ae^{-i\Delta\beta_z}$$

(5.11)

where
$$C_{ij}(z) = \frac{k_0^2}{2\beta_i} \frac{\int\int \psi_i^* \Delta n^2 \psi_j dxdy}{\int\int \psi_i^* \psi_j dxdy}$$

(5.12)

Equations 5.10 and 5.11 represent the coupled mode equations and describe the z-dependence of *A* and *B*.

5.6.2 Co-directional Coupling

In the presence of z-dependent sinusoidal perturbation, we may write:

$$\Delta n^2(x, y, z) = \Delta n^2(x, y)\sin Kz$$

(5.13)

where $K = \frac{2\pi}{\Lambda}$, and Λ is the spatial period of perturbation. This gives

$$C_{ij}(z) = \frac{k_0^2 \sin Kz}{2\beta_i} \frac{\int\int \psi_i^* \Delta n^2 \psi_j dxdy}{\int\int \psi_i^* \psi_j dxdy}$$

(5.14)

$$C_{ij}(z) = 2\kappa_{ij} \sin Kz$$

(5.15)

$$\kappa_{ij} = \frac{k_0^2}{4\beta_i} \frac{\int\int \psi_i^* \Delta n^2(x, y)\psi_j dxdy}{\int\int \psi_i^* \psi_j dxdy}$$

(5.16)

Substituting in Equation 5.10 we get

$$\frac{dA}{dz} = -2i\kappa_{11}A\sin Kz - B\kappa_{12}e^{i(\Delta\beta+K)z} + B\kappa_{12}e^{i(\Delta\beta-K)z}$$

(5.17)

For weak perturbations, the coupling coefficients, κ_{12} and κ_{21} are small and hence, the typical length scale over the modes amplitude change $(1/\kappa_{12}) \sim (1/\kappa_{21})$, is large. It can be shown that $\Delta\beta \sim K$, the contributions from the first and second terms of the RHS Equation 5.17 are negligible as compared to the third term and hence can be neglected. However, the second term would have made significant contribution if $\Delta\beta = \beta_1 - \beta_2 = -K$. Thus in the presence of a periodic perturbation, coupling takes place mainly between the modes for which $\Delta\beta$ is close to either *K* or –*K*. The

approximation retaining either $e^{i(\Delta\beta-K)z}$ term or $e^{i(\Delta\beta+K)z}$ term in Equation 5.17 is called the synchronous approximation.

Hence under this approximation, Equation 5.17 can be written as

$$\frac{dA}{dz} = \kappa_{12} B e^{i\Gamma z} \qquad (5.18)$$

where $\qquad\qquad \Gamma = \Delta\beta - K \qquad (5.19)$

Similarly, $\qquad\qquad \dfrac{dB}{dz} = -\kappa_{21} A e^{i\Gamma z} \qquad (5.20)$

If modes Ψ_1 and Ψ_2 are normalized to carry unit power, then under the weakly guiding approximation, we may write:

$$\frac{\beta_i}{2\omega\mu_0} \iint \psi_i^* \psi_i dxdy = 1 \qquad (5.21)$$

Using orthogonality condition, we can show that:

$$\kappa_{12} = \kappa_{21} = \kappa \qquad (5.22)$$

Thus the two coupled equations become

$$\frac{dA}{dz} = \kappa B e^{i\Gamma z} \qquad (5.23)$$

$$\frac{dB}{dz} = -\kappa A e^{i\Gamma z} \qquad (5.24)$$

These two equations describe the coupling between two modes propagating along the same direction i.e β_1, β_2 have the same sign. Such kind of coupling is co-directional coupling, as explained earlier also.

5.6.2.1 Co-directional Coupling under Phase Matching Condition

Phase matching condition is given by $\Gamma = 0$

i.e $\qquad\qquad \beta_1 - \beta_2 = K \qquad (5.25)$

Thus the periodic perturbation should have period

$$\Lambda = \frac{2\pi}{\beta_1 - \beta_2} = \frac{\lambda_0}{(n_{e1} - n_{e2})} \qquad (5.26)$$

where $\beta_1 = \frac{2\pi n_{e1}}{\lambda_0}$ and $\beta_2 = \frac{2\pi n_{e2}}{\lambda_0}$, n_{e1}, n_{e2} are the effective refractive indices of the

two modes. Then equations (5.23) and (5.24) become

$$\frac{dA}{dz} = \kappa B \qquad (5.27)$$

$$\frac{dB}{dz} = -\kappa A \qquad (5.28)$$

Differentiating (5.28) and making substitution from (5.27), we obtain

$$\frac{d^2 B}{dz^2} = -\kappa^2 B \qquad (5.29)$$

Its solution is $\qquad B = b_2 SinKz - b_1 CosKz \qquad (5.30)$

Similarly $\qquad A = b_1 SinKz - b_2 CosKz \qquad (5.31)$

Initial conditions assume that $z=0$, the mode, ψ_1 is launched with unit power,

$$A/_{z=0} = 1 \qquad (5.32)$$

And initially, ψ_2 had no power in it,

$$B/_{z=0} = 0 \qquad (5.33)$$

Thus $b_1 = 0$ and $b_2 = -1$ and therefore

$$A(z) = \cos \kappa z \qquad (5.34)$$

Similarly $\qquad B(z) = -\sin \kappa z \qquad (5.35)$

Thus the powers carried by the two modes vary with z as;

$$P_1 = |A(z)|^2 = \cos^2 \kappa z \qquad (5.36)$$

and
$$P_2 = \left| B(z) \right|^2 = \sin^2 \kappa z \qquad (5.37)$$

5.6.3 Contra-directional Coupling

When coupling takes place between the two modes propagating in opposite directions, it is known as contra-directional coupling. In such a case, we have to choose

$$\psi(x, y, z) = A(z)\psi_1(x, y)e^{-i\beta_1 z} + B(z)\psi_2(x, y)e^{i\beta_2 z} \qquad (5.38)$$

Here the mode with propagation constant β_1 is propagating in the $+z$ direction and the mode with propagation constant β_2 is propagating in the $-z$ direction. Following an exactly similar procedure, one obtains coupled mode equations for contra-directional coupling as:

$$\frac{dA}{dz} = \kappa B e^{i\Gamma z} \qquad (5.39)$$

$$\frac{dB}{dz} = \kappa A e^{-i\Gamma z} \qquad (5.40)$$

The signs on the RHS of Equations 5.39 and 5.40 are same unlike that in co-directional coupling, therefore the solution in this case are not oscillatory.

5.6.4 Long Period Gratings

The pattern of refractive index modulation in the fiber core acts as a perturbation that serves to couple power between the "matched" modes of the optical waveguide. Figure 5.9 depicts the propagation constant of various spatial modes in the fiber. The forward propagating guided modes have their propagation constants β that lie in the range $\frac{2\pi n_2}{\lambda} < \beta < \frac{2\pi n_1}{\lambda}$ where n_1 and n_2 are indices of refraction of the core and cladding respectively.

For a single-mode fiber, the propagation constant of the guided mode can be represented by $\beta_{co} = \frac{2\pi n_{co}}{\lambda}$, where n_{co} is the effective index of the mode. For mode coupling to occur between two modes, the propagation constant difference between

these modes $\Delta\beta$ (represented as $\Delta\beta_{FBG}$ in Figure 5.9) should match the "phase vector" of the grating:

$$\Delta\beta = \frac{2\pi}{\Lambda}$$

(5.41)

where Λ is the periodicity of the grating. For coupling to occur from the forward to the reverse propagating guide mode ($\beta = -\beta_{co}$), $\Delta\beta$ needs to be relatively large and thus the periodicity of the required grating is small. Such short-period gratings, commonly called as Braggs gratings, have typical periodicity around 0.5 μm for coupling in the 1550 nm window. The overlap interval between the two coupling modes over the grating cross-section determines the magnitude of the power coupled. Long-period gratings are utilized to couple the forward-propagating guided mode to one or more forward-propagating guided or cladding modes [24]. Since the required propagation constant difference $\Delta\beta$ (depicted as $\Delta\beta_{LPG}$ in Figure 5.9) between the coupled modes is relatively small, Equation 5.41 predicts that the required grating periodicity is fairly large.
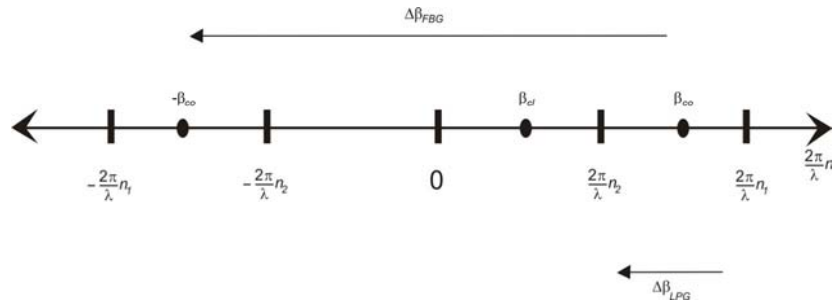

Figure 5.9 Depiction of mode-coupling in short- and long-period fiber gratings based on the difference between propagation constants of the coupling modes.

The optical power transmitted through the fiber as core modes at a wavelength λ, is coupled between core modes and cladding modes at the grating region. In one approach this coupling process may be expressed as

$$\lambda = \frac{(n_{co} - n_{cl}(p))}{\Lambda}$$

(5.42)

where Λ, n_{co}, $n_{cl}(p)$ are the period of the grating, the effective refractive index of any of the core modes and the effective refractive index of the pth cladding mode respectively. This equation is similar to Equation 5.26. Since, in single mode fibers

121

there exists only one core mode (LP_{01}) and many cladding modes (LP_{1p}), the core-cladding coupling occurs at certain specific wavelengths. These wavelengths can be found out by calculating the various values of $n_{cl}(p)$ which inturn is determined by assuming a step index profile for the cladding and ignoring the presence of the core. The light in the cladding quickly decays due to losses at the cladding / air interface, leaving a series of loss bands or resonance in the guided modes.

Another method of calculating the wavelength separation between the different cladding modes makes use of the cut-off wavelength λ_{cut}, which is the wavelength at which a given mode switches from a cladding mode to radiation mode or vice versa. Consider the transverse component of the propagation constant of the cladding mode κ. This component satisfies the condition

$$\beta_{cl}^{2} + \kappa^{2} = \frac{\omega^{2} n_{cl}^{2}}{c^{2}} \tag{5.43}$$

where β_{cl} is the propagation constant of the cladding mode, ω is the angular frequency of the radiation and c is the velocity of light. The separation in wavelength between the pth cladding mode and λ_{cut}, is found by using the above two equations,

$$\lambda_{p} - \lambda_{cut} \approx \frac{\lambda_{p}^{2} \lambda_{cut}^{2}}{8 n_{cl}(n_{co} - n_{cl})} \frac{p^{2}}{a_{cl}^{2}} \tag{5.44}$$

where n_{co} is the effective refractive index of the guided LP_{01} mode and a_{cl} is the cladding radius. For the first few cladding modes one can further simplify the expression by assuming that λ_{p} and λ_{cut} are in close proximity. The wavelength separation between the pth and the $(p+1)^{th}$ mode can then be approximated by

$$\delta\lambda_{p,p+1} \approx \frac{\lambda_{cut}^{3}}{8 n_{cl}(n_{co} - n_{cl})} \frac{(2p+1)}{a_{cl}^{2}} \tag{5.45}$$

The ratio of power coupled into the nth cladding mode to the initial power contained in the guided LP_{01} mode is then given by

$$\frac{P_{cl}^{(n)}(l)}{P_{01}(0)} = \frac{\sin^{2}\left[\kappa_{g} L \sqrt{1 + \left(\delta/\kappa_{g}\right)^{2}}\right]}{1 + \left(\delta/\kappa_{g}\right)^{2}} \tag{5.46}$$

where δ is the detuning parameter given by

$$\delta = \frac{1}{2}\left\{ \beta_{01} - \beta_{cl}^{(n)} - \frac{2\pi}{\lambda} \right\} \tag{5.47}$$

κ_g is the coupling constant for the grating and L is the grating length. The coupling constant κ_g is proportional to the index change and is typically to maximize the power transfer to the cladding mode. Thus Δn (and hence, κ_g) is increased until the condition $\kappa_g = \pi/2$ is met. Thus the intensity of the perturbation and the length of the grating determine the isolation of the filter. An approximate expression of the full width at half maximum (FWHM) $\Delta\lambda$, for a resonance band, at the complete power transfer condition is [24];

$$\Delta\lambda = \frac{0.8\lambda^2}{L(n_{co} - n_{cl})} \tag{5.48}$$

Thus the FWHM of the resonance is inversely proportional to the length of the grating, L. The spectral response of the LPG depends on the period, the intensity of the perturbation and the grating length.

5.7 Fabrication of LPGs with Electric Arc Technique

Our experimental setup for long period grating fabrication consists of an arc generator, fiber holder mounted on a translational cum rotational stage, optical spectrum analyzer and a white light source, as shown schematically in Figure 5.10. This is similar to the setup described in [54,55,56]. The grating fabrication consists of positioning the uncoated fiber between the electrodes of the arc generator, based on a commercially available fiber optic splicing machine from Furukawa. One end of the fiber is clamped in a fiber holder attached to a motorized translation stage, which moves with a precision of 0.1 μm. At the other end the fiber is attached to a mass (~4 gm) through a pulley to provide constant axial tension. An electric discharge is then produced with a current less than 10mA, for a duration of ~1s. Afterwards the fiber is moved by grating period followed by a new electric discharge. The displacement discharge process is then repeated 15-40 times, giving rise to periodic perturbations along the fiber due to its local heating. A broadband light is launched to the fiber and the transmitted power is monitored using an optical spectrum analyser in order to analyse the evolution of the grating characteristics.

Local section of the normal fiber heated by application of electric arc at periodic intervals is deformed as decreasing core and cladding diameter, due to the

longitudinal tension. The change in the diameter depends on the arc condition and tension applied [56]. The core and cladding diameter reduces with arc time. Decreasing the core and cladding diameter cause increasing of mode coupling coefficients and decreasing core and cladding effective indices. The mode coupling in these gratings can be explained due to the change of glass properties by fast local heating-cooling process. The fast local heating – cooling process anneals periodically residual stresses and create new stresses, and results in mode coupling [53]

Certain experimental setups suggest constant tension applied along the length of the fiber using a mass piece attached to the one end of the fiber [50, 51], whereas minimal or no axial strain is exerted in other cases [52, 54]. The effect of this tension is to cause periodic tapering (i.e. narrowing of fiber diameter) where discharges have occurred, but this phenomenon plays a minor role in the grating quality and is not necessary for LPG manufacture [53]. Adding tension to the fiber does tend to increase insertion loss, but it was also found to be beneficial – fewer discharges are required for a greater isolation loss in LPGs where axial stress was applied during manufacture.

Unlike UV-induced LPGs, gratings manufactured with this method do not undergo changes in their resonant wavelengths (observed in transmission) as the grating strength is increased. Thus the spectral characteristics only depend on the length and the grating period, providing a method to manufacture LPGs whose mode coupling characteristics are quite predictable. There may be an anisotropy introduced in the fiber, because of the asymmetry of the electric discharge [55]. This anisotropy changes the polarization of the excitation signal. Also, resonance wavelength of LPGs induced by single arc per grating is difficult to reproduce, because of irregularity in fiber deforming. So for more stable fabrication, we generate not just one arc, but several weak ones periodically in a single grating.
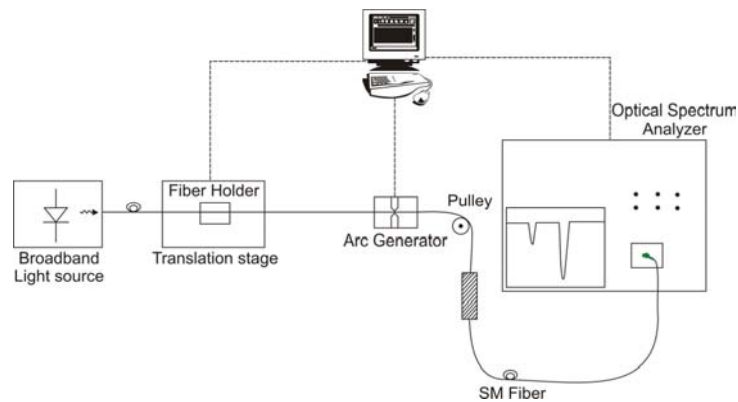
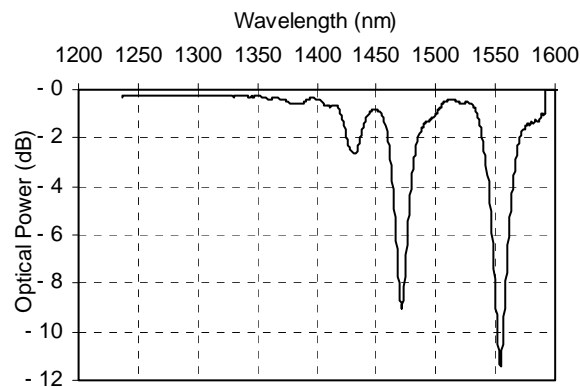Figure 5.10: Fabrication set-up for LPG

Figure 5.11: Transmission spectrum of the LPG

Long Period Fiber Gratings are fabricated with a period of 610 μm on standard Corning SMF-28 fiber (Corning), having dimensions of 9/125 μm. The transmission characteristic of LPG is shown in Figure 5.11. The response shows three resonance wavelengths corresponding to the coupling from the core mode to a particular cladding mode. During the fabrication the spectral response of the grating is monitored after each step. Figure 5.12 shows the growth of LPG at different grating lengths with a constant period of 610 μm. The optical power transfer increases with the grating length. Figure 5.12 shows the evolution of isolation during the fabrication at 15, 25 and 35 arcs respectively. The isolation increases after each arcs, while the loss at non-resonant wavelengths remains almost unaltered. The insertion loss is evaluated to be less than 0.3 dB. The process is stopped at the required isolation. It is observed that both the arc power and arc time has a role in determining the loss and isolation of the grating. The intensity of perturbation and length of the grating

determines the isolation. The peak loss of the resonance wavelength becomes larger as the grating length increases, the lower resonance wavelengths change more slowly than those of the higher modes.

Gratings with different periods have been fabricated, the peak resonance wavelength changes linearly to higher wavelengths, for a specific set of other fabrication parameters (keeping arc current, arc duration and number of grating as constant). Gratings were fabricated with different arc time, while keeping all other parameters as constant. The arc time is varied from 500 ms to 1000 ms. A shift in resonance wavelength is observed for lower wavelength resonance peaks to shorter wavelengths, while that of the higher wavelength resonance peak remains as the same.
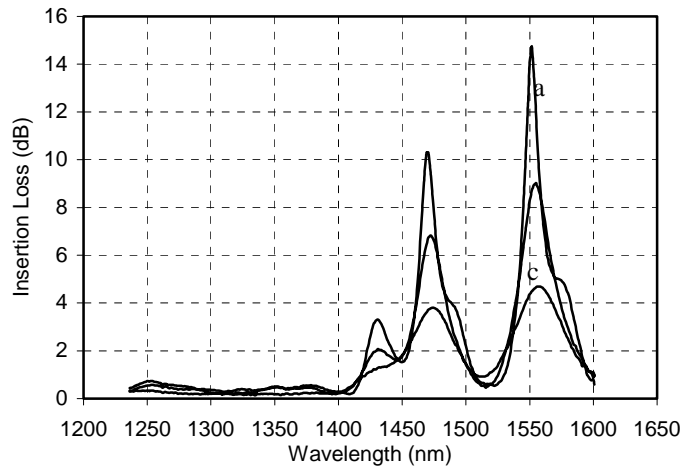

Figure 5.12: Isolation Evolution of the LPG

The local temperature of the fiber during the arc exposure is more than silica glass softening temperature. So for moderate applied tension, a tapering of the fiber is observed, which increases as the axial tension is increased. As the tension on the fiber increases the degree of tapering increases, the insertion loss and isolation also increases. Decreasing the core and cladding diameter cause increasing of mode coupling coefficients at the expense of higher polarization sensitivity and less mechanical strength. Hence it is better to reduce the diameter modulation to the minimum level to reduce the polarization sensitivity. Also, it is observed that the asymmetry of the electric discharge contributes to the polarization sensitivity. Intentional rotation during the grating fabrication is also incorporated. The fabricated

126

LPG show isolation up to 14 dB while keeping the insertion loss at the non-resonant wavelengths to below 0.3 dB. By optimizing the process the isolation can be improved upto 25 dB, with out compromising the polarization performance. The polarization dependent loss of the device is measured by varying the polarization of the input light over all possible states and by observing the variation in insertion loss. With normal process the PDL was around 1.5 dB, but with rotation incorporated, the PDL could be controlled to below 0.3 dB.

The transmission spectrum of LPG is susceptible to both bending and twisting and the resonance peak may shift or split due to these effects. Hence the packaging of these devices needs care for repetitive spectral performance. Packaging of these devices is done by fixing the grating on a quartz substrate with the same tension and bonding it to the substrate with suitable epoxy, as done for the fused couplers. As the thermal expansion of quartz is identical to the fiber, it does not create any additional strain on the grating region, due to temperature variations or external perturbations. A Kovar tube protects this preliminary package.

5.8 Integration of LPGs in Fused WDM

WDMs are fabricated using the fused fiber coupler station as described in Chapter 2, where the fibers are biconically tapered until the desired coupling characteristics are achieved, by online monitoring the CR. Long period gratings are then fabricated on the respective ports of these WDMs, using a set up as described in section 5.7. As the LPGs couple power from guided mode to forward propagating cladding modes – propagating in the same direction, until being completely attenuated by scattering in air-cladding interface and in fiber coating – these devices have excellent back reflection. The process is stopped at the required isolation by real time monitoring the values. The packaging of this integrated WDM is done in a similar fashion of the FBT devices, to make it less sensitive to environmental variations. The fiber is bonded to a quartz substrate whose thermal variation is matched to that of the fiber, with a suitable adhesive. The substrate is then encapsulated with in a Invar tube for overall protection.
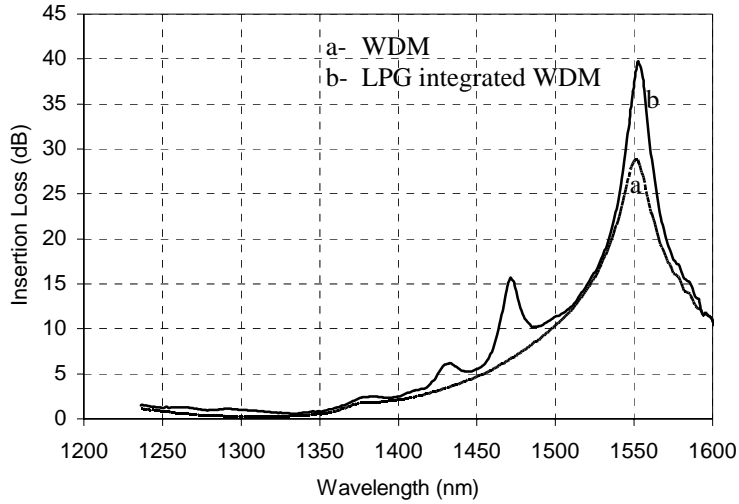
5.9 Results and Discussions

Figure 5.13: Spectrum of the 1310nm port of 1310/1550nm WDM

LPGs have been integrated with 1310/1550 nm WDM. Long Period Fiber Gratings are fabricated with a period of 610 μm on standard Corning SMF-28 Fiber. The isolation of fused WDMs at 1310 nm port and that of the LPG integrated WDM are shown in the Figure 5.13. The isolation of the single fused WDM is around 22-24 dB and that of the LPG integrated fused WDM is 32-35 dB. Hence it is obvious that the isolation is improved while keeping the insertion loss in the pass wavelength band well below 0.6 dB. This insertion loss value is comparable to the concatenated WDM solution. As LPGs couple the undesired wavelength power to the forward propagating cladding modes, it does not contribute to the back reflection or directivity performance of the LPG integrated WDMs. The back reflection of the combined device is found to be better than -55 dB, which is same as the concatenated WDMs.
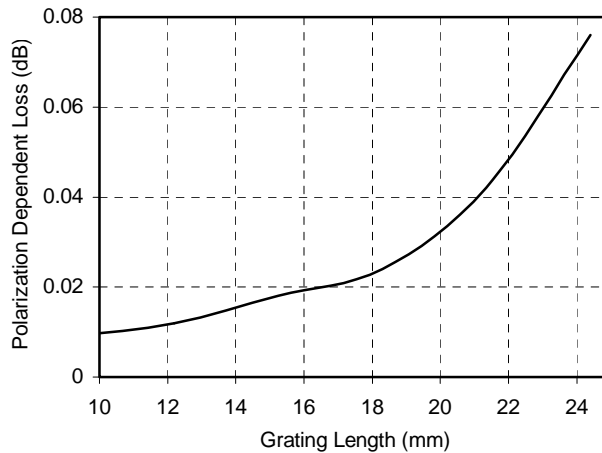

128

Figure 5.14: Polarization sensitivity of grating assisted WDM

The polarization dependence of the device is plotted in Figure 5.14. The polarization dependent loss of the device is measured by varying the polarization of the input light over all possible states using the Lefevre's loop controller and by observing the variation in insertion loss. Though the isolation increases with grating strength, polarization dependent loss also increases as discussed in the previous section. Thus there exists a trade off between the achievable isolation and the PDL of the device. The PDL of the device is function of the grating strength. This polarization dependence comes mostly from the fiber asymmetry of the electric arc discharge during the grating fabrication and the contribution of the same from WDM is limited. To reduce the effects of polarization states to the minimum level, intentional rotation is provided during fabrication.
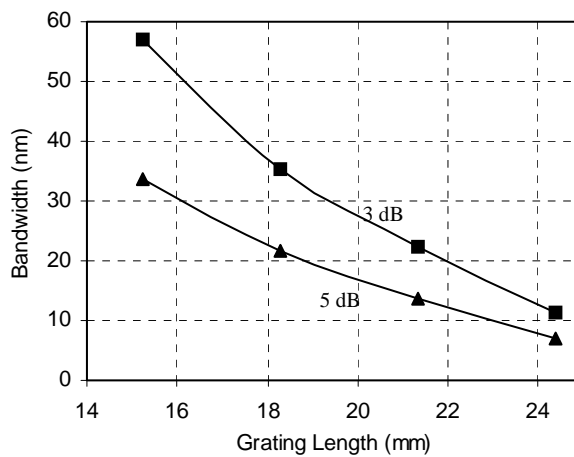

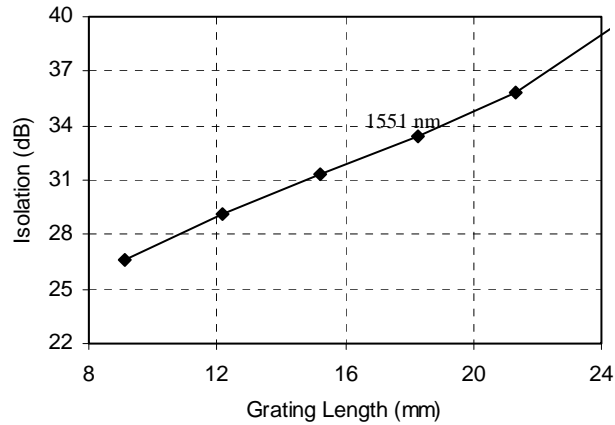Figure 5.15: Isolation Bandwidth of WDM

Figure 5.16: Evolution of Isolation

Defining Isolation bandwidth as the wavelength range over, which the isolation is greater than, or equal to some value, it is observed that the isolation increases while the isolation bandwidth decreases with grating strength. The variation of isolation bandwidth and isolation with grating length is shown in Figure 5.15 and 5.16 respectively. The typical isolation bandwidth achieved is in the range of 10-30 nm, which makes use of this application novel, especially in Coarse Wavelength Division Multiplexing applications. Typically the isolation bandwidth provided by the short taper fiber filter is in the range of more than 100nm. Isolation bandwidth in the case of cascaded WDMs depends on the similarity of the spectral shapes of the individual WDMs used, thus making the performance requirements of individual WDMs very stringent. From Figure 5.16, it is evident that the isolation has reached the level of 35 dB, where the 3 dB bandwidth is around 20 nm. The isolation improvement with grating length owes to greater amount of optical power transfer at the resonant wavelength, but the loss at the non-resonant wavelengths remains the same thus not contributing to the insertion loss at the ports.

To validate the packaging technique and to ensure the optical performance over various environmental conditions, 11 samples have been subjected to various accelerated tests. The effect of temperature variation on the spectral performance is studied by subjecting the packaged grating to temperature variations from 0 to $+70^{0}$C. The resonance wavelength shift of LPG was measured to be around 0.04 nm/^{0}C. The resonance wavelength shift of the device does not make appreciable changes in the

performance, over the temperature range. Comparison of the typical performance of a standard WDM and High Isolation WDM is summarized in Table 5.1.

Parameters	Standard WDM	High Isolation WDM
Wavelength (nm)	1310 & 1550	1310 & 1550
Insertion Loss (dB)	0.3	0.5
Peak Isolation (dB)	22	36
Polarization Dependent Loss (dB)	0.2	0.3
Back Reflection (dB)	-60	-60
Operating Temperature (^{0}C)	- 10 to +75	-10 to +75
Fiber Type	SMF-28	SMF-28
Dimension (L)	50 mm	70-75 mm

Table 5.1: Comparison of the performance of
standard WDM and a grating integrated WDM

5.10 Conclusions

A novel method has been suggested to improve the isolation of fused wavelength division multiplexers using inline spectral filters based on Long Period Grating. The gratings are fabricated on the same SMF28 fiber used to fabricate WDM couplers, using electric arc technique. The performance of the device is also analyzed in detail. This technique finds application in improving the adjacent channel isolation in fused CWDM devices. The advantage of this process comes from three points: 1. LPGs are fabricated on the standard fiber 2. Narrow isolation bandwidth makes this suitable for CWDM applications 3. Easy and flexible fabrication technique. This technique also offers the possibility of integrating the Gain Flattening Filter into the WDM module for EDFA applications.

References

1. G. E. Keiser, "A review of WDM technology and applications", Optical Fiber Technology, Vol. 5, pp. 3-39, 1999

2. V. J. Tekippe, C. M. Lawson, P. M. Kopera and T. Y. Hsu, "Monomode wavelength division multiplexer / demultiplexer", Fiber Optic Couplers, Connectors and Splice Technology II, Edited by D. W. Stowe, Proceeding of SPIE, Vol. 574, pp. 105-109, 1985

3. M. Eisenmann and E. Weidel, "Single-mode Fused Biconical Couplers for wavelength division multiplexing with channel spacing between 100 and 300nm", J. Lightwave Technology, Vol.6, pp. 113-119, 1988.

4. I. J. Wilkinson and C. J. Rowe, "Closely-spaced fused fiber wavelength division multiplexers with very low polarization sensitivity", Electron. Letters, Vol. 26, pp. 382-383, 1990.

5. M. N. McLandrich, R. J. Orazi and H. R. Marlin, "Polarization independent narrow channel wavelength division multiplexing fiber couplers for 1.55 mm", Journal of Lightwave Technology, Vol.9, pp.442-446, 1991.

6. N. Godbout, X. Daxhelet, A. Maurier, and S.Lacroix, "Long-period fiber grating by electrical discharge", In Proc, ECOC'98, pp. 397-398, 1998.

7. S. G. Kosinski, G. A. Ten Eyek, and A.M. Vengsarkar, "Method for making long-period fiber gratings," European patent EP0840146, 1998

8. G. Keizer, "WDM Concepts and Components", Chapter 10: Optical Fiber Communications, 3rd Edition, Mc-GrawHill, pp. 379- 422, 2000

9. F. Tong, "Multi-wavelength receivers for WDM systems", IEEE Communication Magazine, Vol.36, pp. 42-49, 1998

10. J. M. Senior and S. D. Cusworth, "Devices for wavelength multiplexing and demultiplexing", IEE Proceedings, Pt. J. 136, pp. 183 – 186, 1989

11. ITU-T G.983.3, "A broadband optical access system with increased service capability by wavelength allocation", 2001.

12. S. Bourgeois, "Fused Fiber developments offer passive foundation for optical slicing", Special report in Lightwave (Penn Well Corporation), No. 3, pp. 17-19, 2000.

13. C. M. Lawson, P. M. Kopera, T. Y. Hsu and V. J. Tekippe, "In-line single-mode wavelength division multiplexer / demultiplexer", Electron. Letters, Vol.20, pp. 963 -965, 1984

14. GR-1209-CORE, "Generic Requirements for Fiber Optic Branching Components", Issue 3, 2001.

15. D. T. Cassidy, D. C. Johnson and K. O. Hill, "Wavelength-dependent transmission of monomode optical fiber tapers", Applied Optics, Vol.24, pp.945-949, 1985.

16. J. V. Wright, "Wavelength dependence of fused couplers", Electron. Letters, Vol. 22, pp. 320-321, 1986.

17. C. Yijiang, "Theoretical investigation of wavelength flattened fused coupler", Optical and Quantum Electronics, Vol.21, pp.123-125, 1989.

18. D. C. Johnson and K. O. Hill, "Control of wavelength selectivity of power transfer in fused biconical monomode directional couplers", Applied optics, Vol. 25, pp. 3800-3803, 1986.

19. F. P. Payne, "Fused single-mode optical fiber couplers", Journal for the Institution of Electronics and Telecommunications Engineers (India),Vol. 32, pp. 319-322, 1986.

20. J. D. Minelly and M. Suyama, "Wavelength combining Fused Taper Couplers, with low sensitivity to polarization for use with 1480nm pumped Erbium-Doped Fiber Amplifiers, Vol. 26, pp. 523 – 524, 1990

21. V. J. Tekippe, "Insertion Loss and Isolation of fused wavelength division multiplexers/demultiplexers", Proceedings of SPIE, Vol. 839, pp. 20-24, 1987

22. M. S. Yataki, D. N. Payne and M. P. Varnham, "All-fiber wavelength filters using concatenated fused tapered couplers", Electron. Letters, Vol. 21, pp 248-249, 1985

23. F. Gonthier, S. Lacroix, X. Daxhelet, R. Black and J. Bures, "Compact all-fiber wavelength filter synthesis for 1300/1550 nm demultiplexing isolation", Proc. SPIE, Vol. 988, 1998.

24. A. M. Vengsarkar, P. J. Lemaire, J. B. Judkins, V. Bhatia, T. Erdogan and J.E.Sipe, "Long period gratings as band rejection filters", Journal of Lightwave Technology, Vol.14, pp. 58-65, 1996.

25. G. Rego, O. Frazão, F. M. Araújo, V. Sulimov, Long-period Fiber Gratings Produced Using the Electric Arc Technique for DWDM Communication Systems, 5th World Multi-Conference on Systemics, Cybernetics and Informatics, Orlando, USA, 2001.

26. C. R. Giles, "Lightwave applications of fiber bragg gratings", Journal of Lightwave Technology, Vol.15, pp. 1391-1404, 1997

27. D. M. Bird, J. R. Armitage, R. Kashyap, R. M. A Fatah, and K. H. Cameron, "Narrow line semiconductor laser using fiber grating," Electron. Letters, Vol. 27, pp. 1115-1117, 1991.

28. K. O. Hill, B. Malo, K. A. Vineberg, R. Bilodeau, D. C. Johnson, and L. Skinner, "Efficient mode conversion in telecommunication fiber using externally written gratings," Electron. Letters, Vol. 26, pp.1270-1272, 1990.

29. A. M. Vengsarkar, J. R. Pedrazzani, J. B. Judkins, P. J. Lemaire, N. S. Bergano, and C. R. Davidson, "Long-period fiber grating based gain equalisers," Optics Letters, Vol. 21, pp. 336-338, 1996.

30. P. F. Wysocki, J. B. Judkins, R. P. Espindola, M. Andrejco and A. M. Vengsarkar, "Broad-band erbium-doped fiber amplifier flattened beyond 40 nm using long-period grating filter", IEEE Photonics Technology Letters, Vol. 9, pp. 1343-1345, 1997

31. O. Frazão, G. Rego, M. Lima, A. Teixeira, F. M. Araújo, F.M, P. André, P, J. F. Da Rocha, and H. M. Salgado, "EDFA gain flattening using long-period fibre gratings based on the electric arc technique", 2001. Proceedings of the London Communication Symposium, 2001 from http://www.ee.ucl.ac.uk/lcs/ prog01/LCS041.pdf.

32. X. J. Gu, "Wavelength-division multiplexing isolation fiber filter and light source using cascaded long-period fiber gratings", Optics Letters, Vol.23, pp. 509-510, 1998.

33. B. Ortega, L. Dong, W. F. Liu, J. P. De Sandro, L. Reekie, S. I. Tsypina, V. N. Bagratashvili and R. I. Laming, "High-performance optical fiber polarizers based on long-period gratings in birefringent optical fibers. IEEE Photonics Technology Letters, Vol.9, pp.1370-1372, 1997.

34. A. S. Kurkov, M. Douay, O. Duhem, B. Leleu, J. F. Henninot, J. F. Bayon, and Rivoallan, L, "Long-period fibre grating as a wavelength selective polarisation element", Electron. Letters Vol. 33, pp. 616-617, 1997.

35. A S. Kurkov, S. A. Vasil'ev, I. G. Korolev, O. I. Medvedkov, E. M. Dianov, "Fibre laser with an intracavity polariser based on a long-period fibre grating", Quantum Electronics, Vol. 31, pp. 421-423, 2001.

36. L. Zhang, Y. Liu, L. Everall, J. A. R. Williams, and I. Bennion, "Design and realization of long-period grating devices in conventional and high birefringence fibers and their novel applications as fiber-optic load sensors", IEEE Journal of Selected Topics in Quantum Electronics, Vol.5, pp.1373-1378, 1999.

37. K. S. Chiang, Y.Liu, M.N Ng and S. Li, "Coupling between two parallel long-period fibre gratings", Electron. Letters, Vol. 36, pp.1408-1409, 2000.

38. G. Laffont and P. Ferdinand, (2000). "Fiber Bragg grating-induced coupling to cladding modes for refractive index measurements". Proceedings of SPIE, 4185, pp. 326-329, 2000.

39. P. K. Lam, A. J Stevenson and J. D. Love, "Bandpass spectra of evanescent couplers with long period gratings", Electron. Letters, Vol. 36, pp.967-969, 2000.

40. Y. Zhu, C. Lu, B. M Lacquet, P. L Swart, S. J. Spammer, "Wavelength tunable add/drop multiplexer for dense wavelength division multiplexing using long-period gratings and fibre stretchers", Optics Communications, Vol.208, pp.337-344, 2002

41. B. J. Eggleton, R. E. Slusher, J. B. Judkins, J. B. Stark and A. M. Vengsarkar, "All-optical switching in long-period fiber gratings", Optics Letters, Vol. 22, pp. 883-885, 1997

42. M. Das, K. Thyagarajan, "Dispersion compensation in transmission using uniform long period fiber gratings", Optics Communications, Vol. 190, pp. 159-163, 2001

43. Hill K. O., Fujii Y., Johnson D. C., and Kawasaki B. S. "Photosensitivity in optical waveguides: Application to reflection filter fabrication," Appl. Phys. Letters, Vol.32, pp.647 – 649, 1978.

44. G. Meltz, W. W. Morey and W. H.Glenn, "Formation of Bragg gratings in optical fibres by transverse holographic method", Optics Letters, Vol.14, pp. 823 – 825, 1989.

45. M. Douay, W. X. Xie, T. Taunay, P. Bernage, P. Niay, P. Cordier, B. Poumellec, L. Dong, J. R. Bayon, H. Poignant, and E. Delevaque, "Densification involved in the UV based photosensitivity of silica glasses and optical fibers", J. Lightwave Technology, Vol. 15, pp. 1329-1342, 1997.

46. D. Z. Anderson, V. Mizrahi, T. Erdogan, and A. E. White, "Phase-mask method for volume manufacturing of fiber phase gratings," Post-deadline paper PD16, Technical Digest of Post-Deadline Papers Proc. Conf. on Optical Fiber Communications, OFC '93, pp. 68-70, 1993.

47. S. W. James, and R. P. Tatam, "Optical fibre long-period grating sensors: characteristics and applications", Measurement Science and Technology, 14(5):R49-R61, 2003.

48. C. D. Poole, H. M. Presby and J. P. Meester, "Two-mode fibre spatial-mode converter using periodic core deformation", Electron. Letters Vol. 30, pp.1437-1438, 1994.

49. Wang, L.A., Lin, C.Y. & Chern, G.W, "A torsion sensor made of a corrugated long period fibre grating", Measurement Science and Technology, Vol. 12, pp. 793-799, 2001.

50. C. Y. Lin, G. W. Chern, and L. A. Wang, " Periodical corrugated structure for forming sampled fiber Bragg grating and long-period fiber grating with tunable coupling strength", Journal of Lightwave Technology, Vol.19, pp.1212-1220, 2001.

51. G. Kakarantzas, T. E. Dimmick, T.A. Birks, R. Le Roux and P.St. J. Russell, "Miniature all-fiber devices based on CO_2 laser microstucturing of tapered fibres", Optics Letters, Vol. 26, pp.1137-1139, 2001.

52. P. Palai, M. N. Satyanarayan, M. Das, K. Thyagarajan, and B. P. Pal, "Characterization and simulation of long period gratings fabricated using electric discharge", Optics Communications, Vol. 193, pp.181-185, 2001.

53. G. Rego, O. Okhotnikov, E. Dianov and V. Sulimov, V, "High-temperature stability of long-period fiber gratings produced using an electric arc", Journal of Lightwave Technology, Vol. 19, pp.1574-1579, 2001.

54. G. Humbert, and A. Malki, "Electric-arc-induced gratings in non-hydrogenated fibres: fabrication and high-temperature characterizations", Journal of Optics A: Pure and Applied Optics, Vol. 4, pp.194-198, 2002.

55. A. Malki, G. Humbert, Y. Ouerdane, A. Boukhenter and A. Boudrioua, "Investigation of the writing mechanism of electric-arc-induced long period fiber gratings", Applied Optics, Vol. 42, pp. 3776 – 3779, 2003.

56. M. Kim, D. Lee, B. Hong and H. Chung, "Performance characteristics of Long Period Fiber Gratings made from periodic tapers induced by Electric arc discharge", J. of the Korean Physical Society, Vol.40, pp. 369-373, 2002

An All-Fiber Mode Conditioner
for Multimode Networks

Laser based transmission over multimode fiber is affected by differential mode delay, due to the interaction between laser spot and index profile defects. Thus single mode laser sources needs to be adapted for transmission over multimode fibers, to get guaranteed link distances. Conventionally, mode conditioning is done through offset launch method, which requires precise tools. An all-fiber mode conditioning element based on Long Period Grating is proposed and evaluated.

A growing demand for greater information bandwidth in LANs requires operation at Gbps. This has lead to the development of many techniques to increase the bandwidth of multimode fiber based local area networks [1]. In order to support gigabit speeds, the systems need laser sources such as Fabry-Perot lasers or Vertical Cavity Surface Emitting Lasers (VCSEL). When laser sources are used with multimode fibers having refractive index profile defects, it may cause excitation of far separated mode groups. Such a condition causes the laser signal to disintegrate into an *uneven* power distribution among the modes. The resulting degraded optical power profile, often translates into bit errors. Thus, control over modal power distribution is essential to achieve guaranteed link distances at gigabit speeds over multimode fiber [2].

This chapter discusses various methods to ensure reliable high speed transmission over existing multimode fiber installations. There are different methods reported in literature to achieve the mode conditioning which include offset splicing, offset alignment, dough-nut launching and mode-field matched centre launching etc [3, 1]. Many of those techniques available today require launching condition with sophisticated launching tools or devices that are sensitive to environmental stresses. Long period fiber gratings offer coupling between co-propagating modes of a fiber are potentially useful as spectral shaping elements and mode conversion devices [4]. Mode conditioning using long period gratings, written at single mode to multimode interface is demonstrated, with comparable optical performance to other methods.

6.1 Transmission over Multimode Fiber

Fibers with large core and high numerical aperture typically allow propagation of many modes. Each mode is an independent, self-supporting, electro magnetic field that propagates axially along an optical fiber independent of other modes. Each mode will propagate with its own velocity and have a unique field distribution. The variation of the longitudinal propagation velocity with either optical frequency or path length introduces fundamental limit to fiber transmission. The dispersion in propagation velocity between different frequency components of the signal or between different modes of a multimode fiber produces a signal distortion and inter-symbol interference in digital systems, which is not desirable [5]. However, multimode optical fiber has been an attractive option for cost effective premises networks offering a transmission capability up to 1Gbps and beyond [6]
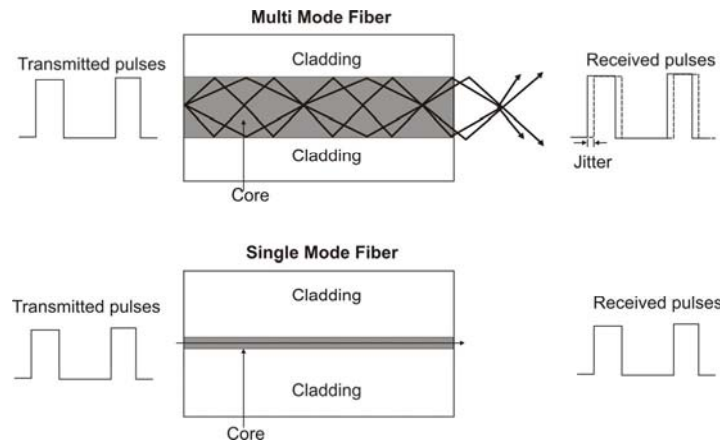
Figure 6.1: Propagation of signals over a multimode and single mode fiber. Multiple modes of light arrive over a range of propagation delays causing jitter.

Different modes traversing different optical paths in the MMF spread in time, causing pulse broadening. The parameter used to express pulse broadening due to intermodal dispersion is differential mode delay (DMD). Figure 6.1 shows the schematic representation of pulse broadening effect in multimode and single mode fibers. DMD is measured by launching a test pulse into a MMF at highly controlled radial positions across the fiber core, from the core center to the cladding region. Only a few modes are excited at each step, and their arrival times are recorded. The DMD of the fiber is the difference between the earliest and latest arrival times of all modes at all steps [7, 8]. From DMD measurements, one can calculate the effective modal bandwidth of the fiber expressed in units of MHz·km.

When light of different wavelengths propagate in a material, it does so with different velocities. VCSELs used with multimode fiber have a finite spectral width and, as a result, a pulse of light containing spectral content will be dispersed. Chromatic dispersion describes this broadening of the pulse width and has the effect of reducing signal quality, thereby degrading link performance. The velocity of light is determined by the refractive index of the medium. The refractive index profiles in modern graded index fibers used for data communication applications follow approximately a power law where the refractive index is defined as:

$$n(r) = n_1 \left(1 - 2\Delta \left(\frac{r}{a} \right)^g \right)^{0.5} \quad r < a$$
$$= n_2 \qquad\qquad r > a \tag{6.1}$$

where n_1 is the core refractive index, n_2 is the cladding refractive index, r is the radial position, a is the core radius, g is the profile parameter and $\Delta = \left(n_1^2 - n_2^2 \right)/2n_1^2$ is the relative refractive index difference between the core and the cladding. The optimum profile for minimum modal dispersion is $g \approx 2$; the index profile becomes parabolic. In a graded index fiber, the modes that travel nearest the centre of the core are subject to higher refractive index than are those that travel the longer paths through the outer portion of the core. When the profile is optimized, the varying index equalizes the travel time of all mode groups and differential mode delay is minimized. All modern fiber is designed to be as close to optimum as possible but the actual range can be as much as $1.8 < g < 2.2$. However, in real cases, perturbations in the refractive index can occur. Defects at the core/cladding interface, changing profile parameter g as a function of radius or a central index dip have all been reported [9].

The number of modes that propagate in a multimode fiber is given by [10]

$$N = \left(\frac{g}{g+2} \right) \Delta \left(\frac{2\pi n_1 a}{\lambda} \right)^2 \tag{6.2}$$

where λ is the wavelength of the light propagating in the fiber and M is the number of modes.

The modes of the square law fiber can be calculated using Hermite polynomials, $H(p,x)$ as:

$$H(p,x) = \sum_{m=0}^{\frac{p}{2}} \frac{(-1)^m \, p! \, (2x)^{(p-2m)}}{m! \, (p-2m)!} \tag{6.3}$$

where p is the mode index.

The total mode field distribution may then be expressed as the product of functions of x and y coordinates (x and y in plane of the fiber end face, z along axis of the fiber) as [11]

$$\chi(p,x,\omega_0) = \left(\frac{2}{\pi}\right)^{\frac{1}{4}} \cdot \left(\frac{1}{\sqrt{2^p \cdot p! \cdot w_0}}\right) \cdot H\left(p, \sqrt{2} \cdot \frac{x}{w_0}\right) \cdot e^{-\left(\frac{x}{w_0}\right)^2} \tag{6.4}$$

and

$$\psi(q,y,\omega_0) = \left(\frac{2}{\pi}\right)^{\frac{1}{4}} \cdot \left(\frac{1}{\sqrt{2^q \cdot q! \cdot w_0}}\right) \cdot H\left(q, \sqrt{2} \cdot \frac{y}{w_0}\right) \cdot e^{-\left(\frac{y}{w_0}\right)^2} \tag{6.5}$$

where p and q are mode indices, w_0 is the e^{-1} waist of the lowest order fiber mode given by

$$w_0 = \left[\sqrt{\frac{2R}{\frac{2\pi n_1}{\lambda} \cdot \sqrt{2\Delta}}}\right] \tag{6.6}$$

where λ is the wavelength of the source.

A single transverse mode laser source may be defined as a Gaussian beam having an electric field distribution described by the following equations:

$$F_x(x,w_x,\delta) = \sqrt{\frac{2}{w_x \pi}} \cdot e^{-\frac{(x+\delta)^2}{w_x^2}} \tag{6.7}$$

$$F_y(y,w_y,\varepsilon) = \sqrt{\frac{2}{w_y \pi}} \cdot e^{-\frac{(y+\varepsilon)^2}{w_y^2}} \tag{6.8}$$

where w_x and w_y are the waists of the beam in the x and y directions. δ and ε are the offsets in the x and y axis from the center of the fiber core.

The field excitation coefficients, $C(p,q,w_0,w_x, w_y, \delta, \varepsilon)$, may be calculated from the overlap integral of the excitation field and the modal field distributions of the fiber:

$$C(p,q,w_0,w_x,w_y,\delta,\varepsilon) = \int_{-\infty}^{\infty}\int_{-\infty}^{\infty} F_x(x,w_x,\delta) \cdot F_y(y,w_y,\varepsilon) \cdot \chi(p,x,w_0) \cdot \psi(q,y,w_0) dx dy \tag{6.9}$$

The double integral may be evaluated as the product of an integral over x multiplied by an integral over y so that:

$$C(p,q,w_0,w_x,w_y,\delta,\varepsilon) = C_p(p,w_0,w_x,\delta) \cdot C_q(q,w_0,w_y,\varepsilon) \tag{6.10}$$

Evaluation of the integral results in the following solutions:

$$C_p(p,w_0,w_x,\delta) =$$

$$\sqrt{\frac{2}{w_x \cdot w_0}} \cdot \frac{1}{2^{\left(\frac{p}{2}\right)} \cdot \sqrt{p!}} \cdot \frac{w_x w_0}{\sqrt{w_x^2 + w_0^2}} \cdot \left(\frac{w_0^2 - w_x^2}{w_0^2 + w_x^2}\right)^{\frac{p}{2}} \cdot H\left[p, \frac{\sqrt{2} \cdot \delta}{w_0^4 - w_x^4}\right] \cdot e^{-\left(\frac{\delta^2}{w_0^2 + w_x^2}\right)}$$

$$\tag{6.11}$$

and

$$C_q(q,w_0,w_y,\varepsilon) =$$

$$\sqrt{\frac{2}{w_y \cdot w_0}} \cdot \frac{1}{2^{\left(\frac{q}{2}\right)} \cdot \sqrt{q!}} \cdot \frac{w_y w_0}{\sqrt{w_y^2 + w_0^2}} \cdot \left(\frac{w_0^2 - w_y^2}{w_0^2 + w_y^2}\right)^{\frac{q}{2}} \cdot H\left[q, \frac{\sqrt{2} \cdot \varepsilon}{w_0^4 - w_y^4}\right] \cdot e^{-\left(\frac{\varepsilon^2}{w_0^2 + w_y^2}\right)}$$

$$\tag{6.12}$$

The power coupling per mode, PC $(p,q,w_0,w_x,w_y, \delta, \varepsilon)$ may be calculated to be:

$$PC(p,q,w_x,w_y,\delta,\varepsilon) = \left(C_p(p,w_0,w_x,\delta) \cdot C_q(q,w_0,w_y,\varepsilon)\right)^2 \tag{6.13}$$

According to the WKB method, the modal propagation time, $\tau(g,p,q)$ for the power law fibers may be calculated as:

$$\tau(g,p,q) = \left(\frac{n_1 \cdot L}{c}\right) \cdot \frac{1 - \dfrac{4 \cdot \Delta}{g+2} \cdot \left(\dfrac{M(p,q)}{N(g)}\right)^{\frac{g}{g+2}}}{\left[1 - 2 \cdot \Delta \cdot \left(\dfrac{M(p,q)}{N(g)}\right)^{\frac{g}{g+2}}\right]^{0.5}} \tag{6.14}$$

where L is the fiber length, c is the speed of light, g the power law of the refractive index curve, $M(p,q) = (p+q+1)^2$ and $N(g)$ the total number of guided modes.

The RMS width of the impulse response of the fiber may then be calculated as [12]:

$$\sqrt{\sum_p \sum_q PC(p,q,w_o,w_x,w_y,\delta,\varepsilon) \cdot \tau(g,p,q)^2 - (mean\_delay)^2} \tag{6.15}$$

where the total power is normalized to one. Here dispersion effects are not included since modal dispersion predominates. Modal bandwidth is a measure that characterizes the effect of pulse broadening in a fiber. Typical specifications are in the range from 200 MHz to 1 GHz. This helps to determine how far a system will perform at what rate [13].

6.2 Modal Bandwidth: Launch Dependence

A simple model for the bandwidth characteristics considers the fiber consisting of a number of discrete delay lines, each of which corresponds to a particular mode [14, 15, 16]. A conceptual model is shown in Figure 6.2. Here the lower order modes corresponds to the modes of rays propagating down the centre of the fiber; the higher order modes propagate near the core / clad interface and the intermediate modes propagate in between. In an ideal fiber all of the delays are tuned to be identical. Thus when a temporary narrow pulse of light is launched into the fiber, its shape is maintained at the output. However, as shown in Figure 6.2, exaggerated delay error causes the output pulse to be broadened. The higher order power arrives late relative to most of the power in the intermediate modes and the lower order modes arrive early. Thus the bandwidth is reduced and information carrying capacity is limited. The modal dispersion in multimode fibers (MMFs) is one of the main performance-limiting factors in fiber optic LANs.
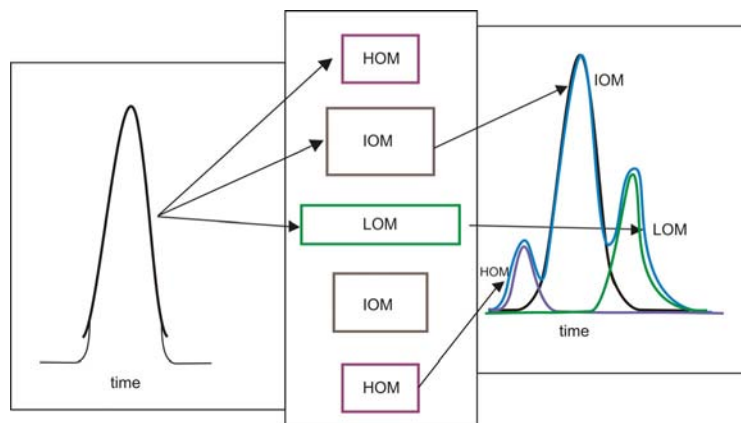

Figure 6.2: Conceptual Model for Multimode Bandwidth

The output as shown in Figure 6.2 corresponds to an overfilled launch, where all of the modes are excited with the maximum amount of power they can carry. This

launch is referred as over filled launch [17], where 100 percent of the optical power is launched to the full area of the fiber core. If the launch power distribution is reduced only the lower and intermediate modes are excited, the pulse width decreases and the bandwidth goes up. When the launch is restricted to only lower order modes, the output pulse will become very narrow. Such a type of excitation will occur when a laser is launched to a multimode fiber. Laser light fills only a portion of the core due to the smaller, focused light pattern that lasers emit, such condition is referred as restricted launch. The key aspect in determining the bandwidth of a multimode fiber communications link is the number and distribution of modes within the multimode fiber, which are excited, and therefore carry optical energy. If only low order mode is launched, and there is no mode mixing, the bandwidth will be high. But often, mode mixing occurs, due to fiber profile irregularities, or mechanical perturbations of the fiber, energy will be coupled to higher order modes, and additional pulse dispersion will inevitably result.

6.3 Laser Launch and Differential Mode Delay

The small spot size of lasers concentrate energy near the center of the multimode fibers and hence are sensitive to any central irregularity in the refractive index profile. When an unconditioned laser source, designed for operation on a single mode fiber, is directly coupled to a multimode fiber, differential mode delay will occur. Thus a combination of the restricted launch and a flaw in the index of refraction leads to a reduction in the multimode fiber modal bandwidth [18]. The central index dip is probably the most severe defect and can occur during in the manufacture of the fiber. The central dip can occur due to the evaporation of dopant from the inner surface of the fiber perform when the perform is collapsed during the fabrication of the fiber [19]. This dip in the refractive index profile is schematically shown in Figure 6.3. The better the fiber manufacturing process and the tighter the control of process parameters, the better the quality and the more consistent the optical fiber.

In addition to the modal dispersion, the signal also broadens due to chromatic dispersion. Chromatic dispersion occurs because the index of refraction of glass changes with wavelength, and therefore the various spectral components of the signal travel at different velocities. The modal and chromatic bandwidths combine quadratically to give the fiber's total system bandwidth as given below:

$$BW_t(MHz.km) = \sqrt{\frac{1}{\left(\dfrac{1}{BW_m}\right)^2 + \left(\dfrac{1}{BW_c}\right)^2}}$$

Modal Bandwidth, BW_m is inversely proportional to the differences in propagation time, or modal delays, that exist between multimode fiber modes. Also, for short-distance links, the bandwidth is dependent on the launch conditions. For multimode fiber (whether step-index or gradient-index) the excitation conditions are particularly important. Due to the constitution of the core, the laser beam can be split into two or more modes (or paths) of light. The different modes can be subject to different propagation delays and arrive at the receiver with a time skew, which causes jitter. Fiber bandwidth is a sensitive function of the index profile and is wavelength dependent, and the scaling with length depends on whether there is mode mixing [20]. DMD is the result of beam splitting caused by structural constitution of the core. Both dispersion and DMD produce the same effect - jitter that builds-up as a function of fiber length. Thus the launch dependent modal power distribution of multimode fiber combined with Differential Mode Delay (DMD) can cause serious problems in Gigabit Ethernet LANs. Worst case DMD occurs when equal power is launched into the fastest and slowest fiber mode groups appearing as pulse splitting in the impulse response [21]. Also, the use of a laser to launch a small number of low order modes into a multimode fiber is known to give rise to modal noise [22].
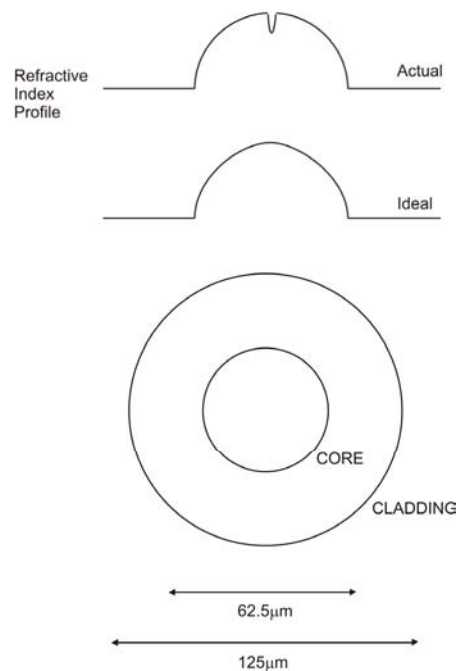
Figure 6.3: Ideal and actual refractive index profiles of graded index multimode fiber

6.4 Mode Conditioning for Gigabit Networks

To achieve useful link distances at Gigabit speeds, the signal from the single mode must be adapted to the multimode fiber. Theoretical studies confirmed that an offset single mode to multimode fiber launch could solve the problem by maintaining a high bandwidth due to mode conditioning effect, where only mid order modes of the multimode fiber are strongly excited. The mid order modes excited is predominately within a small number of mode groups and thus have similar propagation constants. This leads to a reduction in modal dispersion and thus to a significant increase in bandwidth where the enhancement results from the selection of launched modes [2]. Also, the offset launch is tolerant both to the launch conditions and to any imperfections in the fiber refractive index profile.
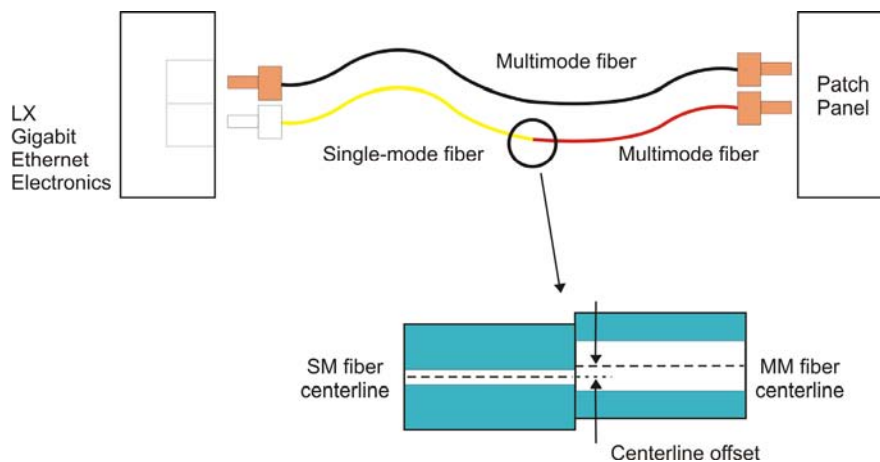
Figure 6.4: Application schematic of a mode conditioning patchcord

This adaption is conventionally done using an optical mode conditioning patch cable (MCP), which is an optical mode conditioner for efficiently conditioning a single mode optical signal propagating in a single mode optical fiber for propagation within a multimode optical fiber. It is based on the principle of enhancement of bandwidth of a multimode fiber by launching optical signals with a deliberate, predetermined offset between the central axis of the single-mode fiber and the multimode fiber. The desired optical intensity profile is a Gaussian mode distribution, similar to that obtained when a multimode light source is used with multimode fiber. This offset launch condition, represents a significant advancement because it has the potential to extend the bandwidth of multimode optical fiber already installed in existing network configurations, such as in a LAN. This is implemented by connecting the GbE electronics to the cable plant using a special patch cord called a "Mode Conditioning Patch Cord". It contains a single-mode fiber (for attaching to the transmitter) connected precisely off-center to a multimode fiber [13] as shown in Figure 6.4. This offset creates a launch that performs very well on multimode fiber. The GbE specification requires the offset launch positioning for LX 1300 nm long-wavelength systems operating on both 62.5μm and 50μm multimode fiber [13].

6.5 Offset Launch Methods

There are different approaches to implement the mode conditioning: offset splicing, offset alignment, special ceramic ferrules and dough-nut launching. In offset splicing technique, a single mode fiber and multi-mode fiber are joined by fusion splicing.

Fusion splicing is accomplished by applying sufficient heat to the fiber ends to fuse the fibers together, thereby creating a single continuous fiber optic path [23]. The fibers are aligned in the fusion splicing process in such a manner as to provide the mode conditioning function. This can be accomplished using commercially available fusion splice device. During the fusion splicing process, the thinner core of the single mode fiber is aligned such that it is slightly offset from the center of the thicker core of the multi-mode fiber as shown in Figure 6.5. The amount of offset is calculated prior to splicing; thus, the fibers do not need to be tuned during the splicing process. Preferably, the two fiber core center offset required for 50/125μm fiber is 10-16μm and that for 62.5/125μm fiber is 17-23μm [13]. This slight offset causes the light of the lowest order propagation mode exiting the single mode fiber to avoid entering the center of the core of the multi-mode fiber. This enable the optical path to avoid the imperfections and obstructions that exist throughout the core centers of older, lower quality multi-mode fibers used in many existing infrastructures. Fibers joined using a fusion splice form a monolithic mode conditioner, that is not susceptible to alignment shifting after installation. In addition, fused fibers do not introduce modal noise [23]. Splice method also do not use epoxy in the optical path, the use of which lowers thermal stability. A tolerance analysis of this approach revealed that some installations could experience unacceptable variability in the splice elements, resulting in poor alignment and ineffective mode conditioning. Also it is very difficult to protect the offseted splice region. A small perturbation can cause break or change in the mode conditioning.
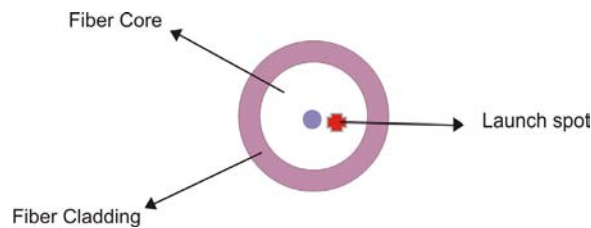

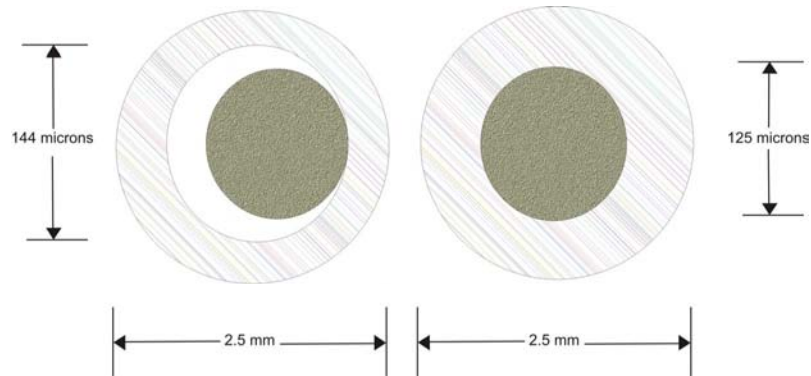
Figure 6.5: Illustration of offset launching technique

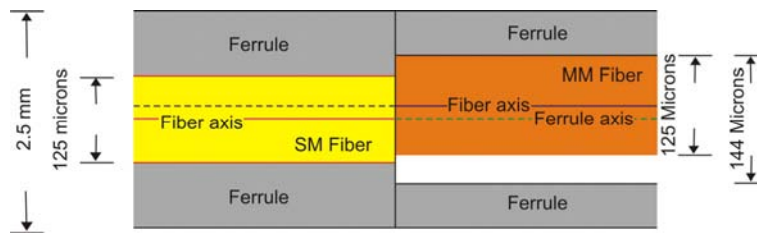Figure 6.6 (a): Cross-sectional view of the fiber in ferrules with different dimensions

Figure 6.6 (b): Lateral Cross-section of the fiber in ferrule

Other methods use special ceramic ferrules or active alignment to achieve the mode conditioning. Special ceramic ferrules are costly; while active alignment is time consuming and complex. In another approach, ferrules with different dimensions are used to achieve the required offset. The concept of this approach is illustrated in Figure 6.6, where ferrules of diameters 125μm and 144μm is used for a 50/125μm fiber. A simple and cost effective method has been proposed based on differentially changing the fiber geometry and then coupling the light from single mode to multimode fiber, through a connector type mechanism [3]. Here in this process the fibers are etched to suitable dimensions to get the offset and the fibers are placed in ferrules with same dimension (125μm ferrule). Only single mode fiber is etched. The required dimensions of the etched single mode fiber is 85μm with a 62.5/125 μm fiber and 99μm with a 50/125μm fiber. This method is attractive because it uses only standard ferrules. This avoids the need for costly offsetted ferrules and also causes significant reduction in the manufacturing time. This mode conditioner does not require as precise an alignment as current methods using ceramic ferrules, which will also contribute to lower manufacturing costs. Recently an angular offset launching

technique for bandwidth improvement has been reported [24]. Bandwidth enhancements based on mode filtering [25] and mode field matched centre launch method [26] also have been reported. Most of these methods are sensitive to environmental stresses and suffer long term performance degradation.

6.6 Coupled Power Ratio

Knowledge about the modal power distribution is desirable to predict the performance of high-speed systems. A wide-field charge-coupled-device camera can be used to measure the two-dimensional spatial distribution of optical power at the output of the multimode fiber [27]. It is possible to characterize the modal distribution by measuring its near field and calculating the Modal Power distribution. The simple method to get a measure of this Modal Power Distribution is the Coupled Power Ratio Measurement. Coupled Power Ratio (CPR) is a qualitative measurement that is commonly used to describe the mode power distribution in multimode fibers. It is the ratio of the total power out of a multimode fiber to the power measured when a single mode fiber is coupled to the multimode fiber [28]. The coupled power ratio is often used to evaluate the launch conditions of transmitters and light sources into multimode fibers and is used in some standards for establishing attenuation measurements criteria for installed fiber plants [29].

The coupled power per mode observed at the output of a multimode fiber that has been excited by a single transverse mode source can be calculated as:

$$CP(p,q,w_0,w_x,w_y,\delta,\delta_1,\varepsilon,\varepsilon_1) =$$
$$\left(C(p,q,w_0,w_x,w_y,\delta,\varepsilon) \cdot C(p,q,w_0,w_x,w_y,\delta_1,\varepsilon_1)\right)^2$$

(6.17)

where δ, ε and δ_1, ε_{11} are the offsets of the input single mode source and the sampling single mode fiber in the x and y directions respectively.

If ε and ε_1 are set to zero, the CPR in dB is then:

$$CPR(w_0,w_x,w_y,\delta,\delta_1) = 10\log\sum_p\sum_q CP(p,q,w_0,w_x,w_y,\delta,\delta_1,0,0)$$

(6.18)

The schematic of the CPR measurement set up is shown in Figure 6.7. The power out of the multimode fiber in the CPR test represents all modes launched into it by the light source. The single mode fiber captures only the lowest order modes. The difference in coupled power between the multimode and single mode fibers (the

CPR) provides a simplified measure of the launched MPD. In the case of an under fill, the single mode fiber captures a greater percentage of light exiting the multimode fiber. The result is a smaller numerical CPR value for the under fill case. The measurement is easily done and gives quantitative and repeatable results. A higher CPR means that there is a high loss when coupled in to the single mode fiber and indicates a more fully filled launch. A low CPR indicates restricted launch conditions corresponding to under filling of the fiber. When measuring CPR, it is important to use single mode fibers at 850nm and 1300nm [29].
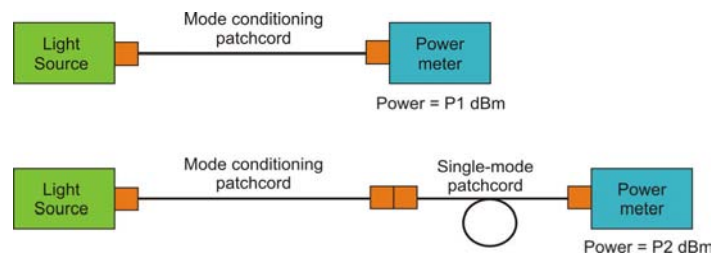

Figure 6.7: Schematic of CPR measurement

The coupled power ratio is measured in two steps. In the first step, the mode conditioner is directly connected to a power meter and the absolute power is recorded as P_1 (dBm). In the second step, a single mode fiber is connected to the multimode fiber and the power coupled to the single mode fiber is recorded as P_2 (dBm). Now, CPR is calculated as, $P_1 - P_2$ (dB). A higher order mode filter is incorporated in the measurement path, by making a mandrel of diameter 30 mm in the single mode launch. The number of turns is five or six. In cases where mechanical instability causes variations >0.5 dB in the successive power readings follow the averaging procedure is followed by taking reading for five times. All the individual readings must be with in the acceptable range. For 50/125 μm fiber the CPR should be in the range of 12-20 dB, while that for 62.5/125 μm is 28-40 dB [13].

6.7 Long Period Gratings

Long Period Grating helps to achieve coupling between co-propagating modes of a fiber. LPGs are designed to couple light between two guided modes of a few-mode fiber [30] and also between the guided mode and the cladding modes of a single mode fiber [31]. The fabrication of an LPG relies on the introduction of a periodic

modulation of the optical properties of the fiber, which can be in the form of index modulation along the fiber core [31] or physical deformation along the fiber [32]. The most widely used method of introducing an index modulation is by exposing a photo-sensitive fiber to UV irradiation. Index modulation has also been achieved by ion implantation, near infrared femto-second pulse irradiation, CO_2-laser irradiation and electrical discharges. The fabrication method of LPGs on standard single mode fiber is detailed in Chapter 5.

Fiber-to-fiber coupling via the cladding mode of the fiber can relax the alignment tolerances substantially [33,34]. A lens-free fiber-to-fiber connector that has a long working distance and a wide alignment tolerance has been implemented by using two matched LPGs written in a double-cladding fiber [35]. Lateral alignment tolerances of ~450 μm and ~3 mm for coupling losses less than 1 dB and 3 dB respectively have been achieved. Laser-to-fiber coupling based on an LPG and a lens has also been demonstrated [36]. A working distance longer than 100 μm and a lateral tolerance of 2.5 μm have been obtained [36]. Fiber-to-waveguide coupling has also been demonstrated with a CO_2-laser-induced LPG [37], which does not require access to the fiber and waveguide end faces. Long period gratings written on the single mode to multimode fiber interface to control the modal power distribution is explored in the following sections. The concept is to couple the power from the guided mode of the first fiber, which is single mode, to the guided modes of the second multimode fiber that is permanently joined to the first fiber. The power coupled is controlled through the long period gratings written on the fibers.

6.8 Mode Conditioner based on LPGs

All-fiber mode conditioning device is realized by fusion splicing a single mode fiber to a multimode fiber and then inscribing a long period grating at the single mode to multimode fiber interface. The long period grating helps to couple power from the core mode of the single mode fiber to the guided modes of the multimode fiber. Long period fiber gratings are fabricated using electric arc discharge method, using a commercially available splicing machine. A set up as described in Chapter 5 is used for the fabrication of the long period grating.

6.8.1 Fabrication

The setup consists of a source at 1310nm, precision translation stages and a power meter. A small weight (~10gm) is attached to one end of the fiber to keep it under

tension. The power coming out of the multimode fiber is captured using a single mode fiber to monitor the CPR value. After exposing the fiber to one arc, the fiber is moved by a distance equal to the grating period, using the precision translation stages. The period of the grating is optimized at 450μm. The single mode fiber used is Corning SMF-28 with a mode field diameter of ~10μm at 1310nm. The multimode fiber used is a graded index fiber from Corning with a core radius of 62.5μm. The single mode fiber is spliced to the multimode fiber, through cladding alignment method. The coupled power ratio is recorded after every five arcs from the splicing machine.

The modal power distribution is characterized by measuring the CPR value as described in section 6.6. The variation in CPR at 1310nm with the length of the grating is shown in Figure 6.8. The CPR value increases almost in a linear fashion with the grating length. It can be seen that a grating length of 10mm is sufficient to get the required CPR value >28dB. The long period grating at the single mode fiber to multimode fiber interface converts, the forward propagating core modes to forward propagating cladding modes. These cladding modes are guided by the multimode fiber as its core modes. The insertion loss is below 0.2 dB when the grating length is 10mm, indicating that the power is coupled to the forward propagating core mode of the multimode fiber. However increase in insertion loss (above 0.5 dB) is observed after a grating length of 15mm, which may be due to the coupling to the lossy cladding modes of the multimode fiber. The splice and grating is protected in the conventional way a splice is protected, using a metal rod assisted package. The length of the package is 40mm, and hence offers a compact all-fiber solution, for mode conditioning.
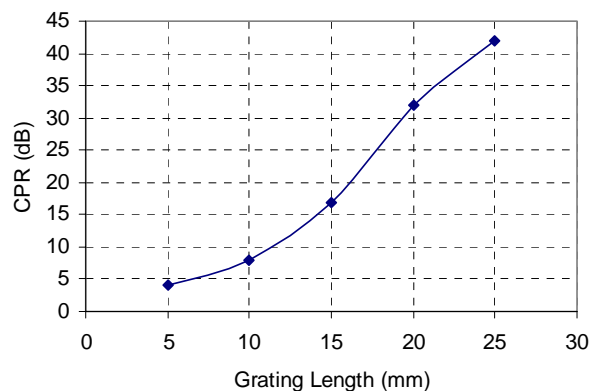

Figure 6.8: Variation of CPR with grating length

A 62.5/125 multimode fiber link is characterized by measuring the bit error. Signal at 1GHz is launched into a 500m MM fiber through LPG based mode conditioning element. The signal is detected using a high speed photo-detector and the bit error rate is monitored. A data pattern of PRBS 2^{31}-1 is used. The Figure 6.9 shows the BER measurement data of the system when mode conditioners with different grating lengths are used. It is found that with grating inscription, the performance of the link is improved.
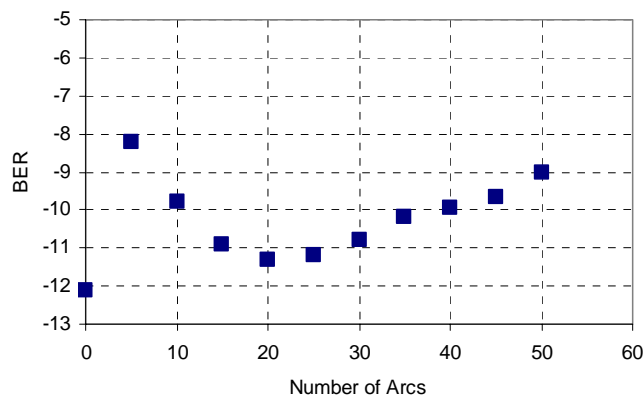

Figure 6.9: Plot of BER versus grating length at 1310nm for 62.5μm link

The CPR distribution of 15 samples of 62.5/125μm mode conditioning samples fabricated is shown in Figure 6.10. It is seen that the CPR values of 75% samples falls in the category of 28-31 dB, which is fairly good value of mode conditioning. More than 95% samples made with the current process confirm to the CPR values as specified by the IEEE requirement, which proves the consistency of the developed method. The CPR values conform to the IEEE 802.3z standard, industry standard which specifically provides for operation of single mode transceivers over multimode fiber optic cables. Though the standard allows an insertion loss value of 0.5 dB, our typical loss is around 0.3dB. The typical back reflection values are greater than 45 dB, in the mode conditioned channel. LPG based mode conditioning offers better back reflection performance, since the long period gratings couple power only to the forward propagating modes and there is no optical discontinuity in the path.
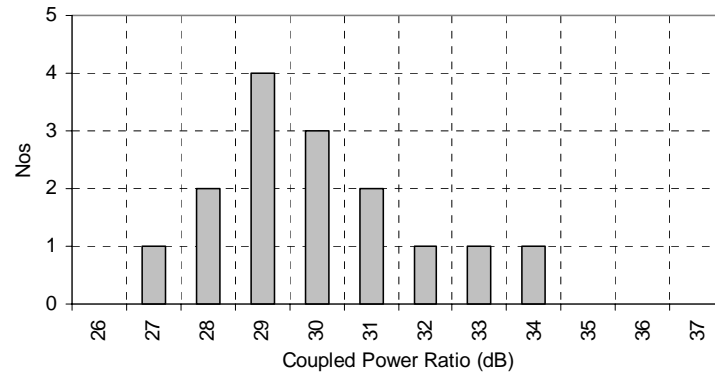
Figure 6.10: Distribution of CPR values of LPG mode conditioners

6.8.2 Sensitivity Studies

The mode conditioning depends on the coupling of power between the modes of the fiber. Here the sensitivity of the position of the grating at the single mode-multimode interface is analyzed. Figure 6.11 shows the variation in CPR and insertion loss of the LPG based mode conditioning element written on a 62.5/125μm fiber. Here a grating of fixed length (10mm) is considered. The centre of the grating is taken as the origin of the grating. It is observed that the CPR value is almost stable when the grating is close to the interface. As the grating centre shifts to the single mode side, both CPR and IL become high. This is attributed to the coupling of power from the guide modes of the single mode fiber to the leaky modes of the multimode fiber. On the other hand, if the grating lies on the multimode fiber, its CPR value is not well controlled. This can be due to the difference in behaviour of grating formed on multimode fibers and needs more analysis.

The effect of combinational effect of misalignment between the single mode fiber and multimode fiber introduced during the splicing and the grating length written on the interface is studied. Figure 6.12 shows the evolution of CPR values with for different lateral mis-alignment between the single mode and multimode fiber combined with the strength of LPGs. The misalignment helps to achieve CPR with less grating strength. However, the insertion loss increases slightly. The insertion loss measurement before the grating inscription shows that the insertion loss increase is not due to the lateral misalignment. Thus the loss increase can be attributed to coupling to some of the leaky modes of the multimode fiber.
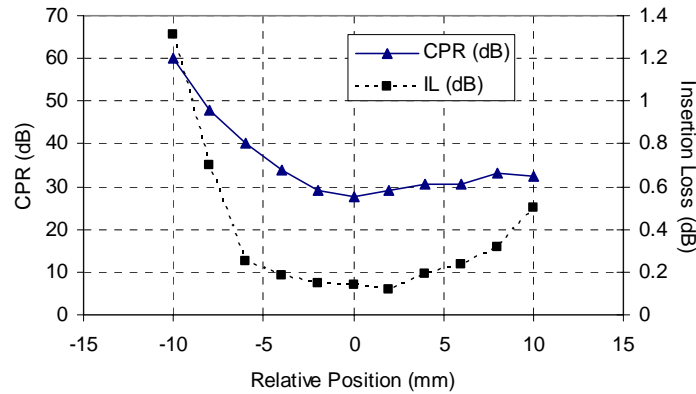
Figure 6.11: Effect of LPG position on the coupled power ratio
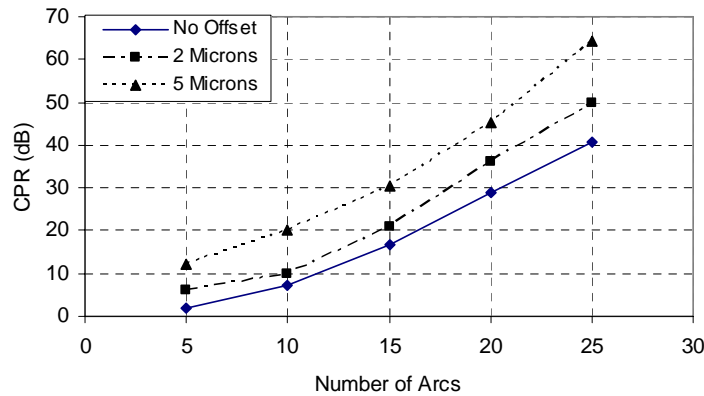and insertion loss of a 62.5/125μm fiber.

Figure 6.12: Effect of misalignment and grating length
on the coupled power ratio of a 62.5/125μm fiber.

6.8.3 Stability Analysis

Even though the products meet performance specifications, they could still suffer
from performance degradation and even failure in the field. Hence product samples
are subjected to accelerated test conditions to ensure the field operability. Our studies
indicate that most field problems can be attributed to: a. Fiber fracture, b. High
Insertion Loss due to fiber misalignment or bending caused by the stress induced
effects. Optical microscopic technique can be used to identify the cause and location
of the failure, if any. Fiber fracture occurs when the fiber inside the assembly were

subjected to stress induced effects. This factor is taken care in our packaging and assembling process.
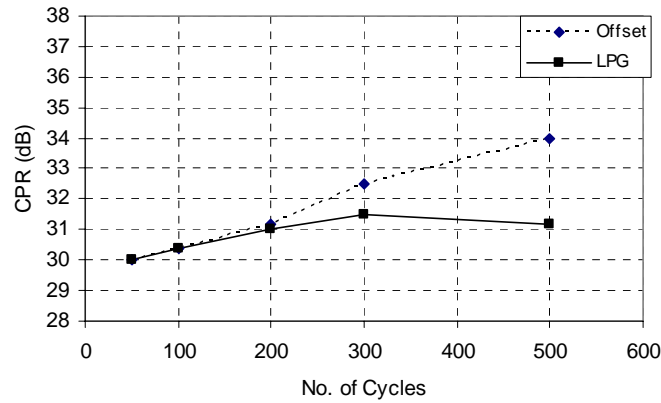

Figure 6.13: Variation in CPR values with temperature cycling
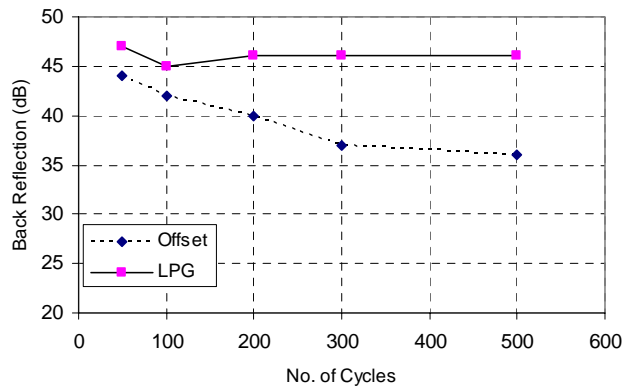

Figure 6.14: Variation in BR values with temperature cycling

To analyze the effect of severe environmental conditions the devices are subjected to the following tests, viz Humidity Aging (HA), Low Temperature, Temperature Life, Impact Test and Vibration Test as per the relevant standards [38]. Variation of the Insertion Loss, Coupled Power Ratio and Back Reflection of the device are measured after each tests. The parameters were measured both before and after the tests. Also online monitoring is done during temperature cycling and humidity aging. A sample size of 11 is chosen, with no failure as the reliability criteria. A device is judged fail if any specification item is not met, during or after the test. With the new method the

CPR stability is within 2dB of the initial value, for a period of 500 thermal cycles from -40 to +85^{0}C. The BR value is highly stable compared to the offset launch technique. The insertion loss during the temperature cycling is stable with in ±0.1 dB.

6.9 Conclusions

An all-fiber solution for the mode conditioning, based on LPG has been proposed, fabricated and evaluated. The coupled power ratio increases almost linearly with the grating strength. The device offers good control on modal excitation and improves the performance of the link. The positional sensitivity of LPG has been studied and found to be best close to the splice point. The thermal stability and back reflection have been compared with existing solution and found to be far better. The back reflection performance of the device is better, since LPGs couple power to the forward propagating modes. This offers the technique to build a compact and stable mode-conditioning device for Gigabit Ethernet LANs. All the 11 samples passed reliability tests, with out any failure, thus proving the process stability and less sensitivity to environmental variations.

References

1. D. H. Shim, Y. Takushima and Y. C. Chung, ">1Tbps.km Transmission over MMF", 2008 Digest of the IEEE/LEOS Summer Topical Meetings, pp. 173-174, 2008.

2. L. Raddatz, I. H. White, D. G. Cunningham and M. C. Nowell, "An experimental and theoretical study of the offset launch technique for the enhancement of the bandwidth of multimode fiber links", IEEE J. Lightwave Technology, Vol. 16, pp. 324-331, 1998

3. Samuel Varghese, Muhammed Iqbal and Suresh Nair, "Development of IEEE 802.3z compliant mode conditioning patchcord for Gigabit Ethernet LANs and its reliability studies", Proceedings of the Sixth International Conference on Optoelectronics, Fiber Optics and Photonics (*PHOTONICS-2002), pp. 89, 2002*

4. S. Ramachandran, Zhiyong Wang and Man Yan, "Bandwidth control of long period grating based mode converters in few-mode fibers", Optics Letters, Vol. 27, pp. 698-700, 2002

5. Tom G. Brown, "Optical Fibers and Fiber Optic Communications", Chapter 1, Fiber Optics Handbook: Fiber, Devices and Systems for optical communications, Edited by Michael Bass, McGraw Hill, 2002

6. Russel Ellis, "The importance of minEMBc laser bandwidth measured multimode fiber for high performance premises networks", White paper from Corning, www.corning.com, 2007.

7. John George, David Mazzarese, "Bandwidth measurement considerations for high speed, short reach multimode fiber systems", Proceedings of National Fiber Optics Engineers Conference, pp. 1273 – 1281, 2003

8. Andrew Oliviero, "Measuring bandwidth of high-speed multimode fiber: Understanding the methods used to ensure fiber performance", White paper from OFS Optics, www.ofsoptics.com, 2003.

9. Peter Pleunis, Myrna Boon and Martien van den Heuvel, "Influences of profile variations in PCVD multimode fiber on DMD characteristics for 10GBbs systems", Proceedings of 50th International Wire and Cable Symposium, pp. 698-702, 2001

10. D. Gloge and E. A. J. Marcatilli, "Multimode theory of graded core fibers", Bell system technical journal, Vol. 52, pp. 1563 – 1578, 1973.

11. J. Saijonmaa and S. J. Halme, "Reduction of modal noise by using reduced spot excitation", Applied Optics, Vol 20, pp. 4302-4306, 1981

12. R. Olshansky and D. B. Keck, "Pulse broadening in graded optical fibers", Applied Optics, Vol. 15, pp. 483-491, 1976

13. IEEE 802.3z , "Information Technology - Telecommunication & Information Exchange Between Systems - LAN/MAN - Specific Requirements - Part 3: Carrier Sense Multiple Access with Collision Detection (CSMA/CD) Access Method and Physical Layer Specifications", www.ieee.org, 2002.

14. Mammel, Cohen, "Numerical prediction of fiber transmission characteristics from arbitrary refractive index profiles", Applied Optics, Vol.21, pp 699-703, 1982

15. K. Peterman, "Simple relationship between differential mode delay in optical fibers and the deviation from optimum profile", Electron. Letters, Vol. 14, pp. 793-794, 1978

16. R. Olshansky, "Pulse broadening caused by deviation from the optimal index profile", Applied Optics, Vol.15, pp. 782-786, 1976.

17. TIA-FOTP-455-204, "Measurement of bandwidth on Multimode fiber", www.tiaonline.org, 2000

18. M. Webster, L. Raddatz, I. H. White, D. G. Cunningham, "A statistical analysis of the conditioned launch for gigabit Ethernet links using multimode fiber", J. Lightwave Technology, Vol.17, pp. 1532-1541, 1999

19. D. G. Cunningham, L. Raddatz, I. White, M. C. Nowell, "Multimode communications systems and method using the same", US Patent 6064786, 2000

20. D. Gloge, E. A. J. Marcatili, D. Marcuse, and S. D. Personick, "Dispersion Properties of Fibers," in S. E. Miller and A. G. Chynoweth (eds.), Optical Fiber Telecommunications, chap. 4, Academic Press, 1979

21. Petar Pepeljugoski, John Abbott and Jim Taum, "Effect of launch conditions on Power Penalities in Gigabit Links using 62.5μm core fibers operating at short wavelength", NIST symposium on fiber optic measurements, Boulder, CO, 1998

22. R. J. S. Bates, D. M. Kuchta, and K. P. Jackson, "Improved multimode fiber link BER calculations due to modal noise and non-self pulsating laser diodes", Optical and Quantum Electronics, Vol.27, pp. 203-224, 1995.

23. P. Schneider, "Improved mode conditioning launch lead", Patent No: WO/2004/005992, 2004

24. C. W. Oh, S. Moon, Suhas. P. Veetil and D. Y. Kim, "An angular offset launching technique for bandwidth enhancement in multimode fiber links", Microwave and Optical Technology Letters, Vol.50, pp. 165-168, 2008

25. Z. Hass and M. A. Santoro, "A mode-filtering scheme for improvement of the bandwidth-distance product in multimode fiber systems", J. Lightwave Technology, Vol. 11, pp.1125-1131, 1993

26. M. D'user and P. Bayvel, "2.5 Gbit/s transmission over 4.5 km of 62.5mm using centre launch technique", Electron. Letters, Vol.36, pp. 57-58, 2000

27. O. G. Leminger and G. K.Grau, "Near-field intensity and modal power distribution in multimode graded-index fibres", Electron. Letters, Vol. 16, pp. 678-679, 1980.

28. "Optical Power Loss Measurements of Installed Multimode Fiber Cable Plant", TIA/EIA-526-14A (OFSTP-14), 1998

29. Mario Simard, Michael Carlson, Francois Babin, Martin Tremblay, "Understanding launch conditions for multimode connector and cable assembly testing", Application Note 092, www.exfo.com, 2005

30. K. O. Hill, B. Malo, K. Vineberg, F. Bilodeau, D.Johnson, and I. Skinner, "Efficient mode-conversion in telecommunication fiber using externally written gratings", Electron. Letters, Vol. 26, pp. 1270-1272, 1990.

31. A. M. Vengsarkar, P. J. Lemaire, J. B. Judkins, V. Bhatia, T. Erdogan, and J. E. Sipe, "Long-period fiber gratings as band-rejection filters", J. Lightwave Technology, Vol.14, pp. 58-65, 1996.

32. S. W. James and R. P. Tatam, "Optical fibre long-period grating sensors: characteristics and application", Meas. Sci. Technol., Vol.14, pp. R49-R61, 2003.

33. W. T. Chen and L. A. Wang, "Optical coupling between single mode fibres by utilizing long-period fibre gratings", Electron. Letters, Vol.35, pp. 421-423, 1999.

34. W. T. Chen and L. A. Wang, "Optical coupling method utilizing a lensed fiber integrated with a long-period fiber grating", Applied Optics, Vol.39, pp. 4490-4500, 2000.

35. M. J. Kim, T. J. Eom, U. C. Paek, and B. H. Lee, "Lens free optical fiber connector having a long working distance assisted by matched long-period fiber gratings", J. Lightwave Technology, Vol.23, pp. 588-596, 2005.

36. W. T. Chen and L. A. Wang, "Laser-to-fiber coupling scheme by utilizing a lensed fiber integrated with a long period fiber grating", IEEE Photon. Technology Letters, Vol.12, pp. 501-503, 2000.

37. B. L. Bachim, O. O. Ogunsola, and T. K. Gaylord, "Optical-fiber-to-waveguide coupling using carbon dioxide- laser-induced long-period fiber gratings", Optics Letters, Vol.30, pp. 2080-2082, 2005.

38. Generic Requirements for Singlemode Optical Connectors and Jumper Assemblies, GR-326-CORE, Issue 3, 1999.

Chapter 7
Packaging and Reliability of All-Fiber Components

Optical splitters are key elements in passive optical networks. Fused couplers with standard packaging techniques are not "well-reliable" for harsh outside plant environment. Field failed coupler samples are analyzed to understand the failure modes of couplers in the outside plant environments. Based on experimental studies, an improved packaging process for fused coupler is proposed. Couplers with the new design are fabricated and long term stability is evaluated, which shows an improvement in performance over conventional coupler designs.

Passive Optical Network (PON) guarantees superior performance with reduced maintenance cost and flexibility to deploy anywhere without power availability. Splitter Array Sub Assemblies (SASAs) are the most critical elements in Fiber-To-The-Home PON deployments. SASAs help to distribute the signals evenly to multiple ports, and share the cost of fiber plant among multiple customers, making PONs a promising solution for today's access networks [1]. The performance quotients of splitters are stated on low excess loss, wavelength independence and good uniformity. Along with these performance specifications, long term performance stability and reliability is equally important for SASAs, which call for reliable and efficient packaging techniques.

Recent developments in wavelength insensitive fused monolithic 1xN couplers has regained the importance of fused coupler based SASAs, as they can offer high uniformity couplers and high port count couplers. Even though these products meet performance and reliability specifications, they could still suffer from performance degradation and even failures in the field. Thus it is very important to analyze the field failure mechanisms in such couplers, to offer zero defect system performance over the expected service life. This chapter describes our studies on the failure modes of fused couplers and the various packaging schemes to improve its performance towards impact and long term stability.

7.1 Basic Packaging Method

In all-fiber components, the constituent material is silica glass in the form of a hair-thin structure. Packaging plays a key role for their deployment in the field and long-term stability. Besides, for fused coupler components, because of the nature of their fabrication, the physical structure and optical characteristics of the glass fibers are modified. As a result, the component becomes susceptible to all known sources of weakness associated with the fused bare fiber. A suitable package is, therefore, required to preserve optical properties against the effects of mechanical and environmental stresses. Packaging protects the component after its realization for a reliable operation in the field [2].

Since the fibers used in fabricating FBT couplers are stripped off the protective coating, and the fused region is tapered to very thin (~ 40μm) fragile structure, the device is extremely sensitive to ambient conditions [3]. This often leads to waist breakage of the device near its centre portion unless it is suitably protected. In order

that the physical structure and device properties, such as excess loss and the splitting ratio of the coupler component are not affected by the package, some essential requirements are to be satisfied. The device after fabrication should be kept suspended under uniform tension from either side in order to get rid of any bend or twist in the waist region. Any minute distortion in the taper shape can cause a large change in the splitting ratio [4, 5, 6] and degrades the loss performance of the device [7, 8]. The packaging substrate must not touch the device anywhere in the tapered region in order to avoid any refractive index modification of the outer surface of the taper [9, 3]. The physical contact can also transmit heat surrounding the device by conduction, which may result in variation of the splitting ratio [10, 11]. The device along with the substrate, in the final packaged form should be sealed air-tight in a tube to avoid any exposure to moisture or dust particles, which otherwise may seriously degrade the performance of the device.
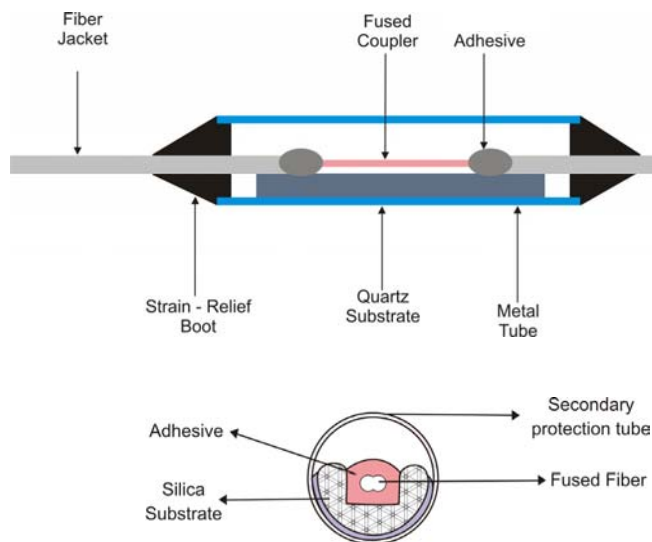
Figure 7.1: Schematic of the quartz substrate package for FBT couplers:
(a) view of the longitudinal section and (b) cross sectional view.

Out of the various packaging schemes of standard FBT components [12], the quartz substrate packaging appears to be very reliable and most widely accepted. The package involves a two-stage protection – the primary package and secondary/outer protection. Primary packaging provides the inner layer of protection for the device (Figure 7.1). The material properties of the primary packaging substrate have a large influence on the performance of the device because of the variations in the thermal

and environmental conditions. The best choice for the material of the primary package is quartz since it exhibits the same behaviour as of the fiber. As shown in Figure 7.1, the substrate is semi-cylindrical with rectangular groove, which can be easily positioned and fixed by a 3-dimentional micro-positioner from underneath the fabricated fiber-device and fixed at the ends using a suitable adhesive. In this investigation, quartz substrates with a length of 47mm and with a groove dimension of 1000x600 μmxμm, is used.

After primary packaging, the device is still bare and needs to be further encapsulated for protection. The device with the primary package is inserted into a metal tube and is shielded at the ends by sealants to keep it air-tight. Invar, a metal alloy that has approximately the same coefficient of thermal expansion as that of silica is used. Care is taken to mount the two ends of the packaged device with the emerging fiber leads such that the package should withstand stress/twist (and stability of the device characteristics) during handling and installation.

7.2 Failure Modes in Fused Couplers

Even though couplers are subjected to standard accelerated tests to simulate the service life in the field, they experience occasional performance degradation and even failures during installation or service. These field problems can cause undesirable service interruption and financial liabilities to the service providers. Field failed samples are cut open and studied for their morphology, structural integrity, surface problems etc. Different techniques such as Optical Microscopy and Scanning Electron Microscopic (SEM) were suggested to analyze the defects [13]

Slow drift in coupling ratio at 85^0C and 85% relative humidity is one of the long term failure mechanisms in fused couplers [14]. Optical adhesive instability at high temperature and humidity is reported as one of the reasons for this drift [15]. Direct diffusion of molecular water (or possibly OH) into the optical fiber can cause coupling ratio drift [14]. As water enters the fiber, the refractive index of the silica decreases, causing an increase in the coupling ratio. Diffusion of water into the coupling region occurs from the humidity chamber. The concentration of water C(r,t) in a cylinder of radius b, with a constant external concentration C_0 and initial internal concentration of zero, as a function of time t and radial position r is given by:

$$C(r,t) = C_0\left(1 - \sum_{n=1}^{\infty} B_n J_o(j_n r/b) \exp\left\{-j_n^2[DH_2O(T)t/b^2]\right\}\right) \qquad (7.1)$$

where
$$B_n \equiv 2/[j_n J_1(j_n)] \tag{7.2}$$

J_n is the nth Bessel function of order n, j_n is the nth zero of J_0(j) and DH_2O(T) is the temperature dependent diffusion constant of water in fused silica. Bell et al [16] gives and expression for the diffusion constant of water in silica based on the measurements in the temperature range from 800[0]C to 1050[0]C as

$$D = 1.0x10^{-6} \exp(-18,300/RT) \text{ cm}^2/\text{sec for T in } ^0\text{K} \tag{7.3}$$

The diffusion constant decreases rapidly with temperature because of the exponential dependence of 1/T.

The waist region of the fused coupler can be modeled as a rectangular waveguide of dimensions ax2a and uniform index of cladding formed by air. The coupling strength can be expressed as [17]

$$\kappa \approx \left[\frac{3\pi\lambda}{32a^2 n_2}\right] X \frac{1}{\left[1+\left(\frac{1}{V}\right)\right]^2} \tag{7.4}$$

where a is the core radius, n_2 is the cladding refractive index , λ is the wavelength and *V* is the *V*-parameter. As water diffuses into the glass, the index drops, resulting in an increase of the coupling strength. The addition of water into the fiber lowers its refractive index such that a fractional increase in the weight of hydroxyl of 1x10^{-5} lowers the index by 1x10^{-6} [14].

Another field failure mechanism in monolithic fused devices is strain from adhesives causing relative motion between the fused fibers, affecting the structural integrity of the fused region and eventually leading to a device failure. The analysis indicates that such kinds of failures starts from small surface defects caused during the fusion or pre-fusion process and further accelerated by the thermal strains or impact due to rough handling at the outside plant conditions [18]. Factors such as worn-out fiber strippers can cause surface defects [19]. The cracks or small surface defects in the fused region grow slowly, causing a silent disconnection. Incases where only one of the fibers among the fused bundle is having problem, strain will be accumulated on the other fibers, thus leading to no-power condition of the product. Figure 7.2 shows the SEM photograph of a failed monolithic coupler. Another prominent failure mechanism observed is the loss of adhesion between the epoxy and quartz substrate to which the fused fiber is bonded. When the fiber bundle detaches from the quartz substrate, it exerts strain on the fused region, ultimately leading to a no-light

condition. Even when the typical failure rate is less than 0.1%, it can still be severe, as it can disrupt the service to multiple customers, depending on physical location of the device in the network.
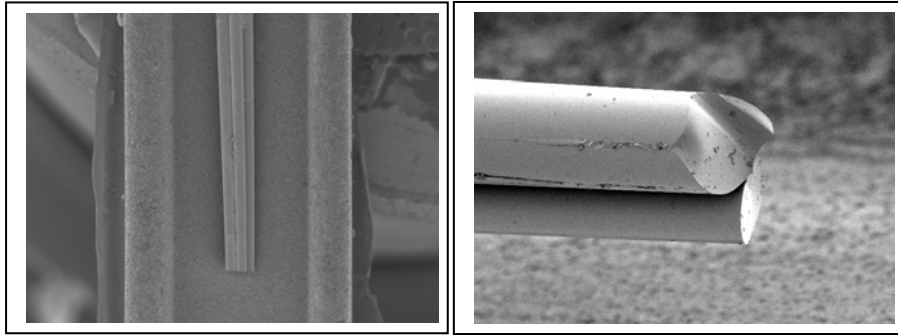

Figure 7.2: SEM picture of failed couplers with magnification of
35 & 400 respectively

Fused couplers must withstand the strains from impact and thermal variations as well as humidity variations at outside plant environments, to offer zero defect PON systems. But all fused couplers are sensitive to environmental effects to some extent, causing long term splitting ratio drifts and increase in polarization dependent loss. Methods were tried to improve the thermal stability of couplers using "glass solder technique", where the glass solder provides a thermally well-matched bond between the quartz substrate and fiber [15]. This method helps to improve the stability of the insertion loss with temperature. However, this doesn't improve the impact resistance. Couplers built with conventional methods and glass solder couplers failed, when bare dropped from a height of 3 ft. The present analysis has been made in specific reference to the fused monolithic 1x4 couplers, made using Corning SMF28 fibers.

7.3 Packaging Design Improvements

Here modifications are suggested for the basic packaging approach described in section 7.1, to improve the performance. Field failures originate from various types of strains, when exposed to outside plant environment. There are mainly two different types of strains that affect the integrity of the fused region. Intrinsic strain sources include strain from twisted fibers, tension in the fused region etc. Extrinsic strains mainly come from adhesives, from substrate or secondary tube. The modelling and analysis of vibrational and thermal strains towards fused region, indicates that change

in the primary packaging technique can effectively isolate various intrinsic and extrinsic strain sources [20].

7.3.1 Thermal Stability

The insertion loss of the coupler should remain stable, when it is subjected to varied thermal conditions. The strain from epoxy can be a problem to the integrity of the fused region, when subjected to continuous thermal / humidity cycling. The exposure to humidity causes water absorption of the adhesive leading to a volume increase, which in turn applies strain on the coupling region. Defects on the surface of the taper grow under the combined effects of humidity and strain and can eventually cause a fiber fracture. Also the epoxy exerts strain due to the thermal expansion thus affecting the thermal stability of the product. The packaging substrate and the optical adhesive to be used should ideally have identical behaviour as that of the fiber glass material. The selection of epoxy shall be made with two parameters: low water absorption and low coefficient of thermal expansion (CTE) to ensure the long-term stability. No adhesive is available which applies zero strain to the fused region; the one having minimum thermal expansion coefficient is 15×10^{-6} in/in/^{0}C. However, the CTE can be further matched to that of fiber, by suitable fillers like quartz powder, which improves the thermal stability considerably. Figure 7.3 shows the thermal stability values with different quartz fill ratios. The variation between the maximum and minimum insertion values, when the coupler is subjected to thermal cycling, is taken as the thermal stability in dB. The thermal stability is measured by monitoring the insertion loss online. Figure 7.3 shows the average thermal stability value of 10 products fabricated with the specified quartz fill ratio. The stability is found to be better when the quartz fill ratio is around 1:1. But above this fill-ratio the thermal stability gets degraded, may be due to the poor adhesion.

Couplers fabricated with a quartz fill ratio of 1:1 were subjected to thermal shock, by varying the temperature between –40 and +90 Degree with a ramp rate of 13^0C/min. Each coupler was tested for this temperature cycle and is actively monitored through out the test. The couplers exhibited minimal sensitivity to changes in temperature; the typical change was less than 0.1dB. The typical thermal stability graph of 1x4 splitter is shown in Figure 7.4.
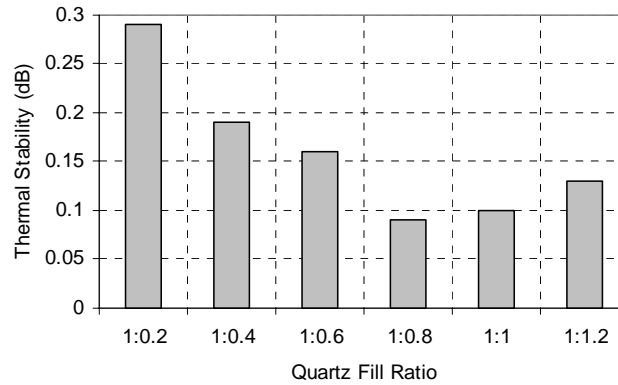
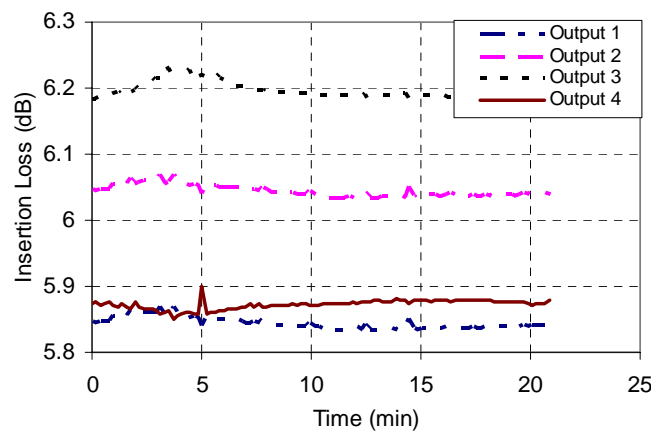Figure 7.3: Thermal stability plot with different quartz fill ratios

Figure 7.4: Insertion loss variation with temperature for a 1x4 coupler

7.3.2 Epoxy Adhesion

Loss of adhesion between the fiber and epoxy is another reason why couplers get failed in fields [21]. Thermally cured epoxies provide the necessary adhesion to maintain the structural integrity of the couplers. But the physical properties of the epoxies are affected by uncontrolled environmental conditions. Exposed to harsh environment (85^0C/85%RH) and in the presence of strains, thermally cured epoxy is found to loose its adhesion with quartz substrate and to hold the fibers in place. It is seen that in some of the couplers, the bond got peeled off from the substrate after exposure to thermal cycling. This effect can be reduced by providing suitable

168

roughness to the quartz substrate. Figure 7.5 shows the performance of the coupler, when quartz substrates of different surface roughness are used. There is an obvious improvement in the performance of couplers made with 50 and 80 micron roughness with respect to the products made with zero surface roughness. However, the 150micron thickness does not give much performance improvement. Here 150micron roughness is created with mechanical process, which might have degraded the structural strength of the substrate. A failure is defined as a change in insertion loss by 0.25 dB. The percentage of failure decreased to <5%, when the surface roughness is increased to of 80μm (rms value).
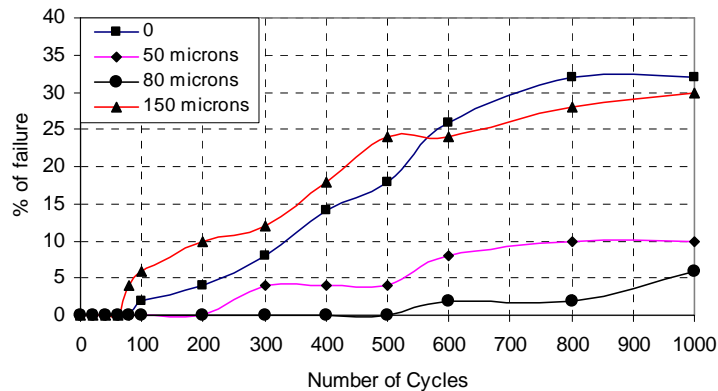

Figure 7.5: Performance chart with different surface roughness
for the quartz substrate

7.3.3 Impact Resistance

Fused couplers are exposed to impact at fields, during installation and handling. It is found that a drop of a product from height of 1ft can make it non-functional, which can happen at any time between the manufacturing process and installation. To minimize the effect of impact towards the fused region, the criticality lies in defining adhesive application points as well as the distance between such points. Traditional epoxy application methods are focussed on holding the fibers to the substrate, but are not applied to absorb the twisting strains. During impact and thermal stress, the twisted portion is still free to move and exert pressure on the fused region, ultimately causing a disconnection. To improve the impact resistance and thus to withstand drop tests, fused couplers shall be affixed to the substrate in such a way that the epoxy absorbs the strains from fiber twists completely. This method of adhesive application restricts the relative motion between the fibers and improves the drop test

performance. But the application of adhesive does not cause changes in the insertion loss of the device. The impact resistance is tested by dropping the couplers from 1ft height on a concrete surface. The insertion loss is online monitored during the drop and a change in IL for more than 0.5dB is judged as a fail. Figure 7.6 shows the number of samples failed when 20 couplers are subjected to drop tests, each batch is made with a specific epoxy length. The epoxy length is measured from the un-stripped portion of fiber towards the fused region. Redefining the epoxy application points improves impact resistance. However, there is a limit on the maximum length of epoxy, since its affects the thermal stability as well as IL due to epoxy wicking. There exists a region, where both the parameters are acceptable. Thus it is necessary to make a balance between the above two factors, to achieve the impact resistance as well as good optical performance.

The bare drop test performance of new couplers is compared with the standard designs and a five-fold improvement is observed. Sample A is selected from a standard coupler manufacturer and Sample B is the optically soldered product. Sample C contains the newly designed couplers. Each lot contains 20 products and the test result is summarized in Table 7.1. Comparative study of samples indicates that the new design offers good performance and withstands bare drop tests. The products were online monitored during drop and passed products showed no variation in their optical performance, during or after the drop. This improvement in drop test performance is attributed to the new method of coupler fixing to the substrate, where the adhesives are applied in such a way that the residual tension at the fused region is minimal.
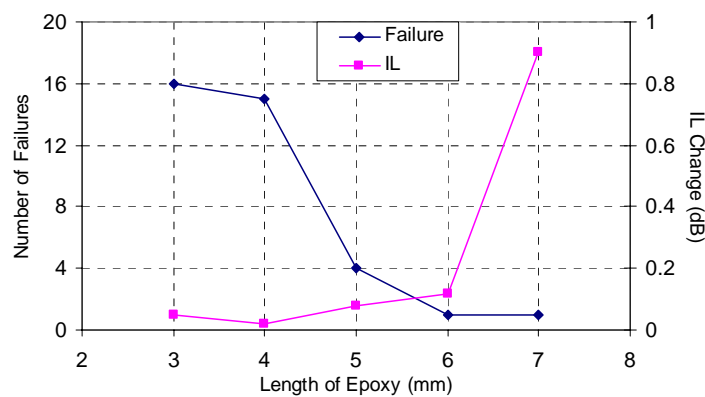

Figure 7.6: Drop test and insertion loss data of fused couplers,

with different epoxy lengths

Product Type	Sample A	Sample B	Sample C
No of Samples	20	20	20
Products Passed	4	9	19

Table 7.1: Bare Drop Test summary of different coupler designs

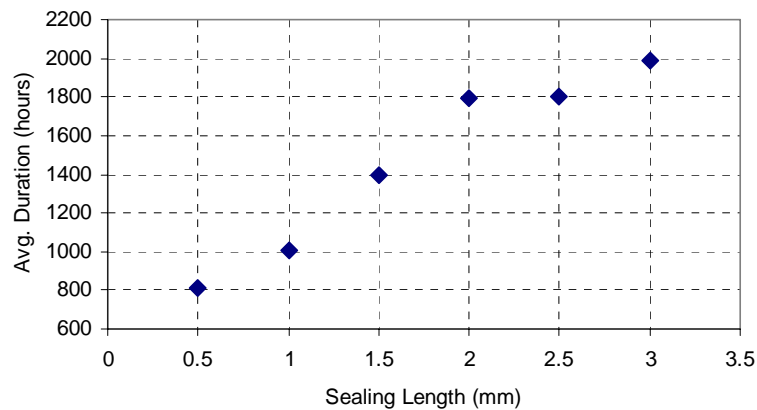### 7.3.4 Humidity Resistance

Figure 7.7: Humidity performance of the couplers with different end sealant lengths.

All epoxies are susceptible to attack from humidity. Swollen epoxies exert pressure on fused region. Also it is recently reported that SiO_2 structure gets loosened at the fusion region [22], causing water molecules to penetrate. This causes shift in coupling ratio of couplers, when exposed to high humid environments. Couplers with enhanced resistance to environmental conditions were demonstrated by Tallent et al with deuterium gas [23]. Performance improvement in humidity can also be achieved with suitable secondary packaging designs. This is achieved by increasing the silicone end booting of the product. Improvements in long term performance are observed by varying the sealant length, which effectively increases the water creeping length. Figure 7.7 shows the average time in hours, the couplers performed with in the criteria when exposed to humidity conditions. The failure condition is defined as variation from the initial value by 0.3 dB.

7.4 Reliability Tests

Monolithic 1x4 couplers are packaged as described in section 7.3. To ensure the performance, these couplers were subjected to temperature cycling and humidity aging tests as per Telcordia standards [24]. A failure is defined as a change in the insertion loss over 0.5 dB in the operating bandpass around 1310, 1490 and 1550 nm. The results of temperature cycling and humidity aging tests are summarized in the Table 7.2. The results show that the optical performance is very stable after these accelerated tests. After humidity aging, the average increase in Insertion Loss in all the ports is less than 0.25 dB. These tests were conducted on a batch of 11 numbers and the performance is tested for all the ports over the entire wavelength range. The test values in Table 7.2 confirm the stability of the new packaging scheme.

Test Condition	Number of Cycles / Days	Average Increase in	
		Insertion Loss	PDL
Temperature Cycling	100 Cycles	0.03	0.01
	200 Cycles	0.05	0.02
	500 Cycles	0.06	0.04
Damp Heat Testing	21 Days	0.08	0.08
	42 Days	0.13	0.12
	83 Days	0.25	0.18

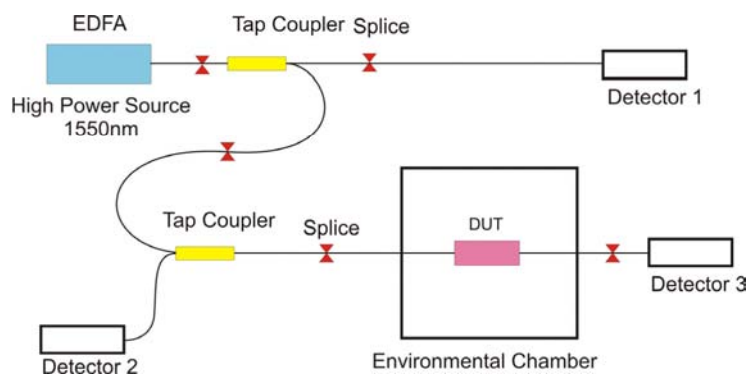Table 7.2: Changes in optical performance parameters

Figure 7.8: High power handling test

The high power handling capability of these couplers are tested , by exposing it to a +23dBm EDFA built in house. The test setup is illustrated in Figure 7.8. The DUT is

placed in elevated environmental condition at 85^0C and 85%RH to see any degradation. No significant drift in IL is observed for 4000 hours.

7.5 Conclusions

Several packaging changes were tried and analyzed to improve the long term performance of monolithic fused couplers. Eventually, a stable packaging technique involving use of quartz substrate, thermally curable epoxy has been developed and successfully tested for their stable performance. The proposed design changes are applicable for all fused devices, including monolithic couplers and wavelength division multiplexers. It is concluded that truly fused 1xN devices could meet the reliability coefficients required for PON applications and SASAs based on these couplers are good choice for future FTTH applications.

References

1. H. Shinohara, ''Broadband access in Japan: rapidly growing FTTH market,'' IEEE Communication Magazine, pp. 72–78, September, 2005.
2. M. Corke, L. Sawyer, J. Vigeant and R. Driver, "Results of large scale environmental testing on fiber optic couplers", Proceedings of SPIE: Fiber Optics reliability: benign and adverse environments II, 992, pp. 280 - 286, 1988
3. F. De. Fornel, C. M. Ragdale and R. J. Mears, "Analysis of single-mode fused tapered couplers", IEE Proceedings Pt. Journal of Optoelectronics, Vol.131, pp. 221-226, 1984
4. B. S. Kawasaki, M. Kawachi, K. O. Hill and D. C. Johnson, "A single-mode fiber coupler with a variable coupling ratio", J. Lightwave Technology, LT-1, pp.176-180, 1983.
5. D. C. Johnson and K. O. Hill, "Control of wavelength selectivity of power transfer in fused biconical monomode directional couplers", Applied Optics, Vol.25, pp. 3800 - 3804, 1986.
6. T. Bricheno and A. Fielding, "A practical model of fused fiber couplers" IEE Colloquium on "All-fiber devices" (London), pp. 1/1 – 1/4, 1988.
7. W. J. Stewart and J. D. Love, "Design limitation on tapers and couplers in single mode fibers", Proceedings of ECOC'85 (Venice), pp.559 - 564, 1985.
8. J. D. Love and W. M. Henry, "Quantifying loss minimization in single-mode fiber tapers" Electron. Letters, 22, pp. 912-914, 1986.
9. C. K. Kao, "Optical Fiber Systems: Technology, Design and Applications", Mc-Graw Hill, Ch. 2, 1982

10. R. G. Lamont, D. C. Johnson, and K. O Hill, "Power Transfer in fused biconical taper single mode fiber couplers: dependence on external refractive index", Applied Optics, Vol.24, pp. 327-331, 1985.

11. M. S. Yataki, "Fused Taper Single mode fiber couplers, Ph. D Thesis, University of Southampton, Ch 2, Aug 1988

12. A. Fielding, "Single mode fused coupler for undersea optical transmission systems", Optics and Laser Technology, Vol.18, pp. 145-150, 1986.

13. T. Wei, B. T, Devlin, H. H. Yuce and J. P. Varachi Jr, "Failure Mode Analysis of Fiber Components", Proceedings of NFOEC-1995, Boston, 1081-1085, 1995

14. C. V. Cryan, J. R. Curley, F. J. Gillham, D. R. Maack, B. Porter and D. W. Stowe, "Long term splitting ratio drifts in single mode fused fiber optic splitters", Proceedings of National Fiber Optic Engineer's Conference (NFOEC) '95, pp. 746-756, 1995

15. H. Daniel, D. Moore and V. Tekippe, "A glass solder process for packaging fiber optic components", Proc. NFOEC '94, V. 4, pp. 71-77, 1994.

16. T. Bell, G. Hetherington and K. H. Jack, "Water in vitreous silica – Part 2: Some aspects of hydrogen-water-silica equilibria", Phys. and Chem of glasses 3, pp. 141-146, 1962.

17. F. P. Payne, C. D. Hussey, and M. S. Yataki, "Modelling fused single mode fiber couplers", Electron. Letters, Vol.21, pp.461-462, 1985

18. Samuel Varghese, Muhammed Iqbal, Baiju C. B, Hari.K, Abraham Thomas, Suresh Nair, "Design improvements of fused couplers for PON applications", Proceedings of Photonics'04, Cochin, pp.134, 2004.

19. I. J. Wilkinson, "Wear-cut Failure Mechanism in Fused Fibre Couplers", Electronics Letters, Vol.29, 1137 –1139, 1993.

20. E. Suhir, "Vibration frequency of a fused biconical taper (FBT) lightwave coupler", J. Lightwave Technology, Vol.10, pp. 898-902, 1992.

21. S. Etemad, P. Grimado, F. DeRosa and A. Dori, "A failure mechanism for optical power branching components: when epoxy lets go of the fiber", Proceedings of NFOEC '95, pp.823-832, 1995.

22. H. Nagata, "Chemical properties of fused fiber coupler surface", Optical Fiber Technology, Vol.6, pp.324-328, 2000

23. J. R. Tallent, A. J. Hoffman, S. Pilevar, "Fiber optic device with enhanced resistance to environmental conditions and method", US Patent 2004/0033023 A1, 2004

24. Telcordia GR-1221, "Generic Reliability Assurance Requirements for Fiber Optic Branching Components" Issue 3, March 2001

General Conclusions and Future Scope

The work presented in this thesis was focused on developing new methods or improving the existing methods to fabricate all-fiber components for passive optical access networks. This chapter derives conclusions based on the results presented in the previous chapters and also describes the future scope of the work in this direction.

All-fiber technology, based on fused couplers and long period gratings, is ideal for realizing various components such as monolithic fused 1x4 couplers, wavelength division multiplexer, mode conditioning device etc for optical access networks. All-fiber components offer unique advantages with respect to other competing technologies. The specific conclusions based on the work are mentioned below.

➢ Fused coupler technology is suited for fabricating monolithic 1x4 couplers having wide band performance and low polarization sensitivity. Monolithic 1x4 couplers with performance over a wavelength range from 1250 nm to 1650nm is reported. The broadband coupler exhibits low excess loss (<0.2 dB) as well as low polarization dependent loss ~ 0.15dB. The power coupling signature in the reported structure is unique due to the symmetric coupling of power from the central fiber to the surrounding fibers. This makes the process relatively simple, and alleviates the need for pre-processing of individual fibers. This method is ideal for mass production of the device. It is found that a small variation in the fiber array geometry does not affect the characteristics of the device. The performance of the device with respect to various process parameters is studied and optimum conditions are suggested. The coupling behaviour of the device depends on the input port in which light is launched and is not recommended as a 4x4 device. But the device is suitable for bi-directional transmission in passive optical networks. Monolithic 1x4 couplers are attractive solution since it offer the advantages of PLC splitter (port count and wide band performance) and fused couplers (epoxy free optical path). It is shown that the method can

be extended to make wavelength independent 1x5 and 1x6 monolithic couplers.

➢ High uniformity monolithic 1x4 couplers are realized with fused fiber technology, which offers similar performance of planar lightwave circuit splitters. A new structure by fusing five fibers is suggested for this. The power launched in the central fiber is completely transferred to the surrounding fibers. Port-to-port uniformity of 0.4dB is achieved, over a spectral range of 400nm. By controlling the process parameters, it is possible to retain a small amount of power in the throughput port, for in-situ monitoring.

➢ Isolation in fused WDMs is limited due to the wavelength dependence of coupling ratio and deviation from ideal coupling characteristics. Long period gratings, fabricated with electric arc technique is integrated with fused WDMs. Integration of the two all-fiber technologies yields a simple and compact solution for high isolation fused WDMs. Isolation value greater than 30dB is achieved with minimal increase in insertion loss.

➢ Mode conditioning patchcords based on long period gratings written on the singlemode to multimode interface is proposed and characterized. This provides an all-fiber method with comparable performance to the conventional offset launching method. The sensitivity of the fabrication to different parameters was studied. The performance of the device under various environmental conditions is also investigated.

➢ The long term reliability and impact resistance of all-fiber components can be improved by suitably adapting the primary and secondary packaging schemes. Various studies are conducted to improve the thermal stability and impact resistance. Devices fabricated with new design exhibits better performance in temperature cycling, humidity aging and drop tests.

Here in the present work, focus has been given to fabricate components based on normal single mode fibers and multimode fibers. However, different types of fibers are being developed recently like bend insensitive fibers, photonic crystal fibers etc. These fibers are likely to be adopted for optical access networks in the near future,

due to various reasons. For instance, hole-assisted fibers offer distinctive advantages to be implemented in customer premises, since it can be easily handled even by un-trained operators. The present work can be extended to develop components based on such specialty fibers. Such components will be required in future networks as well as in special systems such as high power fiber amplifiers and lasers.

Moreover, in this work focus has been limited to access network components. However, metro or back bone networks need more complex functionalities like add drop multiplexers and research needs to be extended to realize such all-fiber components. High power fiber lasers require many additional all-fiber components such as splitters and 1xN combiners, which can be realized with fused fiber technology. Biomedical systems also need many novel all-fiber components.

Appendix A

Derivation of Coupled Mode Equations

In this appendix the coupled-mode equations, which describe the variation in the amplitude of the waves propagating in each individual waveguide of a directional coupler, are derived Let $n_1(x, y)$ and $n_2(x, y)$ represent the refractive index variation in the transverse plane of waveguide 1 in the absence of waveguide 2 and that of waveguide 2 in the absence of waveguide 1. Let $n(x, y)$ represent the refractive index variation of the directional coupler consisting of the waveguides, 1 and 2.

If β_1 and β_2 represent the propagation constants of the modes of waveguides 1 and 2 in the absence of the other then we may write:

$$\nabla_t^2 \psi_1 + \left[k_0^2 n_1^2(x, y) - \beta_1^2 \right] \psi_1 = 0 \tag{A.1}$$

$$\nabla_t^2 \psi_2 + \left[k_0^2 n_2^2(x, y) - \beta_2^2 \right] \psi_2 = 0 \tag{A.2}$$

where

$$\nabla_t^2 = \nabla^2 - \frac{\partial^2}{\partial z^2} = \frac{\partial^2}{\partial x^2} + \frac{\partial^2}{\partial y^2} \tag{A.3}$$

and $\psi_1(x, y)$ and $\psi_2(x, y)$ represent the transverse mode field mode field patterns of wave-guides 1 and 2, respectively, in the absence of the other.

If $\Psi(x, y, z)$ represents the total field of the directional coupler structure, then we have

$$\nabla_t^2 \Psi + \frac{\partial^2 \Psi}{\partial z^2} + k_0^2 n^2(x, y) \Psi = 0 \tag{A.4}$$

We now approximate Ψ as follows

$$\Psi(x, y, z) = A(z)\psi_1(x, y)e^{-i\beta_1 z} + B(z)\psi_2(x, y)e^{-i\beta_2 z} \tag{A.5}$$

which is valid when the two waveguides are not very strongly interacting. In equation (A.5) we have written the total field as a superposition of the fields in the first and second waveguides with amplitudes $A(z)$ and $B(z)$ which are functions of z. For infinite separation between the two waveguides, obviously the waveguides are noninteracting, and A and B would then be independent of z. The coupling between the two waveguides leads to z-dependent amplitudes. Substituting for Ψ in Equation A.4, we obtain

$$Ae^{-i\beta_1 z}(\nabla_t^2\psi_1 - \beta_1^2\psi_1 + k_0^2 n^2\psi_1) + Be^{-i\beta_2 z}(\nabla_t^2\psi_2 - \beta_2^2\psi_2 + k_0^2 n^2\psi_2)$$
$$- 2i\beta_1(dA/dz)\psi_1 e^{-i\beta_1 z} - 2i\beta_2(dB/dz)\psi_2 e^{-i\beta_2 z} = 0$$

(A.6)

where we have neglected terms proportional to d^2A/dz^2 and d^2B/dz^2, which is justified when $A(z)$ and $B(z)$ are slowly varying functions of z. Using Equations A.1 and A.2, Equation A.6 becomes

$$k_0^2 \Delta n_1^2 A\psi_1 + k_0^2 \Delta n_2^2 B\psi_2 e^{i\Delta\beta z} - 2i\beta_1(dB/dz)\psi_1$$
$$- 2i\beta_2(dA/dz)\psi_2\, e^{i\Delta\beta z} = 0$$

(A.7)

where

$$\Delta n_1^2 = n^2(x,y) - n_1^2(x,y)$$

(A.8)

$$\Delta n_2^2 = n^2(x,y) - n_2^2(x,y)$$

(A.9)

$$\Delta\beta = \beta_1 - \beta_2$$

(A.10)

Multiplying equation (A.7) by ψ_1^* and integrating over the whole cross section, we obtain

$$dA/dz = -i\,\kappa_{11}A(z) - i\kappa_{12}Be^{i\Delta\beta z}$$

(A.11)

where

$$\kappa_{11} = \frac{k_0^2}{2\beta_1} \frac{\iint_{-\infty}^{\infty}\psi_1^*\Delta n_1^2\psi_1 dxdy}{\iint_{-\infty}^{\infty}\psi_1^*\psi_1 dxdy}$$

(A.12)

$$\kappa_{12} = \frac{k_0^2}{2\beta_1} \frac{\iint_{-\infty}^{\infty}\psi_1^*\Delta n_2^2\psi_2 dxdy}{\iint_{-\infty}^{\infty}\psi_1^*\psi_1 dxdy}$$

(A.13)

In writing equation (A.11) we have neglected the overlap integral of the modes - that is, we assume

$$\iint_{-\infty}^{\infty}\psi_1^*\psi_2 dxdy << \iint_{-\infty}^{\infty}\psi_1^*\psi_1 dxdy$$

(A.14)

which is valid for weak coupling between the waveguides.

Similarly, if we multiply equation (A.7) by ψ_2^* and integrate, we obtain

$$dB/dz = -i\kappa_{22}B - i\kappa_{21}Ae^{-i\Delta\beta z}$$

(A.15)

where

$$\kappa_{22} = \frac{k_0^2}{2\beta_2} \frac{\iint_{-\infty}^{\infty} \psi_2^* \Delta n_2^2 \psi_2 \, dxdy}{\iint_{-\infty}^{\infty} \psi_2^* \psi_2 \, dxdy} \qquad (A.16)$$

$$\kappa_{21} = \frac{k_0^2}{2\beta_2} \frac{\iint_{-\infty}^{\infty} \psi_2^* \Delta n_1^2 \psi_1 \, dxdy}{\iint_{-\infty}^{\infty} \psi_2^* \psi_2 \, dxdy} \qquad (A.17)$$

We can write Equations A.11 and A.15 in a different form if we define

$$a(z) = A(z)e^{-i\beta_1 z} \qquad (A.18)$$

$$b(z) = B(z)e^{-i\beta_2 z} \qquad (A.19)$$

Substituting from Equations A.18 and A.19 in Equations A.11 and A.15, we have

$$da/dz = -i(\beta_1 + \kappa_{11})a - i\kappa_{12}b \qquad (A.20)$$

$$db/dz = -i(\beta_2 + \kappa_{22})b - i\kappa_{21}a \qquad (A.21)$$

The above two equations represent the coupled mode equations .It follows from equations (A.20) and (A.21) that κ_{11} and κ_{22} represent the corrections to the propagation constant of each individual waveguide mode due to the presence of the other waveguide. These correction factors are normally neglected in the analysis, although one can very easily incorporate them. Thus, the coupled equations may be written as

$$da/dz = -i\beta_1 a - i\kappa_{11}b \qquad (A.22)$$

$$db/dz = -i\beta_2 b - i\kappa_{21}a \qquad (A.23)$$

The quantities κ_{11} and κ_{22} in Equations A.12 and A.16 represent corrections to the propagation constants of each individual waveguide mode due to the presence of the other waveguide and are normally neglected in the analysis, although they can be incorporated easily.

Thus, we write Equations A.11 and A.15 as

$$\frac{dA}{dz} = i\kappa_{12}Be^{i\Delta\beta z} \tag{A.24}$$

$$\frac{dB}{dz} = i\kappa_{21}Ae^{-i\Delta\beta z} \tag{A.25}$$

Differentiating Equation A.24 with respect to z and eliminating B-dependent terms, we obtain

$$\frac{d^2A}{dz^2} - i\Delta\beta\frac{dA}{dz} + \kappa^2A = 0 \tag{A.26}$$

whose general solution is

$$A(z) = e^{i\Delta\beta_z/2}(a_1e^{i\gamma z} + a_2e^{i\gamma z}) \tag{A.27}$$

where

$$\gamma^2 = \kappa^2 + \Delta\beta^2/4,$$
$$\kappa^2 = \sqrt{\kappa_{12}\kappa_{21}} \tag{A.28}$$

Substituting the value of $A(z)$ in Equation A.24, we obtain

$$B(z) = -\frac{1}{\kappa_{12}}e^{i\Delta\beta z/2}\left[\left(\frac{\Delta\beta}{2} + \gamma\right)a_1e^{i\gamma z} + \left(\frac{\Delta\beta}{2} - \gamma\right)a_2e^{-i\gamma z}\right] \tag{A.29}$$

If at $z = 0$, power is incident only in waveguide 1, then

$$A(0) = A_0, B(0) = 0 \tag{A.30}$$

Using these initial conditions in Equations A.27 and A.29, the constants a_1 and a_2 can be determined.

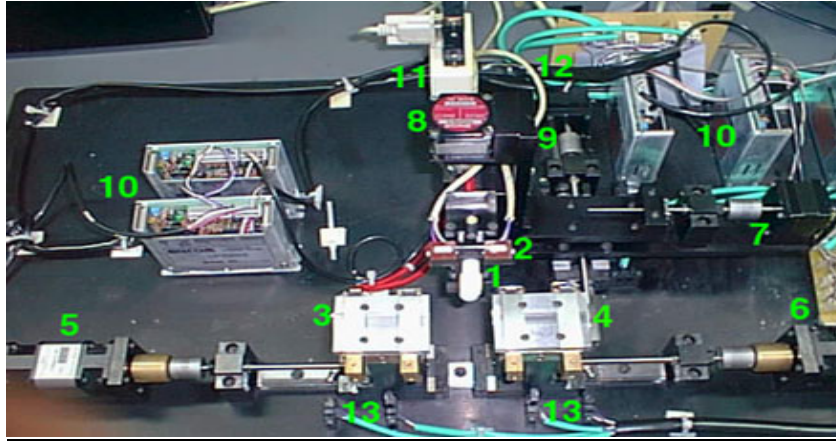Finally, the power in each waveguide at any value of z is given by

$$\frac{P_T(z)}{P_1(0)} = 1 - \frac{\kappa^2}{\gamma^2}\sin^2\gamma z \tag{A.31}$$

$$\frac{P_C(z)}{P_1(0)} = \frac{\kappa^2}{\gamma^2}\sin^2\gamma z \tag{A.32}$$

where $P_1(0)$ is the power launched in to waveguide1. In obtaining the final equations, we have assumed $\kappa_{12} \approx \kappa_{21}$.

iv

Appendix B

A view of the fused coupler fabrication station

1 - Flame Holder

2 - Substrate Holder + Heating Coil

3 - Left Chuck

4 - Right Chuck

5 - Left Pull Motor

6 - Right Pull Motor

7 - Horizontal Flame Stage

8 - Vertical Flame Holder Stage

9 - Forward Flame Stage

10 - Motor Control Card

11 - Gas Flow Controller

12 - Circuit Board

13 - Optical Limit Sensor